IN-76
34047
P- 88

NASA Contractor Report 195407

Final Technical Report

Theoretical Study of Cathode Surfaces and High-Temperature Superconductors

Wolfgang Müller
Analatom, Incorporated
Westlake, Ohio

October 1994

Prepared for
Lewis Research Center
Under Contract NAS3-25085

National Aeronautics and
Space Administration

N95-16598
Unclas
G3/76 0034047
(NASA-CR-195407) THEORETICAL STUDY OF CATHODE SURFACES AND HIGH-TEMPERATURE SUPERCONDUCTORS Final Technical Report (Analatom) 88 p

TABLE OF CONTENTS

1. SUMMARY

The cluster approach has been applied to the study of the electronic structure of cathode surfaces and high-temperature superconductors. The reported calculations are based on the relativistic Xα scattered-wave method of computational quantum chemistry. The study of surface-dipole properties and dipole-dipole interactions for low-work-function surfaces has enabled, for the first time, a systematic theoretical investigation of work-function/coverage curves and a determination of minimum work functions for different model cathode surfaces.

Surface-dipole properties have been obtained for two series of calculations. In the first series, BaO adsorbed on monolayer films of Re, Os, Ir, and Pt on otherwise unchanged bcc W(100) has been investigated to study electronegativity and charge-transfer effects for different coating metals. In the second series, BaO on bcc W(110), hcp Os(10$\bar{1}$0), and fcc Pt(111) has been investigated to study the effects of different substrate crystal structures. It was found that the surface-dipole properties behave monotonically for the monolayer films, while a minimum in the surface dipole and a maximum in the dipole energy is obtained for BaO/Os(10$\bar{1}$0). Alloying with tungsten increases both the surface dipole and barium binding energy for the hcp Os(10$\bar{1}$0) substrate, while it has a small effect in the case of the cubic substrates.

Extended cluster calculations have been carried out for the study of adsorbate interactions and the dependence of the dipole properties on the BaO surface coverage. Larger clusters are found to provide systematically improved results for the surface electronic structure and the adsorbate binding energy. At higher coverages, the calculated binding energies for Ba on B-type cathode surfaces of 4.6-5.4 eV compare very well with the observed energy of desorption of 4.8 eV. The calculated binding energies for Ba and Cs on W(100) of 3.6 and 3.0 eV, respectively, are in excellent agreement with the experimental energies of desorption of 3.8 and 2.8 eV.

The depolarization model of interacting surface dipoles has been employed to determine, from first principles, minimum work functions for a variety of low-work-function surfaces relative to BaO/W. The two important microscopic properties, the initial surface dipoles at low coverages and their polarizabilities, or depolarization, have been determined from calculations for clusters with individual and interacting surface dipoles. Consistent and qualitatively accurate results have been obtained for minimum work functions relative to BaO/W (2.0 eV), namely 1.8 eV for BaO/Os(10$\bar{1}$0), 2.4 eV for BaO/Pt(111), 2.6 eV for Ba/W(100), and 1.4 eV for Cs/W(100).

Comparisons with theoretical results have been made for the Ba, O, and W electronic energies observed in photoelectron spectra of BaO/W(100), the oxygen-induced features of O/W(100) in inverse photoemission spectra, and spectroscopic constants of BaO. Different orientations of BaO on the surface have been considered. For the Ba-O interatomic distance on W, single-adsorbate cluster calculations favor the value of 2.3 Å suggested by Shih et al. (1988), but the question of the orientation of BaO on operating cathodes surfaces remains unresolved.

The electronic structure of the conduction and valence bands and the electronic core levels of the 90K superconductor $YBa_2Cu_3O_7$ have been studied with fully relativistic calculations. Different clusters including between 1 and 4 Cu-O layers and up to 39 atoms have been considered. The generated densities of states for clusters of the size of a unit cell are found to be in good agreement with solid-state calculations and experimental results. Projected densities of states show that the characteristic double maximum observed in photoemission spectra just below the Fermi level is composed of Cu states at its center and O states more to its sides. The high oxygen density of states near the Fermi level and the calculated charge distribution point to substantial vacancies in the O 2p shell. Large covalent contributions in the chemical bonds are found which are expected to be characteristic for the surface of the material.

Core-electron binding energies have been calculated for all core states of the two inequivalent Cu atoms and the four inequivalent O atoms, as well as the 3d states of Y and Ba. Final-state effects in the photoemission process and spin-orbit interactions in the valence band have been investigated for the first time. While final-state effects are essential for the calculation of accurate core-level energies, they are found to be small (0.2 eV) for the localized Cu 3d states in the valence band and do not significantly affect its location relative to the Fermi level. The Cu 3d spin-orbit splittings are 0.3 eV.

The results for BaO/W cathode surfaces and the high-temperature superconductor $YBa_2Cu_3O_7$ have been presented at several scientific conferences and published in the IEEE Transactions on Electron Devices and in Physica C (Müller, 1989).

2. INTRODUCTION

It is well known that the electron emission from impregnated barium dispenser cathodes can significantly be improved by coating the tungsten surface with a platinum-group transition metal, like Re, Os, Os-Ru, or Ir. Similar effects can be achieved by using mixed-metal matrices instead of a pure tungsten matrix. During the activation and early life of the cathode, interdiffusion of W and the other metal(s) occurs and an alloy surface is formed, with a monolayer of adsorbed Ba and O from the impregnant. The best coating metal is Os, followed by Ru, Ir, and Re, while, e.g., Pt gives rise to a degradation of the emission properties.

The improved emission is caused by a lowering of the work function from about 2.0 eV for tungsten (B-type) cathodes to 1.8 eV for alloy (M-type or mixed-metal) cathodes. Pt coating, on the other hand, increases the work function to 2.2 eV (Norman et al., 1987). A clean W surface, for comparison, has a work function of 4.5 eV. The decrease from 4.5 eV for the clean substrate to around 2 eV for cathode surfaces is caused by the adsorption of Ba and O and attributed to the formation of a surface dipole that lowers the electrostatic potential for electron emission. The effect due to the alloy formation is comparatively small, less than 10 percent of the total effect, but nevertheless technologically very important because a work function variation of 0.2 eV changes the emission-current density (at the same temperature) by one order of magnitude.

Several attempts have been made to explain the variation of the work function and emission that is observed for cathodes with different coating materials. From alkali-metal adsorption studies it is known that usually the substrates with the highest work functions give rise to the lowest work functions after adsorption. By analogy, Zalm and van Stratum (1966) explained the emission enhancement for Re, Os, Ru, and Ir by the higher work functions of these metals as compared to W. One would therefore expect that a coating with platinum, which has an even higher work function, should lead to a further improvement. This is, however, not the case.

Norman et al. (1987) have investigated the bonding of Ba and O on W, W-Os, and W-Pt cathodes, using surface extended x-ray-absorption fine-structure (SEXAFS) experiments. They find that Ba is coordinated with one O atom for BaO/W and BaO/Pt-W, but coordinated with two O atoms for BaO/W-Os, and tentatively explain the lowering of the work function by the larger charge transfer from Ba being bridge-bonded to two O atoms. SEXAFS experiments performed by Shih et al. (1988) for the B-type surface, however, contradict the assignments of the earlier experiment, and they propose a bridge-bonded structure for B-type surfaces. Calculations by

Hemstreet et al. (1989) for BaO/W(100) appear to confirm Shih's results, but the calculated work functions are significantly higher than expected.

The purpose of the present theoretical study is to investigate, with first-principles cluster calculations, possible reasons for the observed emission characteristics of different low-work-function surfaces, and to calculate the work functions of different materials.

This report is organized as follows: The results for models of B- and M-type cathode surfaces are presented in Section 3. The electronic structure of O/W and ab initio results for BaO are described in Sections 4 and 5, respectively. An application of the relativistic cluster approach to the recently discovered high-temperature superconductor $YBa_2Cu_3O_7$ is presented in Section 6. The computational methods are briefly discussed in Section 7, and the conclusions are summarized in Section 8.

3. CATHODE SURFACES

In this section, the surface-dipole properties, work functions, and electronic structure of low-work-function surfaces are described. The purpose of these investigations is to identify the microscopic materials parameters that determine the different work functions and significant variations in emission enhancement for B- and M-type cathode surfaces.

3.1 Surface-Dipole Properties

The surface-dipole properties are compared for two series of calculations of model cathode surfaces. The first series involves BaO adsorbed on monolayer films of Re, Os, Ir, and Pt on an otherwise unchanged bcc W(100) substrate. In the second series, effects of the different crystal structures of the coating materials and alloys are investigated. In this series, the dominant crystal faces as present on actual cathode surfaces are employed.

3.1.1 Monolayer Films

In order to investigate the differences in the electronic effects of W, Re, Os, Ir, and Pt without the complications arising from varying crystal structures, different crystal planes, and uncertain adsorption geometries, monolayer-film properties are discussed first. These results reflect the changes in the electronic structure and surface-dipole properties induced by the presence of the coating metal in otherwise identical geometrical environments.

The substrate cluster used is the unit cell (a W_9 cube) of body-centered-cubic tungsten with Ba adsorbed on top of O at the fourfold-hollow site of the (100) face. For the monolayer films, the W surface layer is replaced with Re, Os, Ir, or Pt. Because there are no adsorbate interactions present in these clusters, the results are to be considered as representative of low-coverage conditions.

The calculated properties include the charge distribution with net atomic charges q_i at locations r_i, the resulting

surface dipole $$\mu = \Sigma_i \, q_i r_i \ , \qquad (1)$$

dipole length $$R_{dip} = \mu / q(A) \ , \qquad (2)$$

and dipole energy $$E_{dip} = q^2(A)/R_{dip} = q^3(A)/\mu \ . \qquad (3)$$

q(A) is the net charge on the adsorbate (typically Ba). E_{dip} is a measure of the attractive contribution to the adsorbate binding energy and may be compared with experimental energies of desorption. Atomic units are used, i.e., m = e = $h/2\pi$ = 1. In these units q is expressed in electrons (e), r and R in Bohrs ($1a_0$ = 0.5292 Å), μ in a.u. (= 2.542 Debyes), and E in Hartrees (= 27.21 eV).

The results for the clusters $BaO/M_4W_1W_4$ with a surface layer of M = W, Re, Os, Ir, and Pt are given in Table I. The surface-dipole properties were calculated using the quasirelativistic scattered-wave Xα approach. They are in good agreement with fully relativistic results (see Section 7).

TABLE I.

Dipole properties for $BaO/M_4W_1W_4$ (bcc,100) clusters with M = W, Re, Os, Ir, and Pt from quasirelativistic Xα calculations. q (in electrons) denotes net atomic charges, μ dipole moment, R_{dip} dipole length, and E_{Ba} dipole energy. R(Ba-O) = 4.9 a_0 ≈ 2.6 Å and R(Ba-surface) = 6.0 a_0 ≈ 3.2 Å (Tuck and Norman et al., 1986 and 1987).

Property	M = W	Re	Os	Ir	Pt
q(Ba)	+1.50	+1.53	+1.57	+1.58	+1.52
q(O)	-0.15	-0.17	-0.15	-0.10	-0.25
q(Substrate)	-1.35	-1.36	-1.42	-1.48	-1.27
Electronegativity	1.40	1.46	1.52	1.55	1.44
$q(M_I)$	-0.08	-0.17	-0.25	-0.34	-0.27
$q(W_{II})$	-0.00	+0.06	+0.12	+0.24	+0.18
$q(W_{III})$	-0.25	-0.19	-0.13	-0.09	-0.09
μ (Debyes)	38.4	35.4	31.1	27.3	25.8
R_{dip} (Å)	5.3	4.8	4.1	3.6	3.5
E_{Ba} (eV)	6.1	7.0	8.6	10.0	9.4

Barium is found to be heavily oxidized with a net charge of 1.5-1.6 electrons. Only about 10-20% of this charge has been transferred to oxygen, while the major fraction has been transferred to the substrate. A comparison between the different clusters shows that Ba has the highest oxidation level for the Ir monolayer film. Experimentally, Haas et al. (1983) have found that the oxidation level increases for BaO adsorbed on W to W-Os and Ir,

which is in excellent agreement with the present results. This observed behavior closely parallels and has its origin in the variation of the electronegativities for the different coating metals (cf. Table I).

The largest charge redistributions are found among the substrate atoms. With increasing electronegativity of the atoms in the first substrate layer, this layer acquires more and more electrons from the underlying W atoms. Because of the strong interaction of O with the second-layer W atom in this geometry, the second layer becomes slightly oxidized.

The large charge transfer from Ba to the substrate gives rise to very large surface dipole moments. The calculated dipole moments decrease monotonically in the series from BaO on W to Pt-W, in spite of the maximum in the net charge on Ba for the Ir-W system, because the charge from Ba is increasingly transferred to the first substrate layer at the expense of mainly the third layer. This leads to a significant reduction in the dipole length R_{dip} which, because of a comparatively stable net charge on Ba, determines the observed trend in the surface dipoles.

The dipole energy increases for the monolayer clusters from 6.1 eV for W to 10.0 eV for Ir and then falls back to 9.4 eV for Pt. This trend is expected to reflect the variation of the Ba binding (or desorption) energies at very low coverages, and is qualitatively in agreement with the observed increase of the Ba desorption energy from 4.8 to 5.4 eV for B- to M-type cathodes surfaces (Forman, 1984 and 1987).

The results for the monolayer clusters are summarized in Fig. 1, which shows the monotonic decrease of the surface dipoles and the increase in the dipole energies. Both trends are governed by the increasing electronegativity of the refractory metal (up to Ir) in the first substrate layer. The increasing transfer of charge from the underlying W atoms to the first layer reduces the Ba-substrate dipole and explains the decrease in the surface dipoles (μ). Because the Ba binding energy is proportional to $1/\mu$, the Ba binding energies increase accordingly. The maximum for Ir-W results from the fact that Ir has the highest electronegativity of the refractory metals, and as a consequence the net charge (q) on Ba is a maximum. Because the binding energy is proportional to the second power of q, the effect of the further decrease in R_{dip} (and μ) for Pt-W is more than compensated for and a maximum in the binding energy is obtained.

FIGURE 1.

Surface dipoles and Ba binding energies for BaO on W(100) and on monolayer films of Re, Os, Ir, and Pt on W(100).

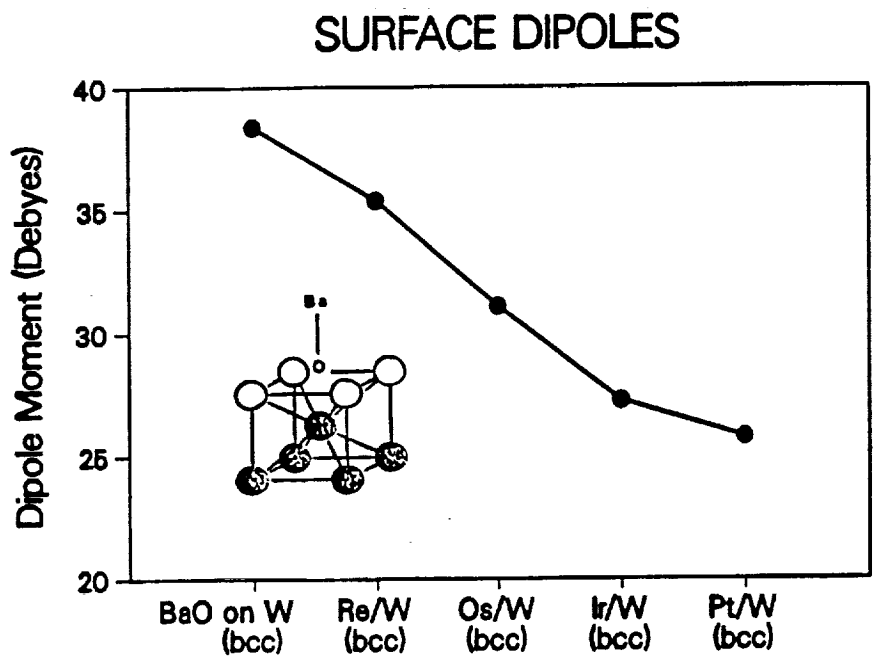

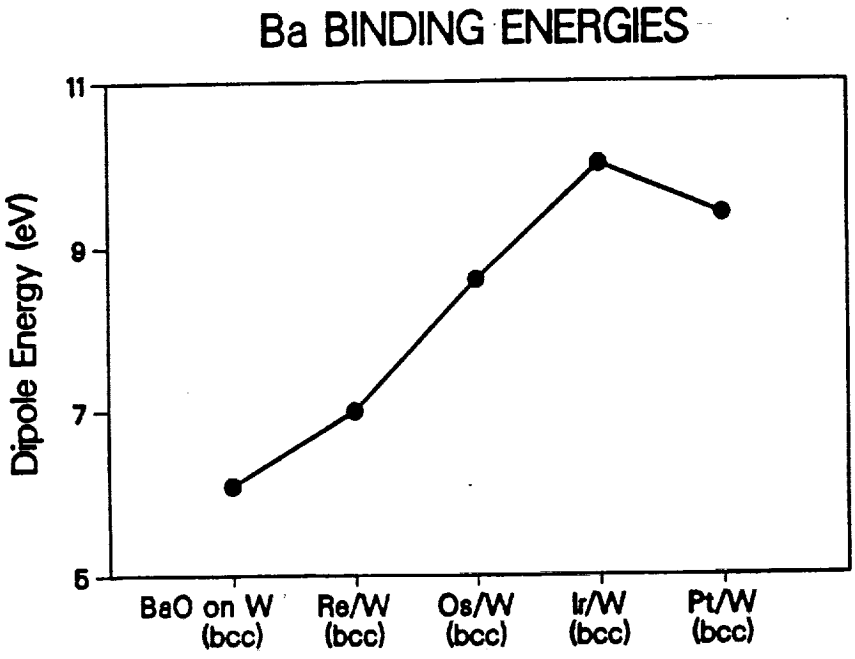

3.1.2 Effects of Crystal Structure

For the study of the effects of different crystal structures the dominant faces as present on actual cathode surfaces are employed. These are the (110) face of bcc W, the (10$\bar{1}$0) face of hcp Os-W, and the (111) face of fcc Pt-W. Lattice constants of 3.16 Å for W, 2.74 and 4.32 Å for Os, and 3.92 Å for Pt are used.

Ba is considered to be adsorbed on top of O at a hollow site in most cases. Despite the recent verification (Shih et al. 1991) that Ba and O are adsorbed at room temperature at different sites (and not on top) for BaO/W(100) with a Ba-O distance of 3.2 Å, the distance on actual cathode surfaces is so much shorter (2.3-2.6 Å) that on-top adsorption is still the most reasonable assumption. For the Ba-W(Os) distances the values suggested by Tuck and Norman et al. (1986 and 1987) were used. The different clusters and Ba-O geometries that were employed for W, Os, Pt, and alloyed substrates are described in Table II. The clusters are shown in Fig. 2.

TABLE II.

Substrates, crystal faces, clusters, Ba-O orientation, and interatomic distances used for the study of cathode surfaces (1 a_0 = 0.5292 Å).

Substrate	Face	Cluster	Ba-O	R(Ba-O)	R(Ba-surface)
bcc W(-Os)	(110)	$BaO/(W\text{-}Os)_9$	on-top	4.95 a_0	7.39 a_0
hcp Os(-W)	(10$\bar{1}$0)	$BaO/(Os\text{-}W)_9$	on-top	4.90 a_0	6.90 a_0
hcp Os(-W)	(10$\bar{1}$0)	$BaO_2/(Os\text{-}W)_9$	bridge	4.90 a_0	5.20 a_0
fcc Pt(-W)	(111)	$BaO/(Pt\text{-}W)_7$	on-top	5.10 a_0	6.90 a_0

In comparison to the monolayer-film results, the trends obtained for the different substrate crystal structures are completely different. As seen in Table III and shown in Fig. 3, the dipole moment exhibits a minimum and the dipole energy a maximum for the Os hcp substrate. The maximum in the dipole energy is consistent with the observed increase in the Ba binding energy from B- to M-type cathode surfaces, but the variation in the dipole moment is completely opposite to expectation. A large (initial) surface dipole is usually indicative of a lower effective work function. The calculated dipole for Os (hcp), however, is smaller and the dipole for Pt (fcc) is larger than that for W (bcc), while an Os surface is a good emitter and a Pt surface a poor emitter.

FIGURE 2.

Clusters for the study of BaO on W(110), Os(10$\bar{1}$0), and Pt(111).

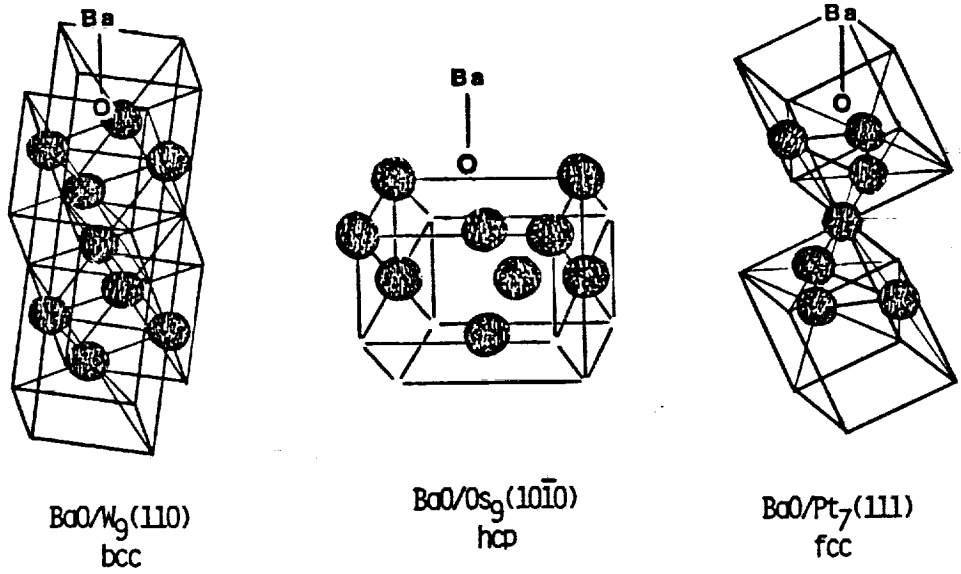

TABLE III.

Dipole properties for BaO/W_9(bcc,110), BaO/Os_9(hcp,10$\bar{1}$0), and BaO/Pt_7(fcc,111) clusters from quasirelativistic Xα calculations. q (in electrons) denotes net atomic charges, μ dipole moment, R_{dip} dipole length, and E_{Ba} dipole energy.

Property	BaO/W_9	BaO/Os_9	BaO/Pt_7
q(Ba)	+1.48	+1.57	+1.48
q(O)	-0.49	-0.42	-0.12
q(Substrate)	-0.99	-1.15	-1.36
$q(M_I)$	+0.00	-0.22	-0.04
$q(M_{II})$	-0.66	+0.17	-0.67
$q(M_{III})$	-0.08	-0.01	-0.23
$q(M_{IV})$	.....	-0.21	.....
μ (Debyes)	39.6	33.3	45.4
R_{dip} (Å)	5.6	4.4	6.4
E_{Ba} (eV)	5.7	8.0	4.9

FIGURE 3.

Surface dipoles and Ba binding energies for BaO on W(bcc,110), Os(hcp,10$\bar{1}$0), and Pt(fcc,111) [full symbols] and their alloys [open symbols].

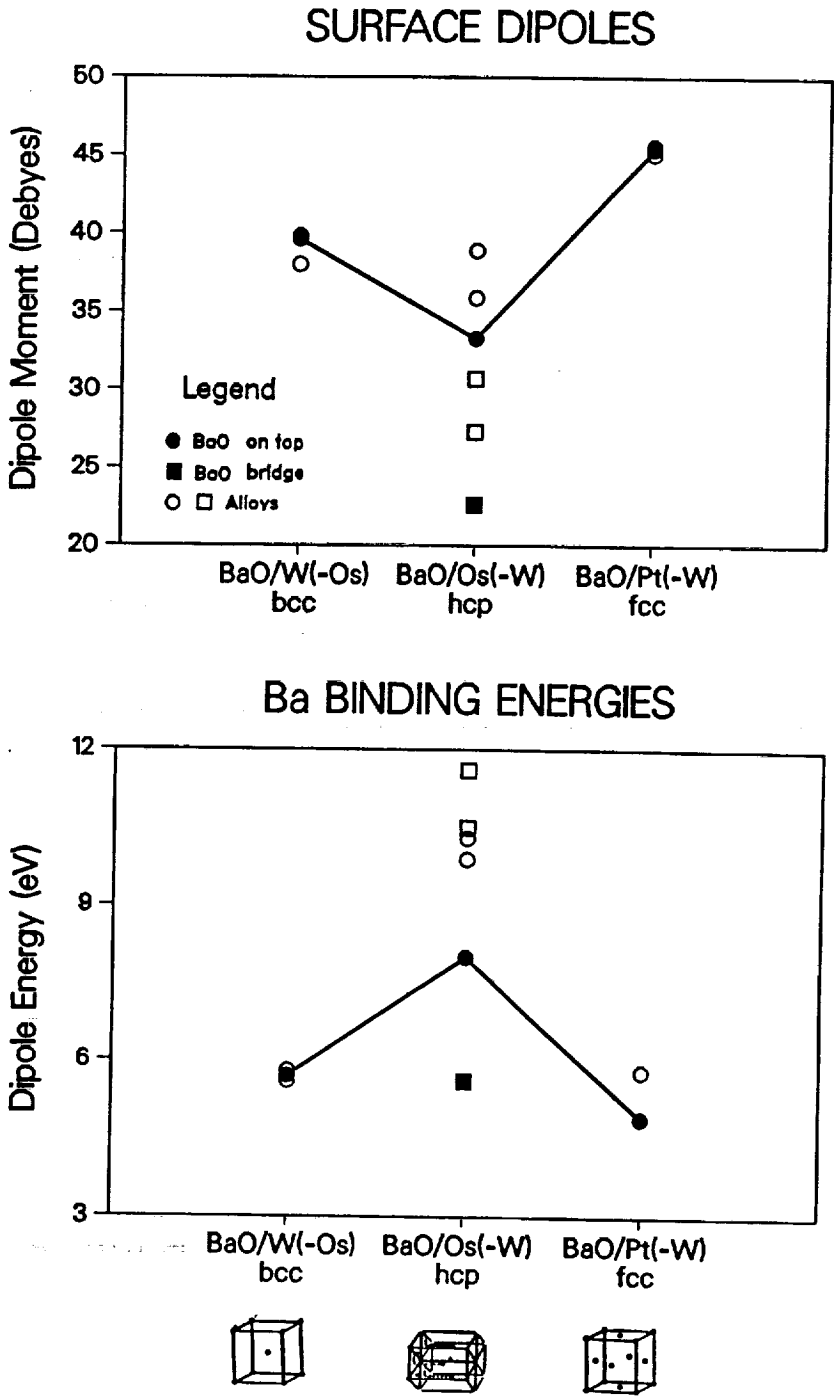

In order to verify these surprising results for more realistic substrates, quasirelativistic Xα calculations have been carried out for randomly alloyed substrate clusters for each crystal structure. Tables IV-VII show that the charge distributions and dipole properties for the alloys with the cubic crystal structure are similar to the results for the pure substrates. The largest effects due to alloying are found for the Os hcp crystal structure, where the net charge on Ba increases by about 0.2 electrons and the net charge on O doubles in most cases. The surface dipole for the Os-W hcp alloy is almost as large as for the W bcc substrate, due to the larger charge transfer but smaller dipole length.

The net charge on Ba and the surface dipole decreases significantly if Ba is bridge-bonded to two O atoms and closer to the surface (cf. Tables V and VII). Alloying again increases the dipole moment and, to a larger extent, the dipole energy. The bridge-bonded results are shown in Fig. 3 by squares.

The effects arising from the different substrate crystal structures of W (bcc), Os (hcp), and Pt (fcc) and their alloys, as compared to the monolayer films, can be explained as follows:

In Table III it is seen that the net charge on Ba runs through a maximum for Os, which is very similar to the monolayer-film results. The dipole moment, however, shows a minimum for the pure Os substrate, while the dipole moment behaved monotonically for the monolayer films. The minimum in the dipole for Os (in spite of the maximum in the charge transfer from Ba) has its origin in the different crystal structures for W, Os, and Pt. For the present faces, the interlayer spacing is smallest for Os and largest for Pt. This obviously has the effect of a better screening of the positive charge outside the surface, with the consequence that the negative charge balancing the positive charge from Ba is located closer to the surface in the case of Os, while more image-like charges are present in the case of W and particularly Pt. An increase in the negative charge on O is also observed for the W and Os substrates relative to the monolayer-film results. The dipole energies behave opposite to the dipole moments as before, and both trends are again governed by the length of the surface dipole, which is affected by the spacing and resultant screening in the substrate layers.

In conclusion, while it is found that the dipole moments and energies vary monotonically for the monolayer-film clusters, the dipole moment exhibits a minimum and the dipole energy a maximum for the hcp crystal structure of the Os substrate, relative to bcc W and fcc Pt. Alloying with W increases both the dipole moment and energy for the hcp substrate.

TABLE IV.

Dipole properties for $BaO/(W\text{-}Os)_9$ (bcc,110) clusters. q (in electrons) denotes net atomic charges, μ dipole moment, R_{dip} dipole length, and E_{Ba} dipole energy.

Property	BaO/W_9	BaO/W_5Os_4	BaO/W_4Os_5
q(Ba)	+1.48	+1.47	+1.48
q(O)	-0.49	-0.47	-0.46
q(Substrate)	-0.99	-1.00	-1.02
$q(W_I,Os_I)$	+0.00	-0.05,-0.04	-0.01,+0.02
$q(W_{II},Os_{II})$	-0.66	-0.54, ----	----,-0.78
$q(W_{III},Os_{III})$	-0.08	+0.20,-0.34	+0.23,-0.36
μ (Debyes)	39.6	38.0	39.8
R_{dip} (Å)	5.6	5.4	5.6
E_{Ba} (eV)	5.7	5.8	5.6

TABLE V.

Dipole properties for $BaO/(Os\text{-}W)_9$ (hcp,$10\bar{1}0$) clusters. q (in electrons) denotes net atomic charges, μ dipole moment, R_{dip} dipole length, and E_{Ba} dipole energy.

Property	BaO/Os_9	BaO/Os_5W_4	BaO/Os_4W_5
q(Ba)	+1.57	+1.77	+1.75
q(O)	-0.42	-0.98	-0.97
q(Substrate)	-1.15	-0.79	-0.78
$q(Os_I,W_I)$	-0.22	-0.19,+0.14	-0.15,+0.18
$q(Os_{II},W_{II})$	+0.17	----,+0.20	-0.19, ----
$q(Os_{III},W_{III})$	-0.01	-0.12,+0.23	-0.22,+0.12
$q(Os_{IV},W_{IV})$	-0.21	-0.49, ----	----,-0.27
μ (Debyes)	33.3	38.9	35.9
R_{dip} (Å)	4.4	4.6	4.3
E_{Ba} (eV)	8.0	9.9	10.3

TABLE VI.

Dipole properties for $BaO/(Pt\text{-}W)_7$ (fcc,111) clusters. q (in electrons) denotes net atomic charges, μ dipole moment, R_{dip} dipole length, and E_{Ba} dipole energy.

Property	BaO/Pt_7	BaO/Pt_4W_3	BaO/Pt_3W_4
q(Ba)	+1.48	+1.56	+1.48
q(O)	-0.12	-0.22	-0.06
q(Substrate)	-1.36	-1.34	-1.42
$q(Pt_I,W_I)$	-0.04	-0.09,+0.09	-0.20,+0.00
$q(Pt_{II},W_{II})$	-0.67	----,-0.76	-0.63, ----
$q(Pt_{III},W_{III})$	-0.23	-0.22,-0.05	-0.43,-0.09
μ (Debyes)	45.4	45.1	45.6
R_{dip} (Å)	6.4	6.0	6.4
E_{Ba} (eV)	4.9	5.8	4.9

TABLE VII.

Dipole properties for bridge-bonded $BaO_2/(Os\text{-}W)_9$ (hcp,$10\bar{1}0$) clusters. q (in electrons) denotes net atomic charges, μ dipole moment, R_{dip} dipole length, and E_{Ba} dipole energy.

Property	BaO_2/Os_9	BaO_2/Os_5W_4	BaO_2/Os_4W_5
q(Ba)	+1.22	+1.66	+1.67
q(O)	-0.41	-0.90	-0.44
q(Substrate)	-0.81	-0.76	-1.23
$q(Os_I,W_I)$	+0.07	+0.11,+0.42	-0.05,+0.31
$q(Os_{II},W_{II})$	-0.11	----,-0.16	-0.61, ----
$q(Os_{III},W_{III})$	-0.08	-0.16,+0.22	-0.26,+0.08
$q(Os_{IV},W_{IV})$	-0.20	-0.41, ----	----,-0.26
μ (Debyes)	22.6	27.3	30.7
R_{dip} (Å)	3.9	3.4	3.8
E_{Ba} (eV)	5.6	11.6	10.5

3.1.3 Dipole Interactions

Two different types of dipole interactions are investigated: (a) adsorbate interactions on a surface and (b) dipole interactions on opposite sites of a symmetrical slab as often used in solid-state calculations.

(a) Adsorbate Interactions

First, a comparison is made for fully relativistic results for vertically and bridge-bonded BaO on W(100) and Os(10$\bar{1}$0) (Müller, IEEE, 1989). Subsequently, the dipole properties are investigated as a function of surface coverage with more extended clusters by using the quasirelativistic Xα scattered-wave approach.

The clusters modeling vertical (BaO/W_9, Ba_2O_2/W_{14}) and bridge-bonded (BaO_2/W_{14} and BaO_2/Os_9) arrangements are shown in Fig. 4. Interatomic distances as proposed by Tuck and Norman et al. (1986 and 1987) are used, i.e., R(Ba-O) = 2.6 Å, R(Ba-W) = 3.9 Å, and R(Ba-Os) = 3.75 Å. For BaO_2/W_{14}, the positions of the oxygen atoms are kept the same as in Ba_2O_2/W_{14} and Ba is moved to the bridge position such that R(Ba-O) = 2.6 Å is maintained.

FIGURE 4.

Cluster models for vertical and bridge-bonded BaO on W and Os.

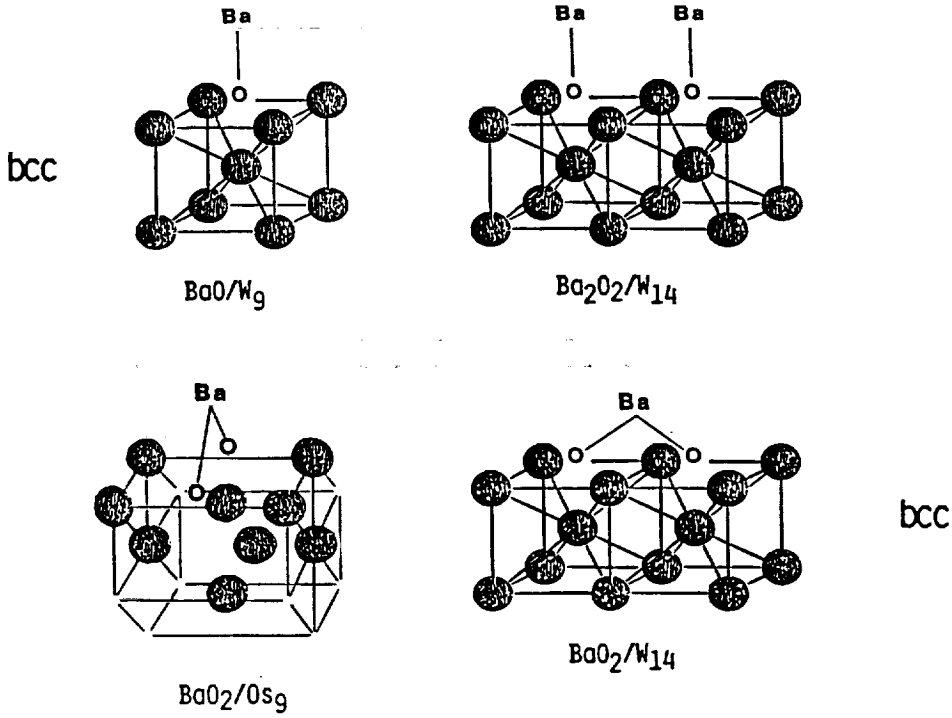

In Table VIII and Fig. 5 net charges, surface dipoles, and Ba binding energies are compared for the different clusters at the fully relativistic level. The interaction of the adsorbate-induced dipoles in Ba_2O_2/W_{14} leads relative to BaO/W_9 to a substantial reduction in the charge transfer, dipole moment, and Ba binding energy per adsorbate. The dipole moment decreases from 37 to 25 Debyes and the binding energy from 6.4 to 5.1 eV. The latter value compares very favorably with the experimental energy of 4.8±0.2 eV for Ba desorption from B-type cathode surfaces (Forman, 1984).

For bridge-bonded barium in BaO_2/W_{14} or BaO_2/Os_9 the dipole moments also decrease strongly, but the Ba binding energies increase relative to BaO/W_9. The Ba overlayer in the bridge-bonded geometry could therefore be more stable and would lead to a minimum in the work function at a higher coverage than for the vertical orientation because of smaller dipole-dipole interactions. The vertical orientation, on the other hand, would lead to an initially steeper slope and possibly lower work function at a smaller coverage. These results are in qualitative agreement with the solid-state calculations of Hemstreet et al. (1989) who find that, for low temperatures, bridge-bonded BaO is more stable while vertically-bonded BaO produces the lower work function. The calculated work functions of 2.7 and 2.6 eV are however significantly higher than observed experimentally.

TABLE VIII.

Ba 6sp and 5d orbital populations p (in electrons), net atomic charges q (in electrons), dipole moments μ, and Ba dipole energies E_{Ba} for BaO/W(Os) clusters from fully relativistic Xα calculations.

Property	BaO/W_9	Ba_2O_2/W_{14}	BaO_2/W_{14}	BaO_2/Os_9
p(Ba,6sp)	0.15	0.16*2	0.13	0.23
p(Ba,5d)	0.34	0.62*2	0.50	0.46
q(Ba)	+1.51	+1.22*2	+1.37	+1.31
q(O)	-0.24	-0.35*2	-0.33*2	-0.36*2
$q(M_I)$	+0.06	+0.01[a]	+0.86[b]	+0.05
$q(M_{II})$	-0.33	-0.89	-0.85	-0.15
$q(M_{III,IV})$	-1.00	-0.86[a]	-0.72[b]	-0.49
μ (Debyes)	37.5	24.6*2	26.7	19.7
E_{Ba} (eV)	6.4	5.1*2	6.7	7.9
Ba Coverage	1/4	1/3	1/6	1/4

[a] W_I:-0.18 center,+0.19 periph., W_{III}:-0.38 center,-0.48 periph.
[b] W_I:-0.08 center,+0.94 periph., W_{III}:-0.32 center,-0.40 periph.

FIGURE 5.

Cluster results for vertical and bridge-bonded BaO on W and Os.

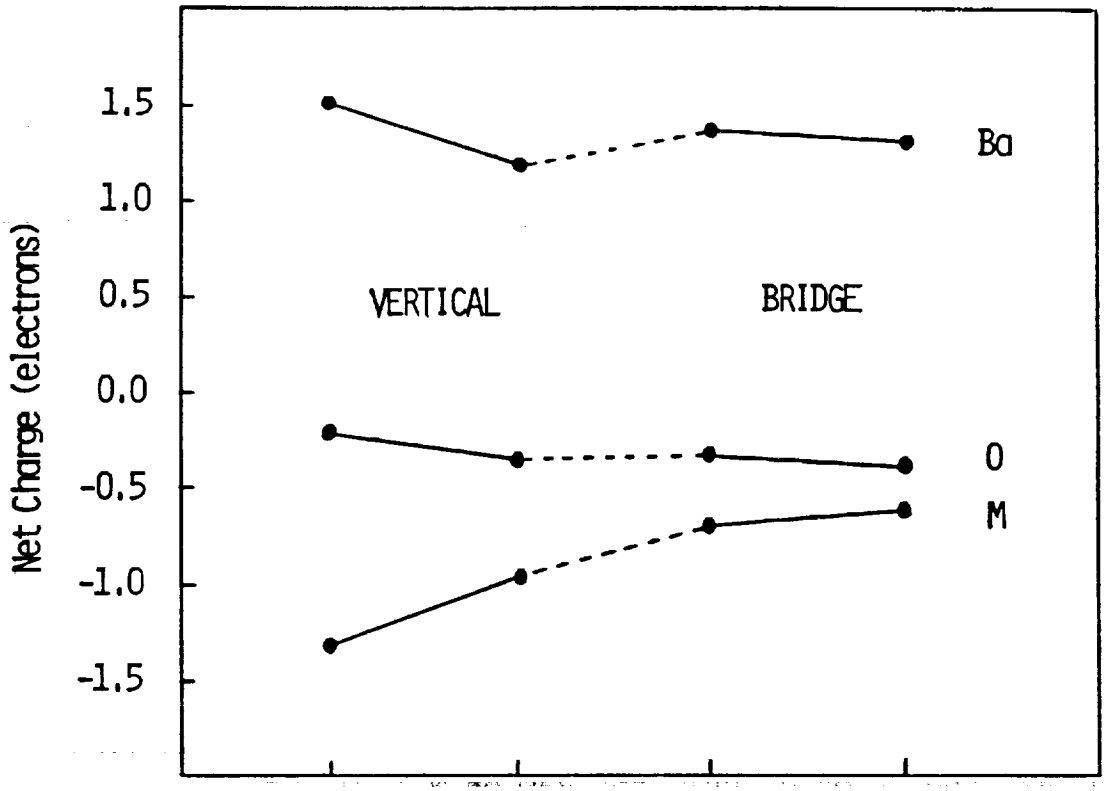

Cluster	Ba O W_9	Ba_2 O_2 W_{14}	Ba O_2 W_{14}	Ba O_2 Os_9
Ba Coverage	1/4	1/3	1/6	1/4
μ(D)	37	25	27	20
E_{Ba} (eV)	6.4	5.1	6.7	7.9

More extensive calculations for the study of adsorbate interactions have been carried out for BaO, Ba, and Cs on W(100), and BaO on other substrates by using the quasirelativistic approach. The surface-dipole results are given in Table IX.

Fig. 6 shows the clusters used for the BaO/W(100) study, which contain 2 or 3 adsorbed BaO molecules and up to 24 W substrate atoms. The formal cluster surface coverages (BaO : W surface) range from 0.20 to 0.38. The calculated dipole moments and dipole energies per adsorbed BaO for BaO/W(100) are plotted in Fig. 7 as a function of formal coverage. At coverages of 0.25 and less, the dipole moment and energy reach a constant value which represents initial adsorption conditions. At higher coverages, repulsive dipole-dipole interactions give rise to a large depolarization. For a formal coverage of 0.38, the calculated dipole energy for BaO/W(100) is close to the experimental value for Ba desorption from B-type cathode surfaces.

Similar calculations have been carried out for Ba and Cs on W(100) with Ba- and Cs-surface distances of 4.5 and 5.2 a_0, respectively, and for BaO on W(110), Os(10$\bar{1}$0), and Pt(111). As for W(100), the larger clusters for the other substrates are obtained by combining two or more single-adsorbate clusters (cf. Figs. 2 & 4). The substrate clusters used for W(110) are W_{30}, W_{23}, and W_{16}; for Os(10$\bar{1}$0): Os_{21} and Os_{15}; and for Pt(111): Pt_{16} and Pt_{12}.

For W(110), the W_9 substrate clusters are combined such that R(Ba-Ba) = 5.98 a_0 for the smallest combined unit, which is the

TABLE IX.

Dipole moments μ (Debyes) as a function of surface coverage for BaO, Ba, and Cs on W(100), and BaO on W(110), Os(10$\bar{1}$0), and Pt(111) from quasirelativistic Xα calculations. q_0 are the net charges on Ba (or Cs) for the clusters with the smallest surface coverage.

System	q_0	Cov = 0.15	0.20	0.25	0.29	0.33	0.38	0.40
BaO/W(100)	1.62	----	30.0	31.2	----	26.4	18.0	----
Ba/W(100)	1.30	----	20.5	21.8	----	15.9	12.8	----
Cs/W(100)	0.92	----	----	18.4	----	19.1	16.0	----
BaO/W(110)	1.60	42.2	43.7	----	33.7	25.7	----	----
BaO/Os(10$\bar{1}$0)	1.71	----	----	40.5	----	32.4	25.7	----
BaO_2/Os(10$\bar{1}$0)	1.26	----	----	16.6	----	17.7	14.1	----
BaO/Pt(111)	1.82	----	----	----	----	51.9	----	34.5

FIGURE 6.

Clusters for the study of adsorbate interactions on W(100).

Formal Coverage (BaO : W)

0.20

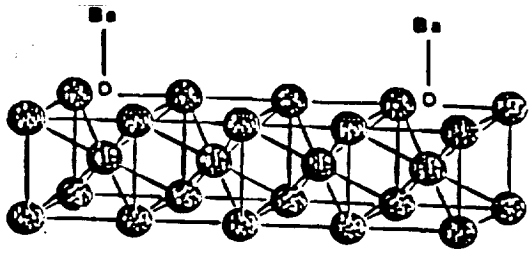

0.25

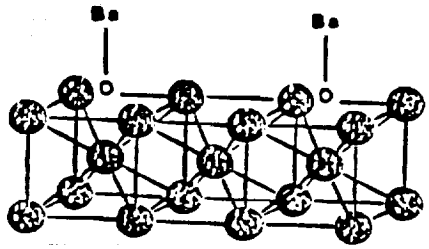

0.33

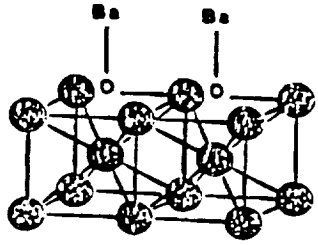

0.38

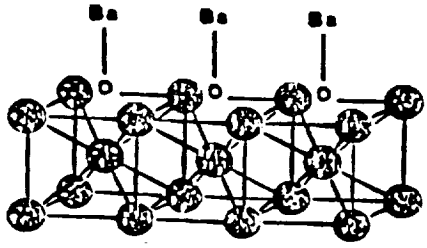

FIGURE 7.

Dipole moments and dipole energies for BaO/W(100) as a function of formal surface coverage.

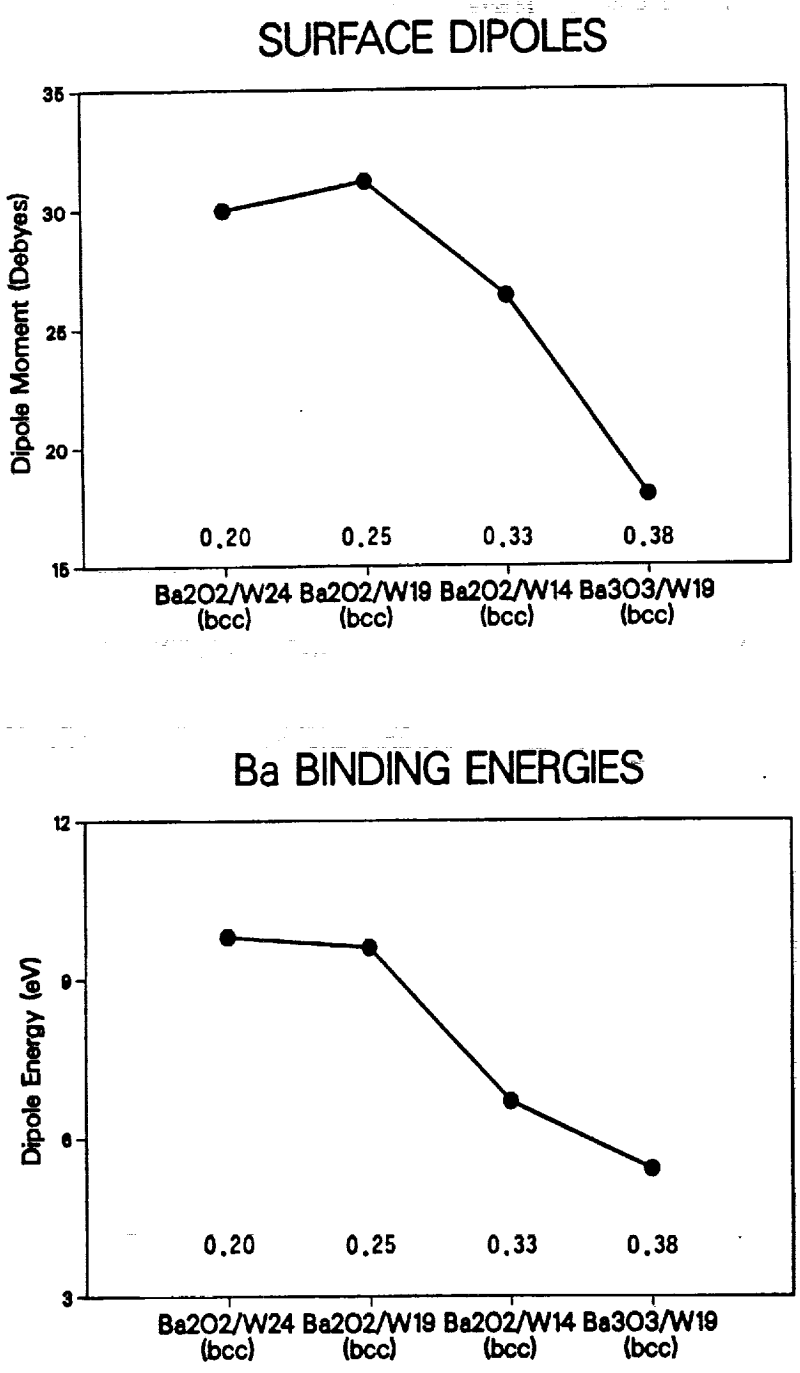

FIGURE 8.

Dipole moments as a function of surface coverage for BaO on W(bcc), Os(hcp), and Pt(fcc).

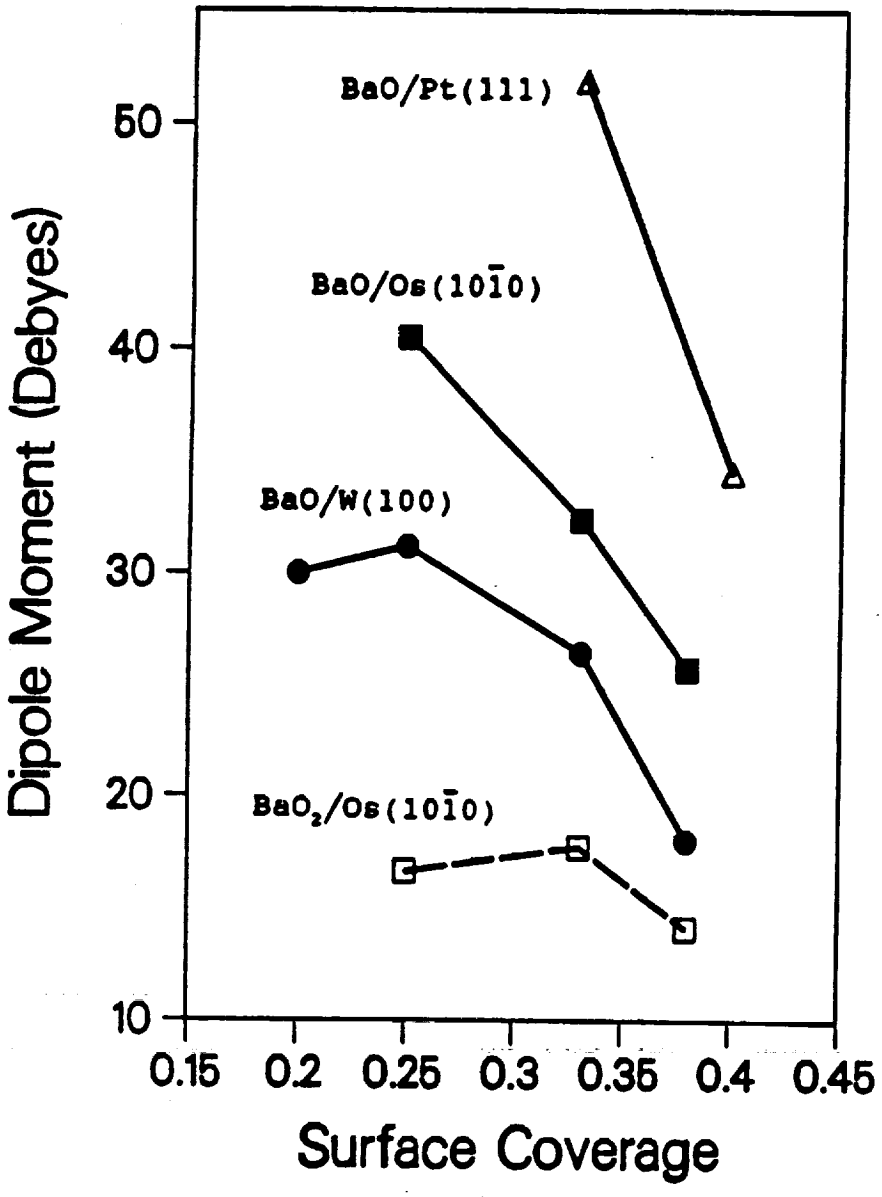

same as for the W(100) systems. For the vertical orientation of BaO on Os, the Os_9 substrate clusters are combined such that R(Ba-Ba) = 5.18 a_0, and for the bridge-bonded orientation such that R(Ba-Ba) = 8.16 a_0. For Pt(111), portions of the Pt_7 cluster are added such that R(Ba-Ba) = 6.04 a_0.

The results for BaO on W(100), Os(10$\bar{1}$0), and Pt(111) are compared in Fig. 8. The surface dipoles on Pt exhibit the largest interaction (or depolarization), as is reflected in the steeper slope of the dipole/coverage curve at higher coverages. The depolarization of vertically-bonded BaO is similar on Os and W, while bridge-bonded BaO_2 on Os shows the smallest depolarization. These data will form the basis for the determination of work-function/coverage curves in Sec. 3.2 below.

(b) Symmetrical Slab

In solid-state band-structure calculations of surface properties, the missing periodicity in the "z" direction perpendicular to the surface is usually enforced by representing the substrate by a slab with a thickness of a few atomic layers, and adsorbates positioned on both sides of the thin substrate film. The electronic structure of the combined overlayer-substrate system is then calculated for a periodical arrangement in which the slab is repeated in the z direction at sufficiently large separations to prevent interactions between neighboring slabs.

The magnitude of the artificial interaction of the surface dipoles on both sides of an individual slab can be evaluated with cluster calculations by comparing the results for, e.g., a BaO/W_9 surface cluster with three substrate layers and the symmetrical Ba_2O_2/W_{14} slab-geometry cluster shown in Fig. 9.

FIGURE 9.

Symmetrical slab-geometry cluster Ba_2O_2/W_{14}.

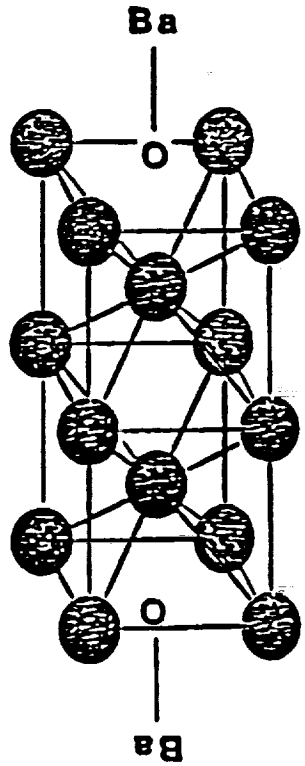

Symmetrical slab-geometry clusters have been investigated for Cs, Ba, and BaO on W using the fully relativistic Xα approach. The data are compared with earlier surface cluster results (Müller, 1988) in Table X. As a general result, it is found that the net charges q on the adsorbate atoms decrease in all cases. The charge on the third, central W layer also decreases significantly, while the charge on the second W layer stays almost constant and the charge on the first W layer increases. The net charge on the adsorbate atoms decreases by about 20% for Cs and 10% for Ba. The extra electrons occupy the 5d states, while the occupation of the 6s and 6p states remains almost the same.

All these charge rearrangements are caused mainly by the interaction of the large surface dipoles on both sides of the symmetrical clusters. The net result is a reduced charge transfer from the metal adsorbate to the substrate, and a larger fraction of this charge is localized near the surface. As a consequence, the surface dipoles are reduced significantly. The calculated surface dipole (in the slab-geometry case defined as $\pm \Sigma_i q_i \cdot |z_i| /2$) is reduced for Cs adsorption from 15 to 11 Debyes, for Ba adsorption from 25 to 20 Debyes, and for BaO adsorption from 38 to 31 Debyes. For comparison, the surface dipole per BaO molecule adsorbed in adjacent sites on a W_{14} surface cluster is reduced from 38 to 25 Debyes. The interaction of the antiparallel surface dipoles in a symmetrical slab with 5 W layers is, therefore, about half as strong as the interaction of parallel surfaces dipoles at high coverage. The screening by the intermediate W layers is not very effective. Solid-state results for Cs or Ba(O) on W with only 5 W layers have therefore to be regarded with some reservations.

TABLE X.

Comparison of fully relativistic slab-geometry and surface-cluster results for Cs, Ba, and BaO on W(100). Given are populations p, net atmic charges q, and dipole moments μ. The adsorbate-surface distances are: R(Cs) = 5.2, R(Ba) = 6.0, and R(O) = 1.1 a_0.

Property	Cs/W_9	Cs_2/W_{14}	Ba/W_9	Ba_2/W_{14}	BaO/W_9	Ba_2O_2/W_{14}
p(Cs/Ba,6sp)	0.15	0.17*2	0.43	0.39*2	0.15	0.15*2
p(Cs/Ba,5d)	0.24	0.33*2	0.53	0.72*2	0.34	0.54*2
q(Cs/Ba)	+0.61	+0.50*2	+1.04	+0.89*2	+1.51	+1.31*2
q(O)	.....	.....	.....	.....	-0.24	-0.21*2
$q(W_I)$	+0.04	-0.06*2	-0.21	-0.34*2	+0.06	-0.18*2
$q(W_{II})$	-0.27	-0.30*2	-0.30	-0.29*2	-0.33	-0.32*2
$q(W_{III})$	-0.38	-0.14*2	-0.53	-0.26*2	-1.00	-0.60*2
μ (Debyes)	15.2	11.0	25.1	19.7	37.5	30.9

3.2 Work-Function/Coverage Curves

The important question now to be addressed is if and how the cluster properties for individual and interacting dipoles can be used to obtain information about higher coverages and possibly minimum work functions for actual cathode surfaces.

3.2.1 Depolarization Model

The decrease in the work function from 4.5-5.5 eV for the bare metal substrates to around 2 eV for the cathode surfaces is caused by the adsorption of Ba and O and the creation of a surface dipole that lowers the electrostatic potential for electron emission. At small coverages, a linear variation of the work function with adsorbate coverage is experimentally observed. At higher coverages, the increasing repulsive interaction between the surface dipoles causes the work-function/coverage curve to deviate from the initially linear behavior, and a minimum is eventually reached. At this point the beneficial effect of an additional dipole is completely canceled by the destructive interaction with all other dipoles.

The work function change, $\Delta\phi = \phi - \phi_0$, is given by the Helmholtz equation,

$$\Delta\phi = - e\mu n(2\epsilon_0)^{-1} , \qquad (4)$$

where μ is the effective surface dipole at coverage n and ϵ_0 is the permittivity of vacuum.

The effective surface dipole can be expressed as

$$\mu = \mu_0 - \alpha f , \qquad (5)$$

where μ_0 is the initial surface dipole at low coverages, α an effective polarizability, and f the electric field resulting from all other dipoles. The electric field f for a simple square network of point-dipoles has been evaluated by Topping (1927) and is given by

$$f = 9\mu n^{3/2}(4\pi\epsilon_0)^{-1} . \qquad (6)$$

Substituting f into Eqn. (5), solving for μ, and then substituting μ into Eqn. (4) yields

$$\Delta\phi = - 1.88\ e\mu_0 n\ /\ (1+c\alpha n^{3/2}) , \qquad (7)$$

with μ_0 in Debyes, α in $Å^3$, and n in 10^{15} atoms/cm^2. The constant c is dependent on the actual overlayer formed and on the validity of the point-dipole approximation.

Eqn. (7) has experimentally been verified for alkali adsorption on single-crystal surfaces of W (Schmidt and Gomer, 1966) and was found to be valid up to the work-function minimum. For larger coverages, the work function is more and more determined by the properties of the adsorbate itself, which are no longer described by the depolarization model. At sufficiently large coverages the work function of the pure adsorbate is eventually reached.

By theoretically determining the initial dipole moments μ_0 and the polarizabilities α, the work-function curves should be fully defined up to and somewhat beyond the minimum. To test the validity of this theory, the two important microscopic properties, μ_0 and α, are calculated with the cluster approach. The constant c is determined by making an empirical adjustment for one reference system.

For the initial surface dipoles μ_0, the calculated dipole moments in Table IX for the clusters with the smallest surface coverage are used. The polarizabilities α are calculated from the induced dipole moments μ_{ind} (relative to μ_o) for the clusters with the highest surface coverage according to

$$\alpha = \mu_{ind} \; / \; \Sigma_i f_i \; , \qquad (8)$$

where $\Sigma_i f_i$ is the electric field produced by the other dipoles in the cluster. The electric field f_i due to a dipole μ_0 at distance R is given by

$$f_i = \mu_0 \; [\; R^2 + (0.5\mu_0/q_0)^2 \;]^{2/3}. \qquad (9)$$

Atomic units are used in evaluating Eqns. (8) and (9), i.e., 1 a.u. (polarizability) = 0.1482 Å^3 and 1 a.u. (dipole moment) = 2.542 Debyes. R is in a_0 and q in electrons.

3.2.2 BaO on Tungsten, Osmium, and Platinum

The depolarization model is first applied to a comparative study of the work-function curves for BaO on W(100), Os(10$\bar{1}$0), and Pt(111). The initial surface dipoles μ_0 and polarizabilities α are calculated as outlined in the previous section. The parameter c in Eqn. (7) has been determined such that the change in the work function for the model B-type BaO/W(100) surface equals 2.65 eV, with ϕ_{min} = 2.0 eV, which yields c = 2.7. This value is treated as a universal constant for simple square networks of dipoles and is used for all other systems with cubic crystal structures. For BaO on the hcp crystal structure of Os, an equitriangular network is assumed. (The assumption of a square network is not reasonable and would have led to an unrealistically low work function of 1.3 eV.) The parameter for the equitriangular network is geometrically related to that for the square network by c_{hex} = 11/9 c = 3.3, so that no new adjustment is needed.

The calculated dipole data and derived work-function changes $\Delta\phi$, minimum work functions ϕ_{min}, and optimum coverages n_{min} are presented in Table XI. This table shows that the initial surface dipoles μ_o increase in the series BaO on W(100), Os(10$\bar{1}$0), and Pt(111), while α shows a minimum for Os(10$\bar{1}$0). For BaO_2/Os(10$\bar{1}$0), with Ba bridge-bonded and an excess of oxygen present in the cluster, both μ_o and α are smaller than for BaO/W(100).

TABLE XI.

Calculated initial surface dipoles μ_o (Debyes), polarizabilities α ($\AA^3$), initial, changes Δ, and minimum work functions ϕ (eV), and optimum coverages n_{min} (in 10^{15} atoms/cm^2) for BaO on W(100), Os(10$\bar{1}$0), and Pt(111). $\Delta\phi$ for BaO/W(100) has been adjusted.

System	μ_o	α	ϕ_o	$\Delta\phi$	ϕ_{min}	n_{min}
BaO/W(100)	30.0	14.0	4.65	2.65	2.00	0.14
BaO/Os(10$\bar{1}$0)	40.5	12.3	5.2	3.4	1.8	0.13
BaO_2/Os(10$\bar{1}$0)	16.6	9.8	5.2	1.6	3.6	0.16
BaO/Pt(111)	51.9	27.8	5.3	2.9	2.4	0.09

For the minimum work functions it is found that BaO/Os(10$\bar{1}$0) has a lower and BaO/Pt(111) a higher work function than the model BaO/W(100) surface. The calculated decrease in the effective work function for Os (0.2 eV) and the increase for Pt (0.4 eV) relative to W are in excellent agreement with the observed emission properties of Os(-W) and Pt(-W) dispenser cathodes. The work function for the Ba-bridge-bonded, excess-oxygen BaO_2/Os system is found to be significantly higher than for all other systems, which is consistent with the observed poisoning caused by excess oxygen. The calculated work-function curves are shown in Fig. 10. It should be noted that the work-function curves for coverages larger than n_{min} are spurious, because the actual work functions at higher coverages are known to be similar to those at the minimum or may even drift lower. These effects, which are due to the formation of multiple overlayers, are not included in the theoretical model.

In conclusion, while the initial slope of the work-function curves is determined by μ_o, the minimum work function and optimum coverage are dependent on the interplay between the initial dipole and the depolarization, and also the substrate work function ϕ_0. In spite of the fact that μ_o exhibits a linear behavior in the series BaO on W, Os, and Pt, the lowest work function and the largest change, $\Delta\phi$, are found for BaO/Os.

FIGURE 10.

Calculated work-function curves for BaO on W, Os, and Pt.

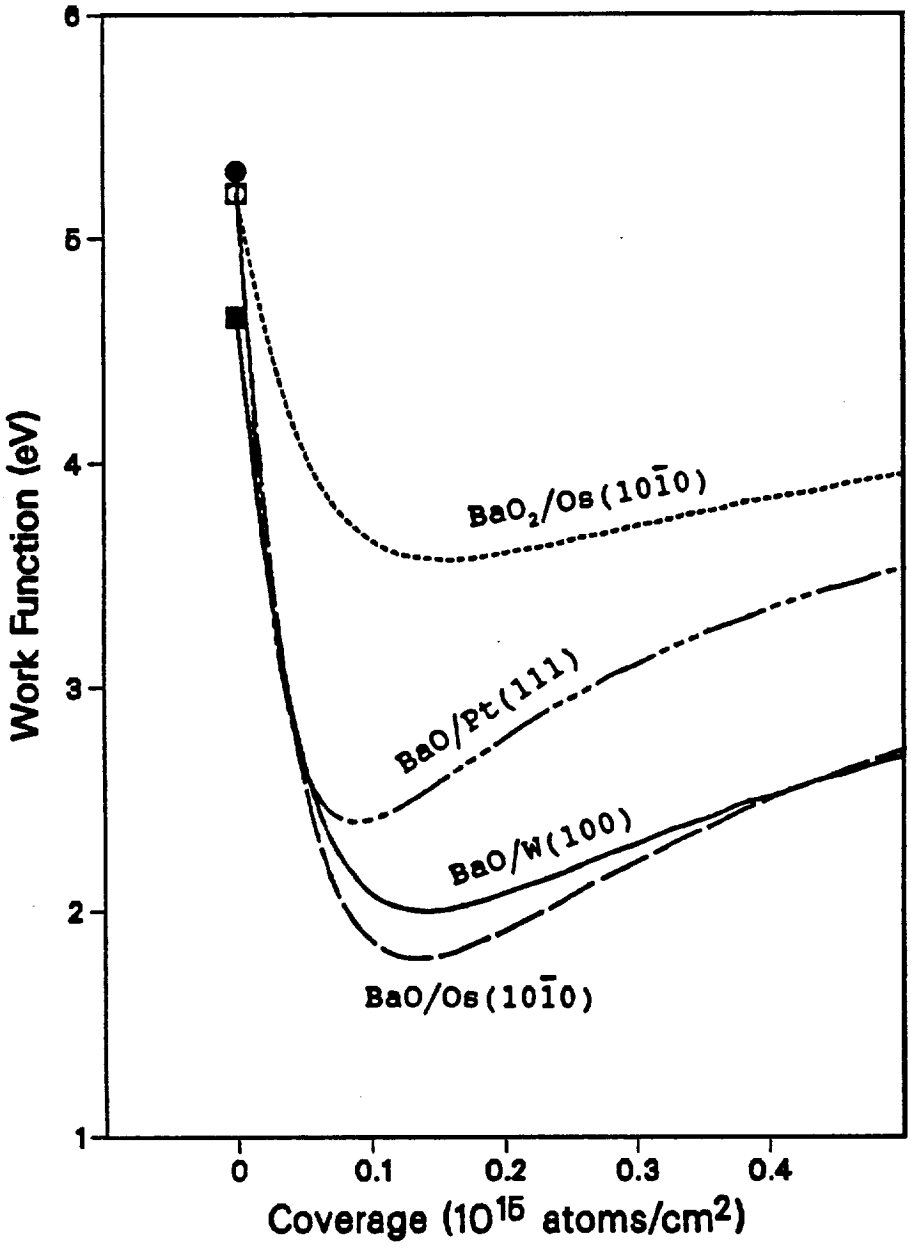

3.2.3 Other Low-Work-Function Surfaces

As a critical test for the validity of the theoretical approach for the determination of work-function/coverage curves for low-work-function surfaces, results are now discussed for Ba and Cs on W(100), and BaO on W(110). The calculated dipole and work-function data are given in Table XII and the work-function curves are shown in Fig. 11. The results for BaO/W(poly) are based on the assumption that μ_o and α for the polycrystalline surface are similar to W(100), which appears to be justified by the fact that a reasonable value for the minimum work function (1.89 eV) is obtained.

For Ba/W(100), the calculated minimum work function is 2.62 eV, which is in excellent agreement with the experimental value of 2.63 eV (Lamouri and Krainsky, 1992). This result confirms the validity of the empirical adjustment for the work-function change of BaO/W(100) through the choice of the parameter c in Eqn. (7). The adjustment could just as well be said as having been made for Ba/W(100) [or BaO/W(110), see below]. The calculated Ba binding energy for Ba/W(100) of 3.6 eV for the highest formal coverage investigated compares well the experimental value of 3.8 eV for Ba desorption from polycrystalline W (Forman, 1984). The calculated optimum coverage of 0.16 monolayers (1 monolayer = 10^{15} atoms/cm^2), however, is significantly smaller than the expected half (0.5) monolayer. The small coverages appear to be a problem with the Ba-related systems, but the work-function values do not seem to be affected.

For Cs/W(100), the minimum work function is calculated at about 1.4 eV, or 0.2 eV below the experimental value of Swanson and

TABLE XII.

Calculated initial surface dipoles μ_o (Debyes), polarizabilities α (Å^3), initial, changes Δ, and minimum work functions ϕ (eV), and optimum coverages n_{min} (in 10^{15} atoms/cm^2) for BaO, Ba, and Cs on W(100), and BaO on W(110).

System	μ_o	α	ϕ_o	$\Delta\phi$	ϕ_{min}	n_{min}
BaO/W(100)	30.0	14.0	4.65	2.65	2.00	0.14
BaO/W(poly)	(30.0)	(14.0)	4.54	2.65	1.89	0.14
Ba/W(100)	20.5	11.8	4.65	2.03	2.62	0.16
Cs/W(100)	18.4	4.9	4.65	3.27	1.38	0.28
BaO/W(110)	42.2	19.4	5.33	3.00	2.33	0.11

FIGURE 11.

Calculated work-function curves for Ba, BaO, and Cs on W.

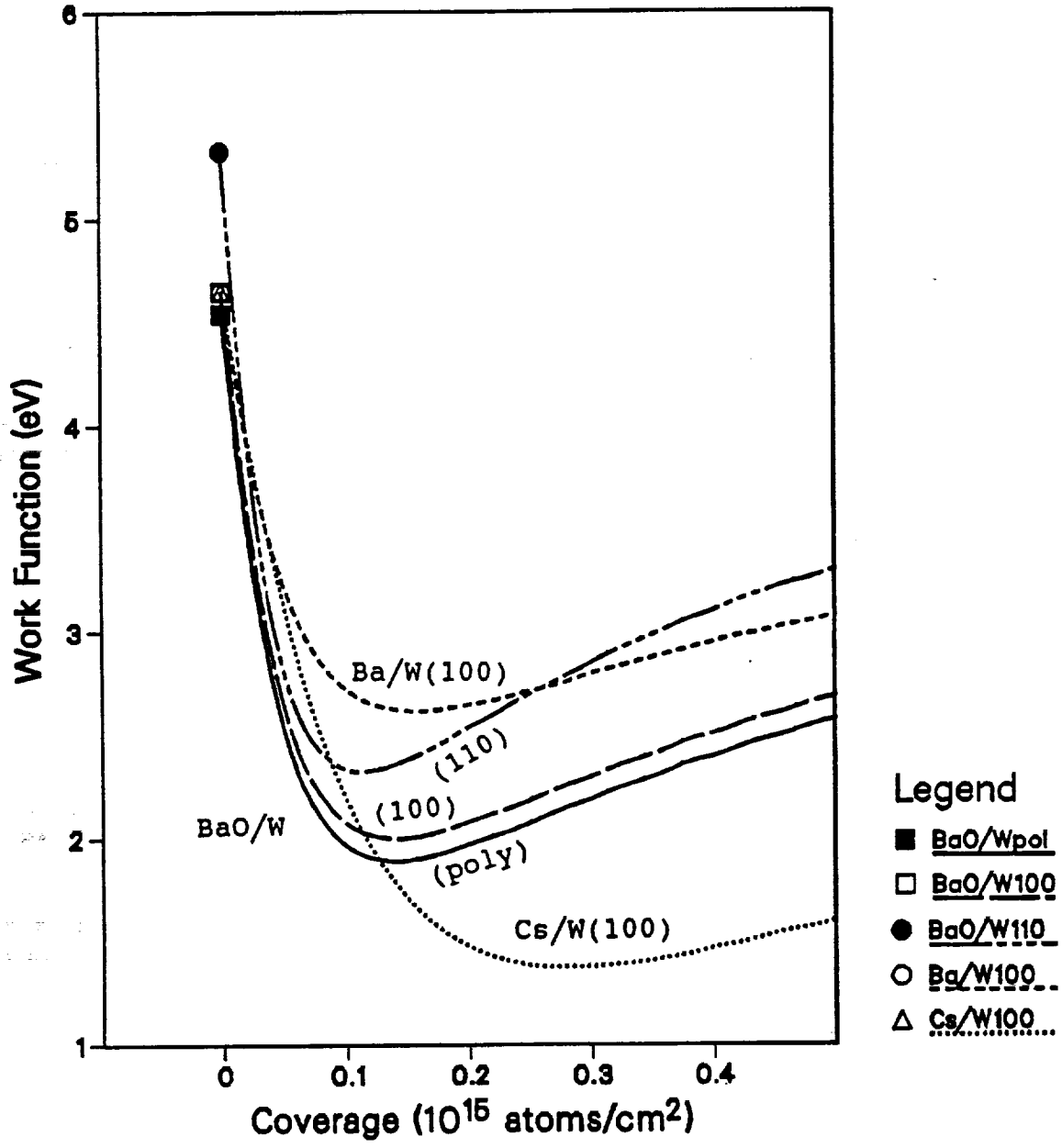

Strayer (1968). In relation to the full work-function change of over 3 eV, this result is quite respectable in that the theory overshoots the total effect by only 7 percent. The minimum in the work function is obtained for a Cs coverage of 0.28 monolayers, which is in excellent agreement with the experimental value of 0.25 monolayers. The calculated Cs binding energy is fairly stable for the different clusters considered, 2.9-3.2 eV, and in very good agreement with the experimental value of 2.8 eV.

For the BaO/W system, additional calculations have been carried out for different geometries of BaO on W(100). When the height of Ba above the O/W(100) surface is decreased or increased by 10%, the surface-dipole properties change significantly and work functions of 1.8 and 1.4 eV are obtained, respectively. While these values are not completely out of range, they show that the actual geometries are critical for an accurate determination of the work functions.

BaO/W(110) has also been investigated. This surface is of particular importance because it makes up about 50% of the surface area of typical B-type cathodes. It is not well known, however, to what extent this surface (or other surfaces) contributes to the emission. The initial bare work function for W(110) of 5.33 eV is significantly higher than that for (100) or polycrystalline W of 4.5-4.6 eV. For a vertical arrangement of BaO on W(110), the calculated change in the work function of 3.0 eV at a coverage of 0.1 monolayer is in excellent agreement with experiment (D. Mueller et al., 1990). The resulting work function of 2.3 eV is, however, too high to be relevant for cathode operation.

The calculated Ba binding energies for the standard geometries of BaO/W(100) and BaO/W(110) are 5.4 and 4.6 eV, respectively, and compare well with the experimental value of 4.8±0.2 eV for BaO on polycrystalline W.

The important issue of the contributions from different crystal faces to the emission of B-type cathode surfaces clearly requires much more work. The knowledge of accurate geometries is crucial, but reliable experimental information is unfortunately not available. Efforts are therefore planned to determine the relevant geometries from either a comparison of theoretical and experimental results or directly from first-principles calculations. With the good quality and consistency of the results obtained so far, the theoretical approach shows promise that the work functions for different crystal faces and alloy substrates can then be determined with high accuracy.

3.3 BaO/W Electronic Structure

3.3.1 Densities of States

Adsorbate interactions have been shown in the previous section to play an important role in determining the minimum work functions and optimum coverages on cathode surfaces. In order to better visualize and compare the results for clusters with isolated and interacting dipoles, total, atom-, and l-projected densities of states (DOS) have been generated for BaO/W(100) from fully relativistic calculations.

In Fig. 12, the densities of states (DOS) are compared for BaO/W_9 and Ba_2O_2/W_{14}. The major differences are the splitting of the Ba 5p levels due to the Ba-Ba interaction and an increase in the DOS just below the cluster Fermi level for Ba_2O_2/W_{14}. The peak positions of the major features are virtually unchanged. The DOS distributions have been generated by broadening the discrete energy levels of the clusters with Gaussian functions. Half-widths of 0.30 and 0.15 eV were used for BaO/W_9 and Ba_2O_2/W_{14}, respectively. The regime of tungsten-derived DOS between -5 and +5 eV is very well covered in both clusters, as indicated with the vertical lines on the horizontal axis which represent the discrete energy levels.

In Figs. 13 and 14, atom-projected DOS are shown for one Ba, O, W_I, W_{II}, and W_{III} atom each in BaO/W_9 and Ba_2O_2/W_{14}, respectively. In Ba_2O_2/W_{14}, the W atoms in the center of the cluster are used. The comparison demonstrates that the peak positions and overall structure are virtually unchanged for the oxygen- and tungsten-related densities of states. The largest difference is observed for the barium-related DOS which is significantly broadened in Ba_2O_2/W_{14} relative to BaO/W_9, due to the strong Ba-Ba interaction.

In Fig. 15, the Ba portion of the DOS and the projections on azimuthal quantum numbers l=0,1,2 are shown for both clusters on identical scales. The 6s and 6p (l=0 and 1) states of Ba are largely unoccupied, while the 5p (l=1) semi-core states are fully occupied. The Ba 6p states, which are somewhat higher in energy than the 6s states, are mixed with W states and are therefore not clearly seen. The 5d (l=2) states are largely unoccupied, but somewhat more occupied in Ba_2O_2/W_{14} than in BaO/W_9. The population analyses give Ba 5d occupations of 0.62 and 0.34 electrons per Ba atom in Ba_2O_2/W_{14} and BaO/W_9, respectively. For higher coverages the Ba 5d states will become more and more occupied and reduce the Ba oxidation level.

FIGURE 12. Densities of states for BaO/W_9 and Ba_2O_2/W_{14}.

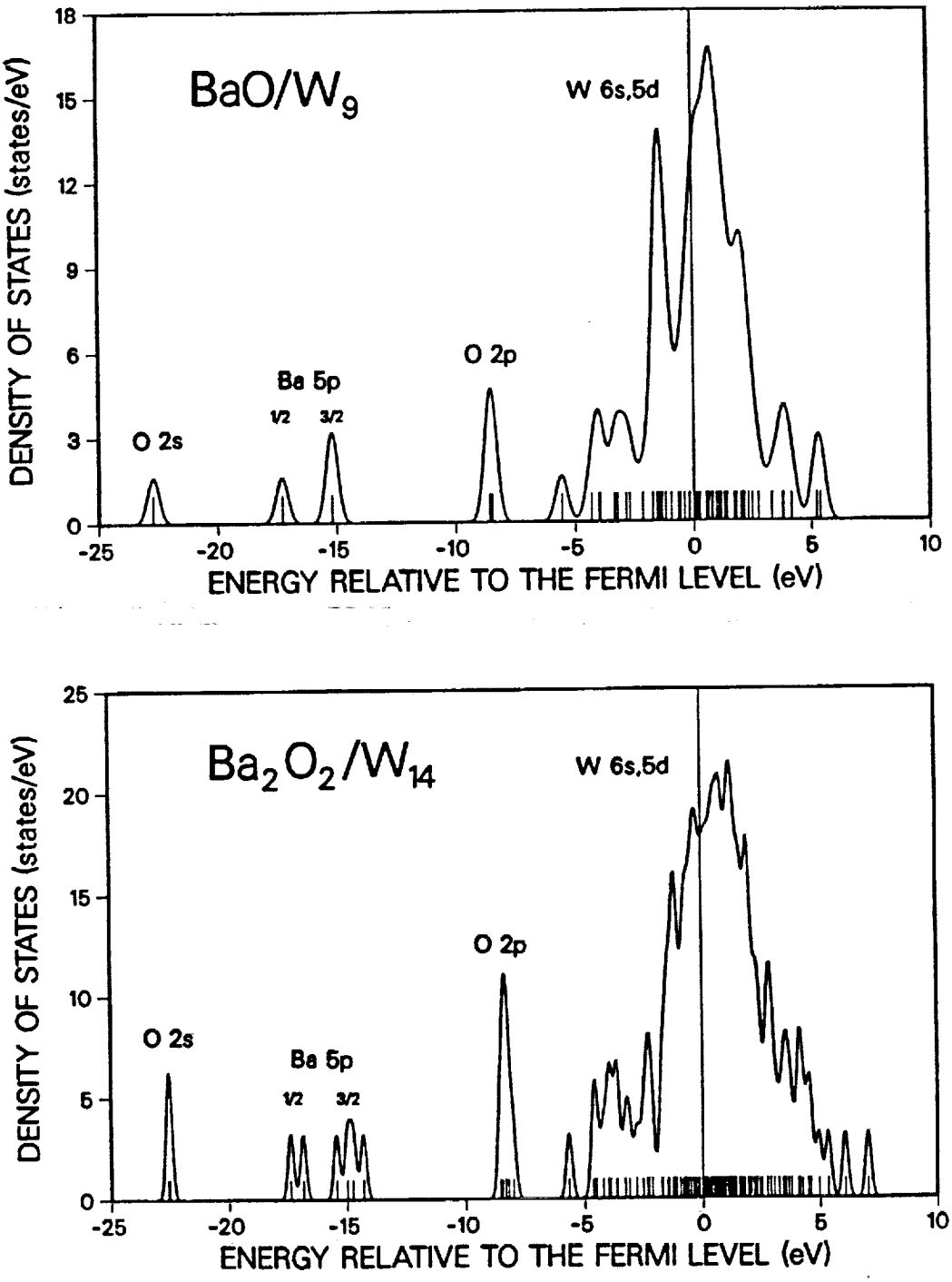

FIGURE 13. Projected densities of states for BaO/W_9.

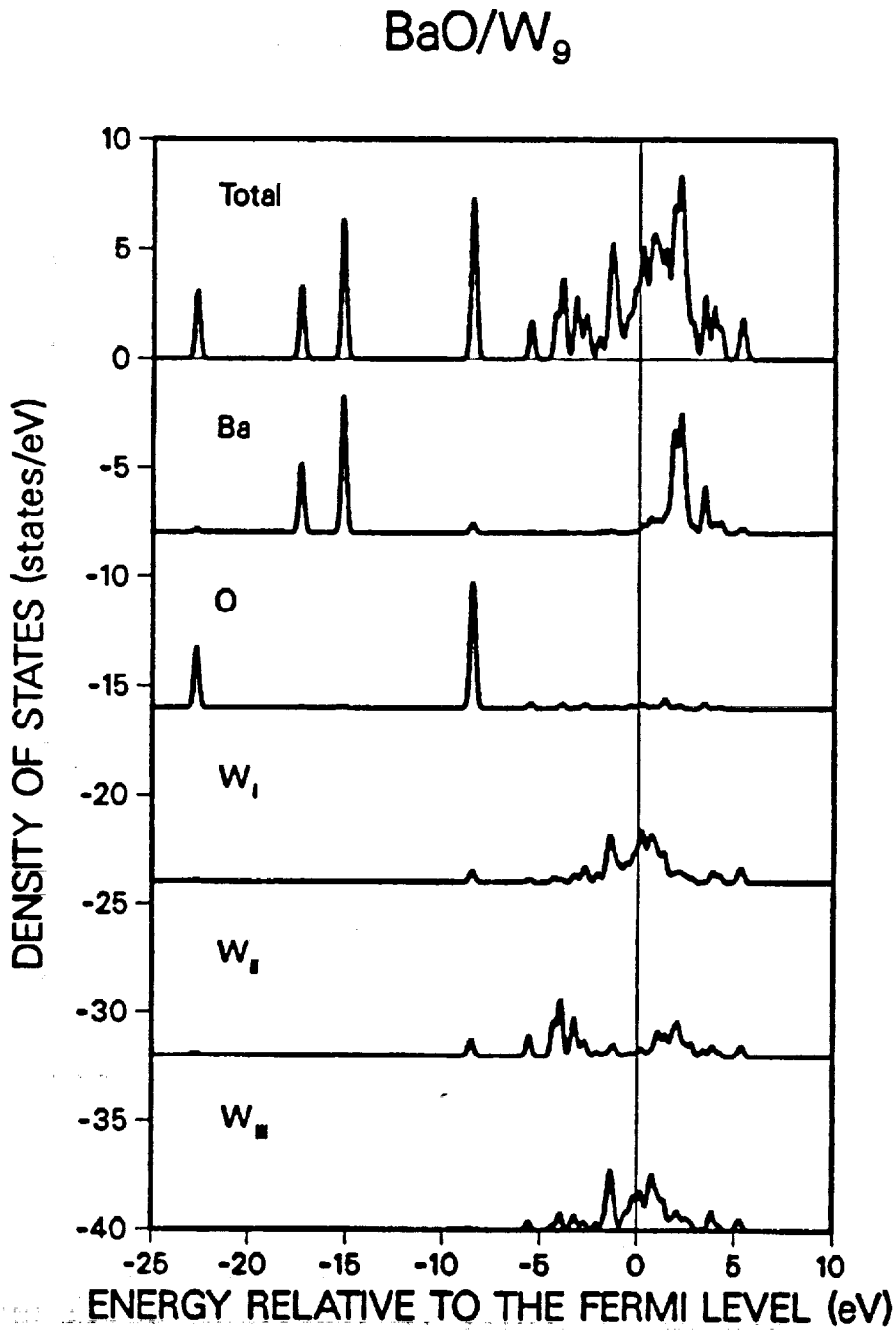

FIGURE 14. Projected densities of states for Ba_2O_2/W_{14}.

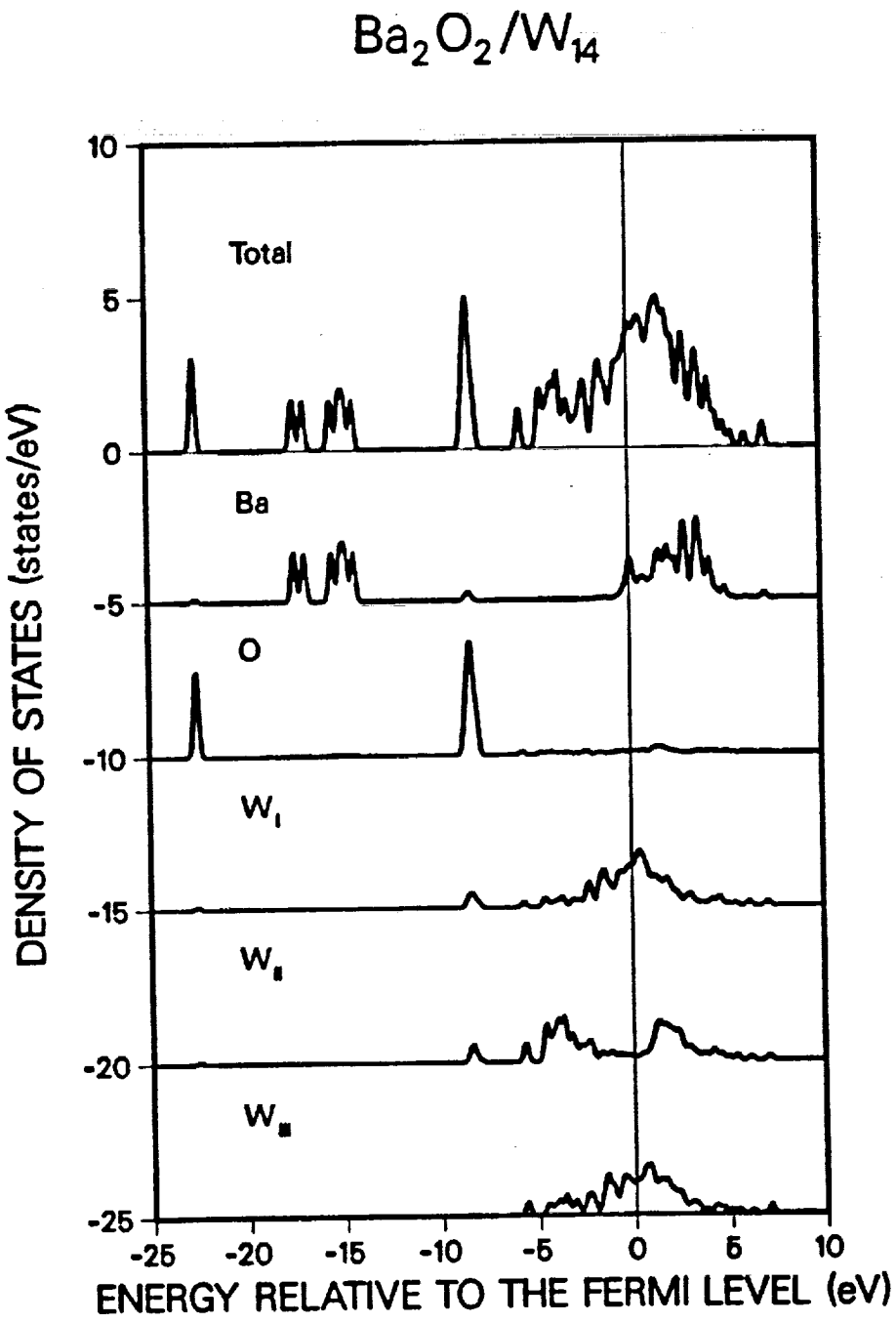

FIGURE 15. Projected DOS for barium in BaO/W_9 and Ba_2O_2/W_{14}.

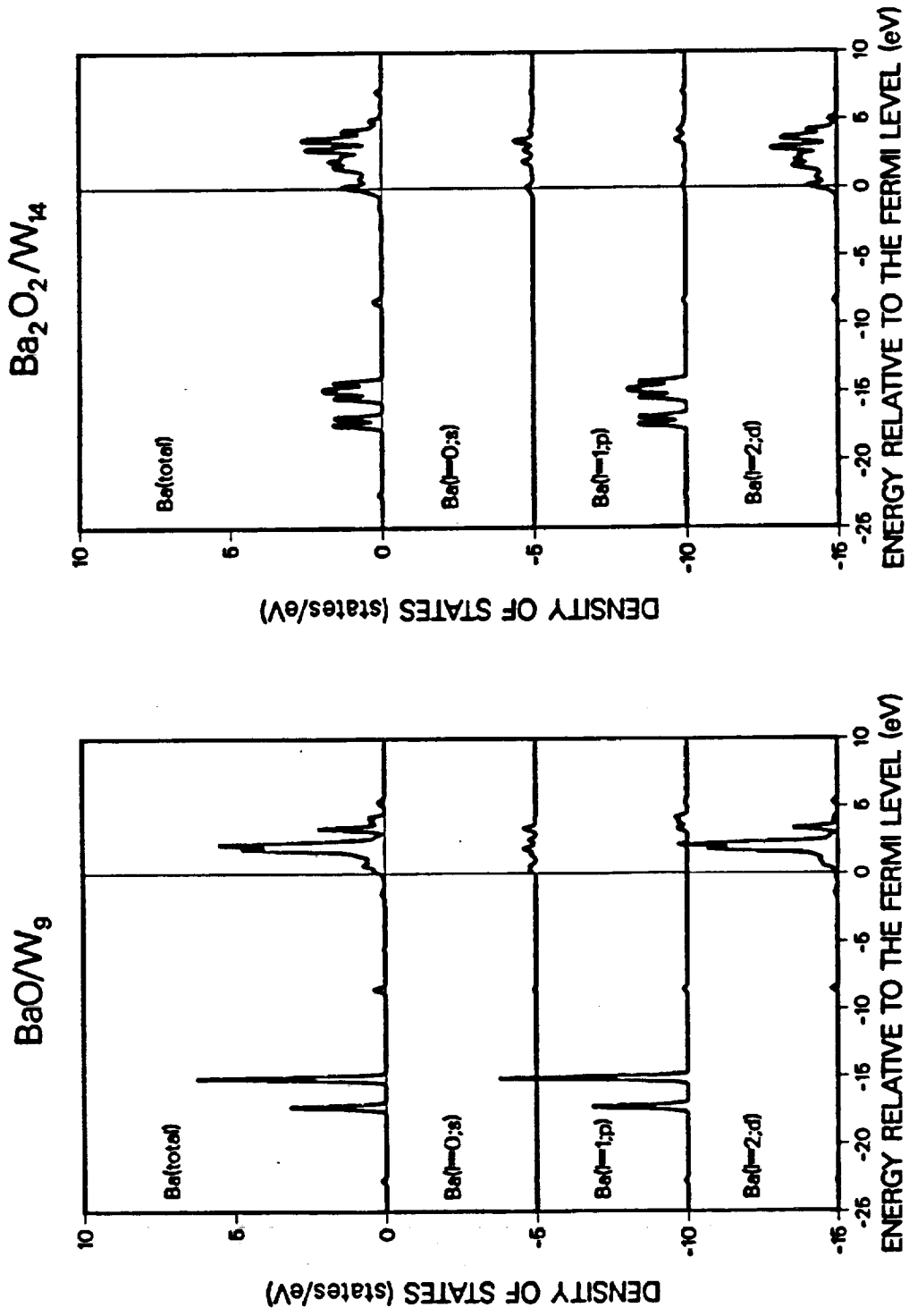

FIGURE 16. Electron densities for BaO/W_9 and Ba_2O_2/W_{14}.

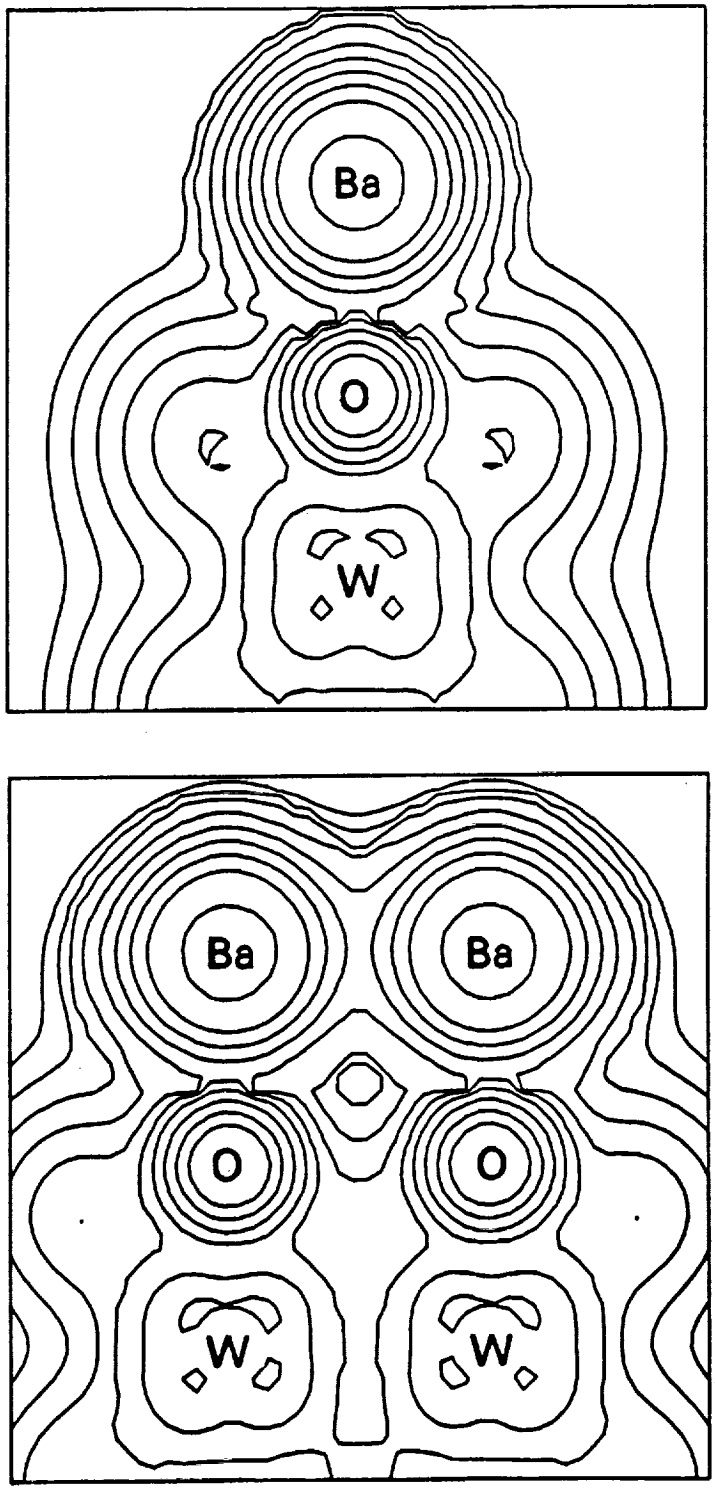

Contour plots are shown in Fig. 16 for the electron densities of BaO/W_9 and Ba_2O_2/W_{14} in a plane perpendicular to the surface. A strong interaction is seen for the Ba, O, and second-layer W atoms in the vertical orientation. In Ba_2O_2/W_{14}, the barium atoms exhibit a large lateral interaction, while the electron density in the $O\text{-}W_{II}$ area is not affected. This observation correlates very well with the results for the respective densities of states in Figs. 13 and 14, which show virtually no changes for the O and W states but a significant broadening of the Ba states.

3.3.2 BaO Geometry Variation

All previous calculations for BaO/W(100) with Ba on top of O were based on the geometry determined by Tuck and Norman et al. (1986 and 1987) from a fit of surface models to experimental SEXAFS data. Their analysis led to R(Ba-surface) = 6.0 a_0 and R(Ba-O) = 4.9 a_0 (or 3.2 and 2.6 Å, respectively). The subsequent measurements of Shih et al. (1988), however, gave 2.3 Å for the Ba-O distance in B-type cathode surfaces. A comparison of the calculated binding energy for the O 2p level of 8.5 eV with the measured value from D. Mueller et al. (1988) for BaO/W(100) of 5.9 eV also hinted at a possibly smaller Ba-O distance than as reported by Tuck and Norman et al.

It is therefore of particular importance to investigate the effects of different geometries on the charge transfer, the dipole moment, and the O 2p binding energy in the BaO/W surface complex. Calculations have been carried out for BaO/W_9 assuming the vertical adsorbate orientation, with Ba-surface distances of 6.0, 6.3, and 6.6 a_0 and the two proposed Ba-O distances of 4.9 and 4.3 a_0 (2.6 and 2.3 Å).

TABLE XIII.

Calculated net atomic charges q (electrons), dipole moments μ (Debyes), and Ba dipole energies E_{Ba} (eV) for different geometries of BaO/W_9 at the fully relativistic level. R(Ba) = R(Ba-surface) and R(Ba-O) are given in Bohrs (1 a_0 = 0.5292 Å).

R(Ba,Ba-O)	q_{Ba}	q_O	μ	E_{Ba}
6.0, 4.9	1.51	-0.24	37.5	6.4
6.3, 4.9	1.51	-0.32	38.0	6.3
6.6, 4.9	1.49	-0.39	38.2	6.0
6.0, 4.3	1.36	-0.36	33.4	5.2
6.3, 4.3	1.33	-0.43	32.6	5.0
6.6, 4.3	1.29	-0.48	31.9	4.7

The results for the surface-dipole properties and the electronic binding energies are presented in Tables XIII and XIV, respectively.

The following effects are observed: When R(Ba) = R(Ba-surface) is increased or R(Ba-O) is decreased, the net charge on O increases which leads to smaller O 2p binding energies. When R(Ba-O) is changed from 4.9 to 4.3 a_0, the net charge on Ba, the cluster dipole moment, and the Ba desorption energy all decrease. The decrease in the net positive charge on Ba leads to slightly smaller electronic Ba binding energies, while the W electronic levels are not affected. The increase in the negative charge on O for larger Ba-surface distances gives rise to increases in the negative O-W contributions to the dipole moment, which offset the increases due to the larger Ba-surface distances and leave the total dipole moments within R(Ba-O) = 4.9 and 4.3 a_0 virtually unchanged.

A comparison of the results for the original geometry with R(Ba,Ba-O) = 6.0, 4.9 a_0 to those based on 6.6, 4.3 a_0 shows significant improvements with respect to the experimental data.

TABLE XIV.

Fully relativistically calculated electronic binding energies (in eV) relative to the highest occupied cluster level for different geometries of BaO/W_9. The final results for R(Ba,Ba-O) = 6.6, 4.3 a_0 include the final-state contributions (ΔFS). R(Ba) = R(Ba-surface) and R(Ba-O) are given in Bohrs (1 a_0 = 0.5292 Å).

	W_I				Ba			O			W_{II}
R(Ba,Ba-O)	$5p_{1/2}$	$5p_{3/2}$	$4f_{5/2}$	$4f_{7/2}$	5s	$5p_{1/2}$	$5p_{3/2}$	2s	2pσ	2pπ	6s
6.0, 4.9	45.8	36.0	30.0	27.7	30.9	17.3	15.2	22.7	8.6	8.5	5.6
6.3, 4.9	45.8	36.0	30.0	27.8	30.8	17.2	15.1	21.8	7.8	7.7	5.6
6.6, 4.9	45.8	36.0	30.1	27.8	30.6	17.0	14.9	21.0	7.3	6.9	5.6
6.0, 4.3	45.8	36.0	30.0	27.8	29.2	15.6	13.6	21.6	7.3	7.0	5.6
6.3, 4.3	45.8	36.0	30.1	27.8	28.9	15.3	13.2	20.8	6.9	6.2	5.5
6.6, 4.3	45.8	36.0	30.1	27.8	28.6	15.0	12.9	20.1	6.6	5.5	5.3
ΔFS	0.9	0.7	4.1	4.0	3.1	2.3	2.5	1.4	0.1	0.7	0.2
Final	46.7	36.7	34.2	31.8	31.7	17.3	15.4	21.5	6.7	6.2	5.5
Expt.[a]	....	36.8	33.5	31.3	....	16.6	14.6	21.9	--	5.9	--
ΔExpt.	....	-0.1	+0.7	+0.5	....	+0.7	+0.8	-0.4	+0.8/-0.4		

[a] D. Mueller et al. (1988)

The calculated Ba dipole (desorption) energy decreases from 6.4 to 4.7 eV (expt. 4.8 eV) and the O 2p binding energy decreases from ~8.5 to around 6 eV (expt. 5.9 eV). Because the W_{II} 6s state has a similar binding energy, a substantial mixing of the W_{II} 6s and O 2pσ orbitals occurs, which increases with decreasing energy separation between these two orbitals. For R(Ba,Ba-O) = 6.6, 4.3 a_0, the state at 6.6 eV actually contains a larger contribution from W_{II} 6s (25%) than from O 2pσ (15%), and the O 2pσ character is found mainly in the state at 5.3 eV.

For the final geometry, R(Ba,Ba-O) = 6.6, 4.3 a_0, additional calculations have been carried out in order to investigate corrections to the orbital energies of the N-electron system due to the reorganization of the charge distribution upon ionization. This is done by performing so-called transition-state calculations in which 1/2 electron is removed from the state under consideration. The (N-1/2)-electron system is the "transition state" between the N- and (N-1)-electron systems. This procedure is known to provide good estimates for the differential reorganization, or final-state, effects (ΔFS). A separate calculation is required for each state, and the electron binding energies are now measured relative to the transition-state energy of the highest occupied orbital.

In comparison with photoemission spectra, only the differences in the calculated energy shifts are relevant in cluster calculations. The differential effect for the electronic state at the cluster Fermi level is zero, by definition, since it is used as the reference. The results in Table XIV show that the final-state contributions (ΔFS) increase with increasing binding energy and localization. For the W_{II} 6s and O 2pσ states, which are significantly mixed, the correction is only 0.1 to 0.2 eV. ΔFS is of the order of 1 eV for the more localized O 2pπ, O 2s, and W 5p electronic states, 2-3 eV for Ba 5p and 5s, and 4 eV for W 4f.

After inclusion of these final-state corrections, all electronic binding energies below 50 eV for BaO/W_9 with R(Ba,Ba-O) = 6.6, 4.3 a_0 are within 1 eV of the photoemission energies from D. Mueller et al. (1988), while the results for the Ba- and O-related energies with R(Ba,Ba-O) = 6.0, 4.9 a_0 would have been too high by 2 eV or more. Fig. 17 shows the densities of states for these two geometries and the final results for R(Ba,Ba-O) = 6.6, 4.3 a_0. The corresponding experimental peak positions are indicated by arrows. Interestingly, the Ba binding energy for the BaO/W_9 cluster with the modified geometry, 4.7 eV, is within the margin of experimental uncertainty (4.8±0.2 eV).

The good agreement between theory and experiment for the modified geometry is strong evidence that the distances proposed by Tuck and Norman et al. for BaO/W(100) are most likely not correct. The present calculations clearly favor the smaller Ba-O distance determined by Shih et al. (1988), although in his model Ba is

bridge-bonded to O, and no fine structure indicative of a Ba-W distance was observed. The better agreement for a larger Ba-surface distance than as proposed by Tuck et al. (1986) could also be a result of the absence of adsorbate interactions in BaO/W_9, which, from the results for Ba_2O_2/W_{14}, can be expected to lead to a somewhat smaller charge transfer, smaller binding energies, and possibly similarly good agreement with experimental binding energies at a slightly smaller Ba-surface distance.

FIGURE 17.

Density of states for BaO/W_9 with R(Ba, Ba-O) = 6.0, 4.9 a_0 (dotted) and with R(Ba, Ba-O) = 6.6, 4.3 a_0 (dashed, and full line after inclusion of final-state effects).

The arrows indicate experimental peak positions.

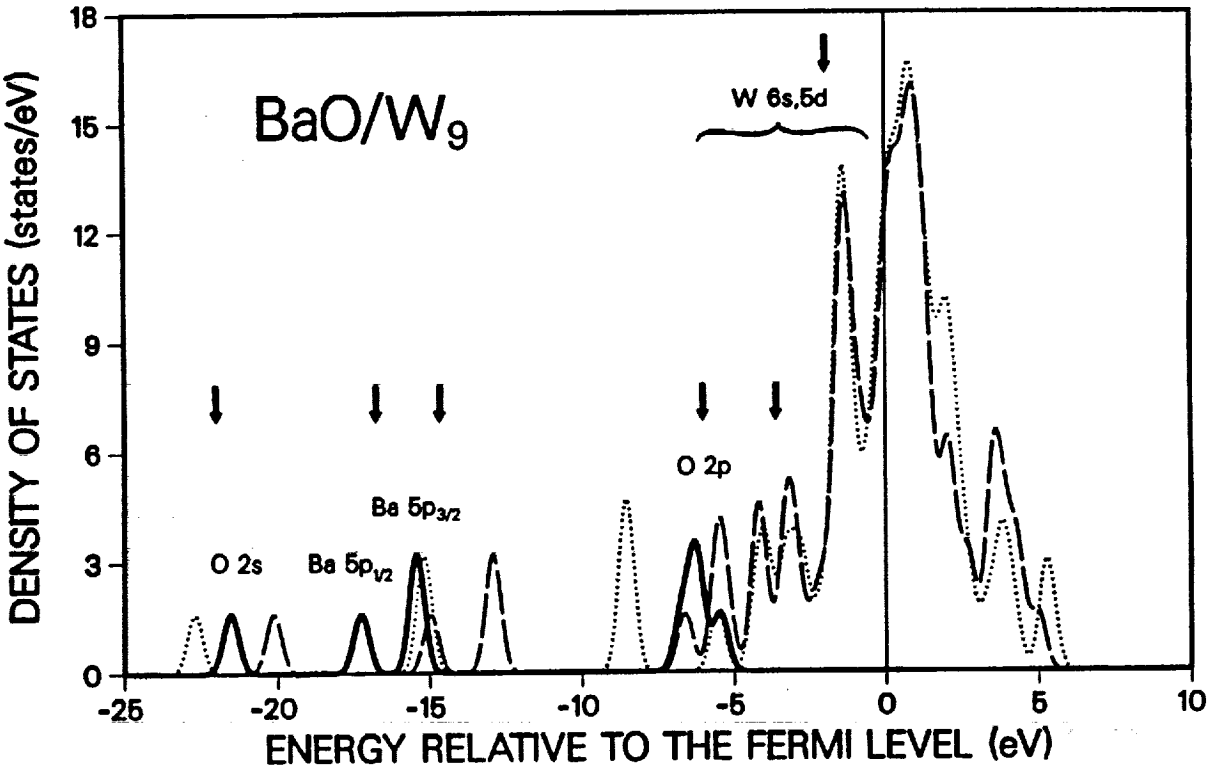

The general conclusions with respect to the charge transfer and surface dipole, on the other hand, are qualitatively similar for the modified and original geometries: Ba is strongly oxidized with q_{Ba} = 1.3 electrons (1.5 orig.) and O is only slightly reduced with q_O = -0.5 electrons (-0.24 orig.), which gives rise to a very large surface dipole of 32 Debyes (37 orig.).

For the determination of the final-state effects for the 5p and 4f core states of the four equivalent W surface atoms in BaO/W_9 the following approximation has been employed: A total of 1/2 electron was removed from the symmetry-equivalent state, which means that only 1/8 electron was removed per site. The calculated energy shift from the transition-state calculation is then scaled by a factor of four.

Because the W_I atoms are related by symmetry, a rigorous transition-state calculation with 1/2 electron removed from one W_I core state would reduce the fourfold symmetry, C_{4v}, to C_s with just one reflection plane remaining. This would substantially increase the computational effort, in particular, since a separate calculation is required for each single state.

The validity of the above approximation is demonstrated by a comparison of the results for the W_I and W_{II} core states in Table XV. The final-state contribution for the W_I 5p and 4f states is calculated to be 0.2 and 1.0 eV, respectively, or after scaling close to 1 and 4 eV. The latter values compare very well with the directly calculated contributions for W_{II} where no scaling is needed.

TABLE XV.

Orbital energies $\Delta\epsilon$, relative to the cluster Fermi level, final-state contributions ΔFS, final calculated, and experimental binding energies for tungsten-related states of BaO/W(100), in eV. R(Ba-surface) = 6.6 a_0 and R(Ba-O) = 4.3 a_0 ~2.3 Å on W_9.

State		-$\Delta\epsilon$	ΔFS	ΔFS(scaled)	Final	Expt.	ΔExpt.
W_I	$5p_{1/2}$	45.8	0.2	0.9	46.7	----	----
	$5p_{3/2}$	36.0	0.2	0.7	36.7	36.8	-0.1
	$4f_{3/2}$	30.1	1.0	4.1	34.2	33.5	+0.7
	$4f_{5/2}$	27.8	1.0	4.0	31.8	31.3	+0.5
W_{II}	$5p_{1/2}$	46.0	1.1	1.1	47.1	----	----
	$5p_{3/2}$	36.5	1.0	1.0	37.5	36.8	+0.7
	$4f_{3/2}$	29.8	4.5	4.5	34.3	33.5	+0.8
	$4f_{5/2}$	27.6	4.3	4.3	31.9	31.3	+0.6

3.3.3 Effects of Bulk and Surface Environments

As a first step toward the simulation of bulk and surface environments in atomic cluster calculations, W_9 and BaO/W_9 clusters have been investigated in which the sphere radii for the various atoms have been modified to more realistically represent the conditions that are present in real, extended systems.

The standard atomic sphere radii for an isolated cluster are chosen as 88 percent of the radii determined from the superposition of nonrelativistic atomic charge densities. A standard body-centered-cubic W_9 cluster, for example, has eight identical W surface atoms and one inner W atom.

If used as a surface model, however, the third-layer tungsten atoms, W_{III}, should be treated differently from W_I, since they have tungsten neighbors in an extended system with similar nearest-neighbor distances as W_{II}. A set of modified calculations has therefore been carried out for W_9 and BaO/W_9, in which the sphere radii for the four W_{III} atoms were reduced to those of W_{II}. In a third set of calculations, the sphere radii were taken from more truly embedded systems, W_{34} and Ba_5O_5/W_{34}, which leads to a reduction of all sphere radii relative to the standard clusters. W_{34} and Ba_5O_5/W_{34} are derived from W_9 and BaO/W_9 by adding the eight nearest neighbors in the first and third W layers, the four nearest neighbors in the second layer, a fourth W layer similar to the second layer, and in the adsorbate cluster the four nearest BaO molecules.

Fully relativistic results for the series of calculations for W_9 are given in Table XVI and Figs. 18-20. The charge distribution is symmetrical for standard W_9, with about 0.05 electrons transferred from each of the surface atoms to the central W_{II} atom. For W_9 with modified and embedded radii, the W_{II} atom acquires 0.7 to 1.0 additional electrons, mainly from the W_{III} atoms. This charge redistribution sets up negative dipole moments perpendicular to the W_I "surface" layer with excess negative charge at or near the surface as present on real metal surfaces. The reduction of the sphere radii in the series leads to a stabilization of the electronic cluster levels, as expressed by the shift in the highest occupied state, ϵ_{max}, which is indicative of an increase in bulk character.

In Figs. 18, 19, and 20 the density of states for W_9 is decomposed into contributions arising from the surface, W(S), subsurface, W(S-1), and third-layer, W(S-2), atoms, respectively. A comparison with the projected densities of states (see insets) from the solid-state calculation of Wimmer et al.(1983) for a 5-layer W film shows good agreement for the surface and subsurface layers.

TABLE XVI.

Net charges q (in electrons), dipole moments μ, and energies ϵ_{max} of the highest occupied state for W_9 clusters with standard, modified, and atomic sphere radii taken from an embedded cluster (W_{34}).

Property	stand. radii[a]	mod. radii[b]	emb. radii[c]
$q(W_I)$	+0.19	-0.44	+0.30
$q(W_{II})$	-0.38	-1.08	-1.39
$q(W_{III})$	+0.19	+1.52	+1.09
μ (Debyes)	0.00	-8.16	-4.06
ϵ_{max} (eV)	-5.07	-5.78	-6.15

[a] $R(W_I)=3.161$, $R(W_{II})=2.672$, $R(W_{III})=3.161$, R(outer sphere)=8.340 a_0.
[b] As for a, except $R(W_{III}) = R(W_{II})$.
[c] $R(W_I)=2.850$, $R(W_{II})=2.593$, $R(W_{III})=2.782$, R(outer sphere)=8.340 a_0.

The densities of states in Fig. 18 for the surface atoms (S) of W_9 with different atomic sphere radii show the prominent surface state at -1 eV, four peaks between -2 and -6 eV, the broad density of unoccupied states around +1 eV, and additional features at higher energies. The surface structure for this simple cluster is in remarkably good agreement with the (non-relativistic) solid-state result for the 5-layer W(100) film which is shown on the inset in the middle figure. The intensity distribution is reasonably well reproduced by all clusters, while the width of the occupied DOS is better described by W_9 with the radii taken from the embedded cluster.

The subsurface-atom (S-1) densities of states for the different W_9 clusters are compared in Fig. 19. The surface state and the high DOS around the Fermi level are now completely missing. Higher DOS are found instead below -2 and above +1 eV, with the consequence that the bulk-like DOS exhibits a minimum where the surface DOS has its maximum. The sharply peaked DOS is characteristic of d-electron metals. Again, the simple cluster result is in good general agreement with the solid-state calculation.

The DOS for the third-layer atoms (S-2) in Fig. 20 is for standard W_9 identical and for the other two calculations similar to the respective surface DOS of Fig. 18. Despite the large changes observed in the calculated charge distributions, the projected densities of states are fairly similar for the different members of the series, and only the second-layer W can be considered as having bulk-like properties.

FIGURE 18.

Densities of states for the surface atoms (S) of W_9 with standard, modified, and atomic sphere radii taken from an embedded cluster.

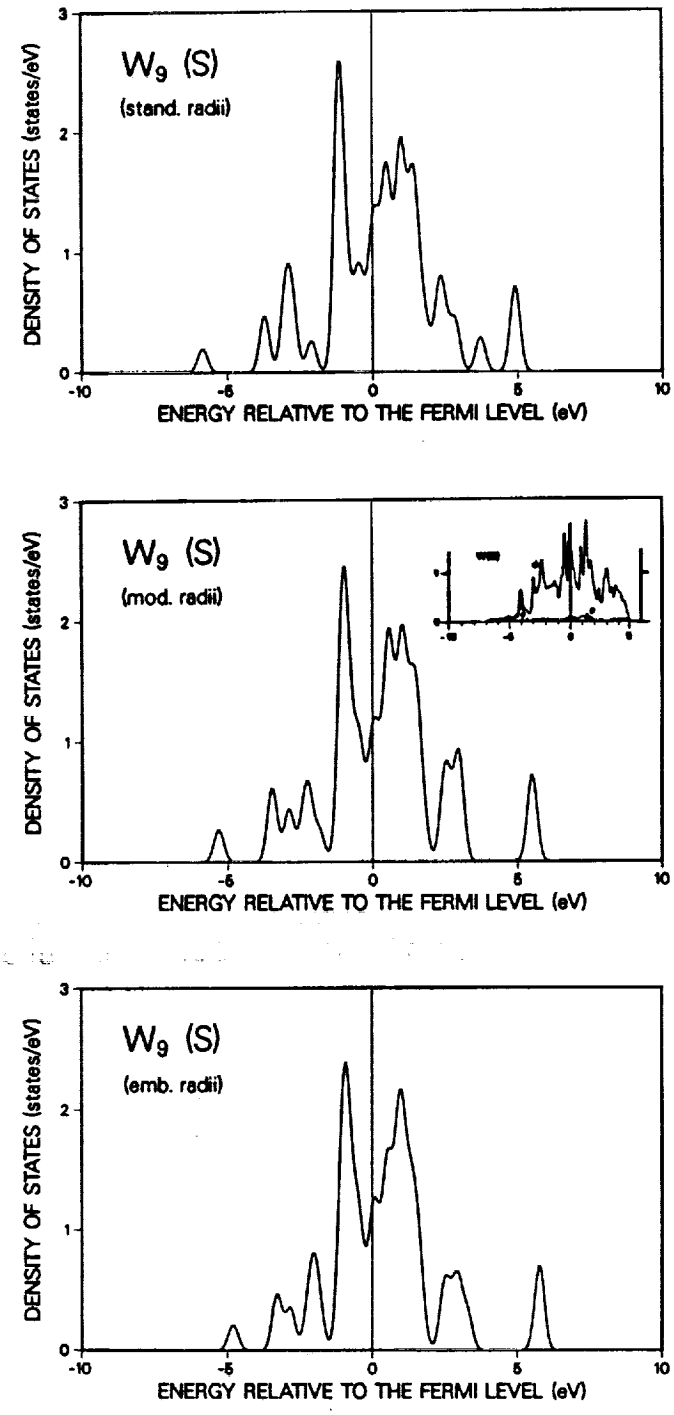

FIGURE 19.

Densities of states for the subsurface atoms (S-1) of W_9 with standard, modified, and atomic sphere radii taken from an embedded cluster.

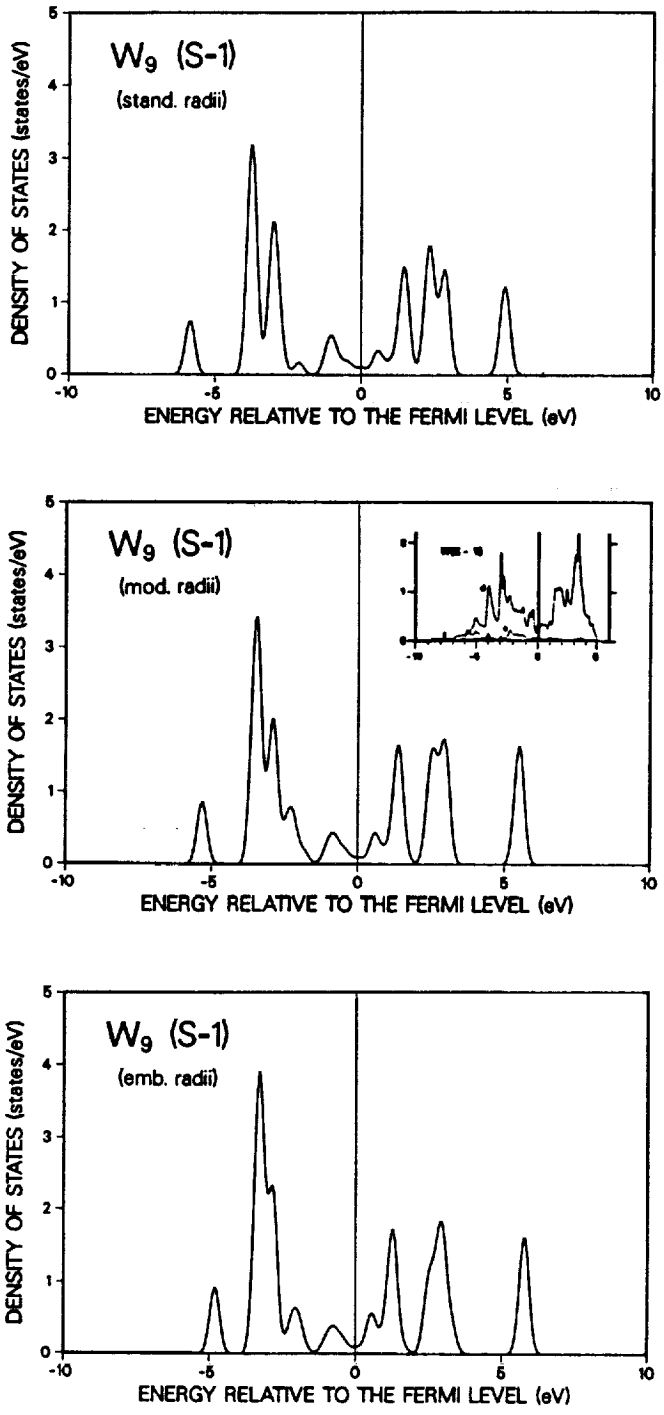

FIGURE 20.

Densities of states for the third-layer atoms (S-2) of W_9 with standard, modified, and atomic sphere radii taken from an embedded cluster.

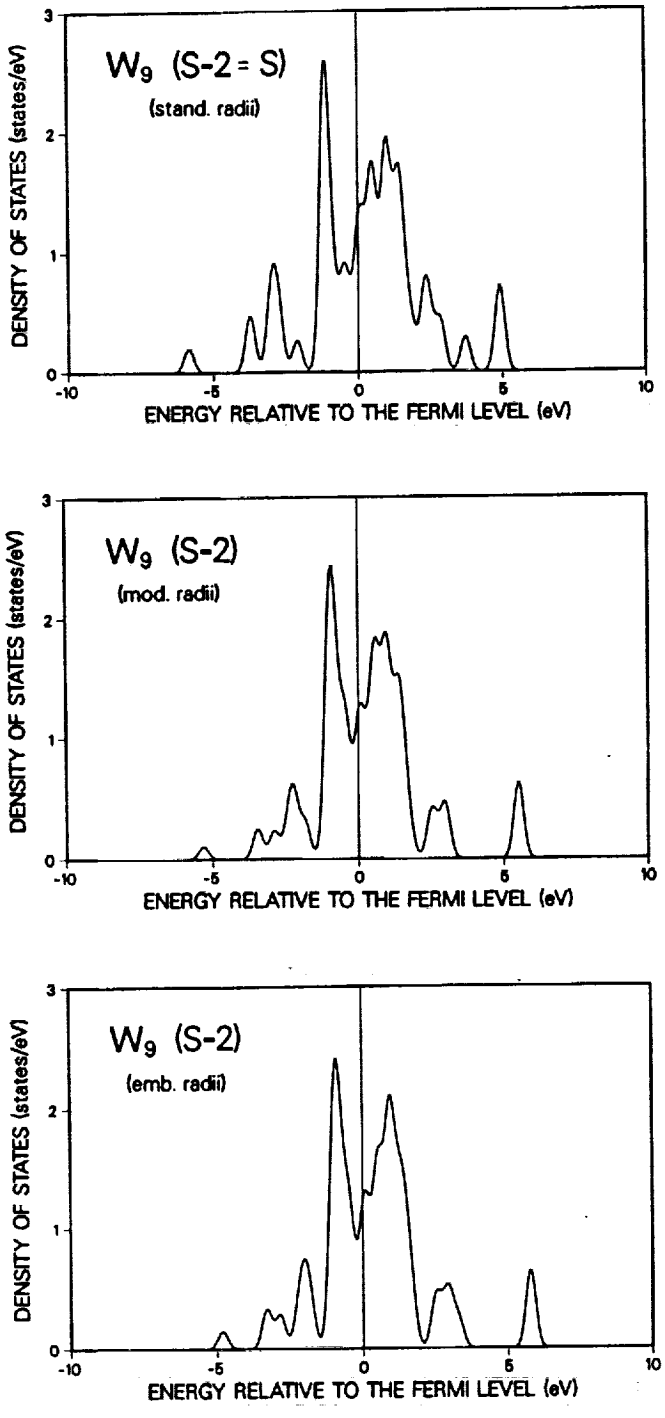

The reduction of the sphere radii in the BaO/W_9 cluster with R(Ba,Ba-O) = 6.0, 4.9 a_0 has the following effects on the fully relativistically calculated charge distribution and dipole properties, as shown in Table XVII: The charge on Ba increases steadily in the series from 1.51 to 1.62 and 1.83 electrons, which is likely to be related to the stabilization of the tungsten electronic structure already observed for bare W_9. The screened negative image charge is now found mainly in the second rather than in the third W layer. A comparison with the charge distributions in the respective bare W_9 clusters (Table XVI) shows, however, that the W_{II} atom already had a similarly large negative charge such that the actual charge transfer is still into the third tungsten layer. The dipole moments, therefore, remain similarly large, while the Ba binding energy increases substantially due to the increasing positive charge on Ba. It is also worth noting that the reduction of the W_I sphere radius from 3.16 to 2.85 a_0 in BaO/W_9 with embedded radii leads to increases in the oxidation level of the W surface layer and the negative charge on oxygen.

TABLE XVII.

Net charges q (in electrons), dipole moments μ, Ba dipole energies E_{Ba}, and energies ϵ_{max} of the highest occupied state for BaO/W_9 clusters with standard, modified, and atomic sphere radii taken from an embedded cluster (Ba_5O_5/W_{34}). R(Ba-O) = 4.9 a_0 ~2.6 Å.

Property	stand. radii[a]	mod. radii[b]	emb. radii[c]
q(Ba)	+1.51	+1.62	+1.83
q(O)	-0.24	-0.23	-0.73
q(Substrate)	-1.27	-1.39	-1.10
$q(W_I)$	+0.06	-0.30	+0.73
$q(W_{II})$	-0.33	-1.13	-1.34
$q(W_{III})$	-1.00	+0.04	-0.49
μ (Debyes)	37.5	37.2	43.2
E_{Ba} (eV)	6.4	7.9	9.8
ϵ_{max} (eV)	-5.39	-5.95	-6.79

[a] R(Ba)=3.769, R(O)=1.777, $R(W_I)$=3.000, $R(W_{II})$=2.613, $R(W_{III})$=3.160, R(outer sphere)=10.486 a_0.
[b] As for a, except $R(W_{III}) = R(W_{II})$.
[c] R(Ba)=3.323, R(O)=1.763, $R(W_I)$=2.684, $R(W_{II})$=2.544, $R(W_{III})$=2.673, R(outer sphere)=10.486 a_0.

The densities of states for BaO/W_9 with standard, modified, and atomic sphere radii from the embedded cluster are compared in Fig. 21. The chief differences are (i) changes in the W-related DOS outside the regime of high surface DOS around the cluster Fermi level and (ii) a shift of the Ba 5p states at -15 eV by 1.5 eV to smaller binding energies relative to standard BaO/W_9. Surprisingly, the Ba 5p levels are not affected by the large reduction of the Ba sphere radius when comparing BaO/W_9 with modified and embedded radii. The O 2s and 2p binding energies remain unchanged for all clusters.

The results for the BaO/W electronic structure can be summarized as follows:

- The O 2s and 2p binding energies can be brought in agreement with the photoemission data of D. Mueller et al. (1988) by changing the Ba-O distance in the vertical arrangement from the value of 2.6 Å proposed by Tuck and Norman et al. (1986 and 1987) to the value of 2.3 Å proposed by Shih et al. (1988). Final-state effects are important for the O 2s (1.4 eV) and O 2pπ (0.7 eV) binding energies. Adsorbate interactions and simulated environments do not affect the oxygen electronic levels.

- The Ba 5p energies also improve with a shorter Ba-O distance. The final-state effects amount to 3.1 eV for Ba 5s and ~2.4 eV for 5p. These states are strongly affected when the smaller sphere radii of embedded W atoms are used, but the effect of adsorbate interactions is small.

- All calculations so far have confirmed a large charge transfer from Ba to the substrate, a relatively small negative charge on O, and a resulting very large surface dipole. The calculated Ba binding energies are in good agreement with experiment.

FIGURE 21.

Densities of states for BaO/W_9 with standard, modified, and atomic sphere radii taken from an embedded cluster (Ba_5O_5/W_{34}).

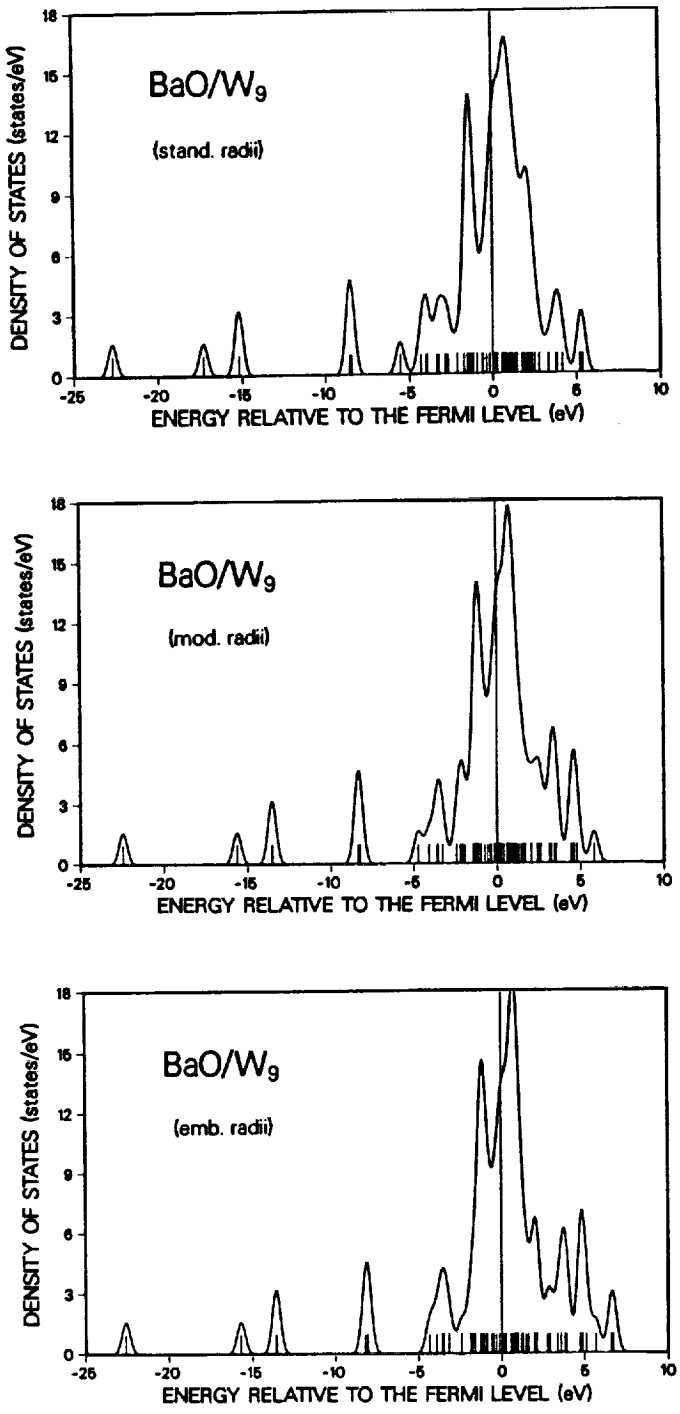

4. O/W ELECTRONIC STRUCTURE

For the O/W(100) system, extended cluster calculations have been carried out and a comparison has been made with oxygen-induced features in angularly-resolved inverse photoemission spectra (Krainsky, 1988).

Figure 22 shows the fully relativistically calculated densities of states (DOS) for a O_2/W_{14} cluster, the W_{14} substrate, the oxygen-related DOS in O_2/W_{14}, the difference $O_2/W_{14}-W_{14}$, and the experimentally observed spectrum of oxygen-induced features for an angle of incidence of 52°, which is representative of the spectra taken between 40° and 76°. The density of the oxygen-induced states in this range is in remarkably good agreement with experiment. The intensities and energies of the observed peaks are well reproduced and significantly improved from earlier results for single-adsorbate O/W clusters. The oxygen-related DOS exhibits only one major peak, the O 2p peak, at 6.3 eV below the cluster Fermi level. This shows that all other features in the difference spectrum originate from changes in the electronic structure of W due to the adsorption of O, and not from unoccupied O levels themselves.

For the purpose of comparison with the above results, quasirelativistic calculations have been carried out for the same system. This comparison revealed significant differences. At the quasirelativistic level, the occupied O 2p states are shifted from -6.3 eV to -4.0 eV, and the peaks near 1 and 2 eV above E_F are now larger in intensity than the state near 4 eV.

Preliminary surveys have also been carried out for oxygen adsorped in a bridge position at room temperature and for a reconstructed surface at elevated temperatures by using the quasirelativistic approach. The adsorption of oxygen in a bridge position on unreconstructed W(100) is modeled with a O_4/W_{12} cluster, where the substrate cluster contains two layers of six W atoms each. A O_2/W_{12} cluster is used for the high-temperature case, where the middle row of the first-layer W atoms has been moved to the third layer and oxygen is now adsorbed on top of the exposed second-layer W atoms. For the unreconstructed surface, the results for $O_4/W_{12}-W_{12}$ with oxygen at a bridge site are similar to those with oxygen at the fourfold-hollow site. For the reconstructed surface, the DOS for $O_2/W_{12}-W_{12}$ shows a further increase in the intensity for the peak near 1 eV, so that none of these results provides an improvement in the description of the observed spectrum.

Because of the shortcomings of the quasirelativistic results with respect to the intensities of the oxygen-induced unoccupied states, it has been decided to further explore the O/W system with fully relativistic calculations for larger clusters, in which proper surface equivalences will taken into account.

FIGURE 22.

Theoretical and experimental oxygen-induced features in the density of states for O/W(100).

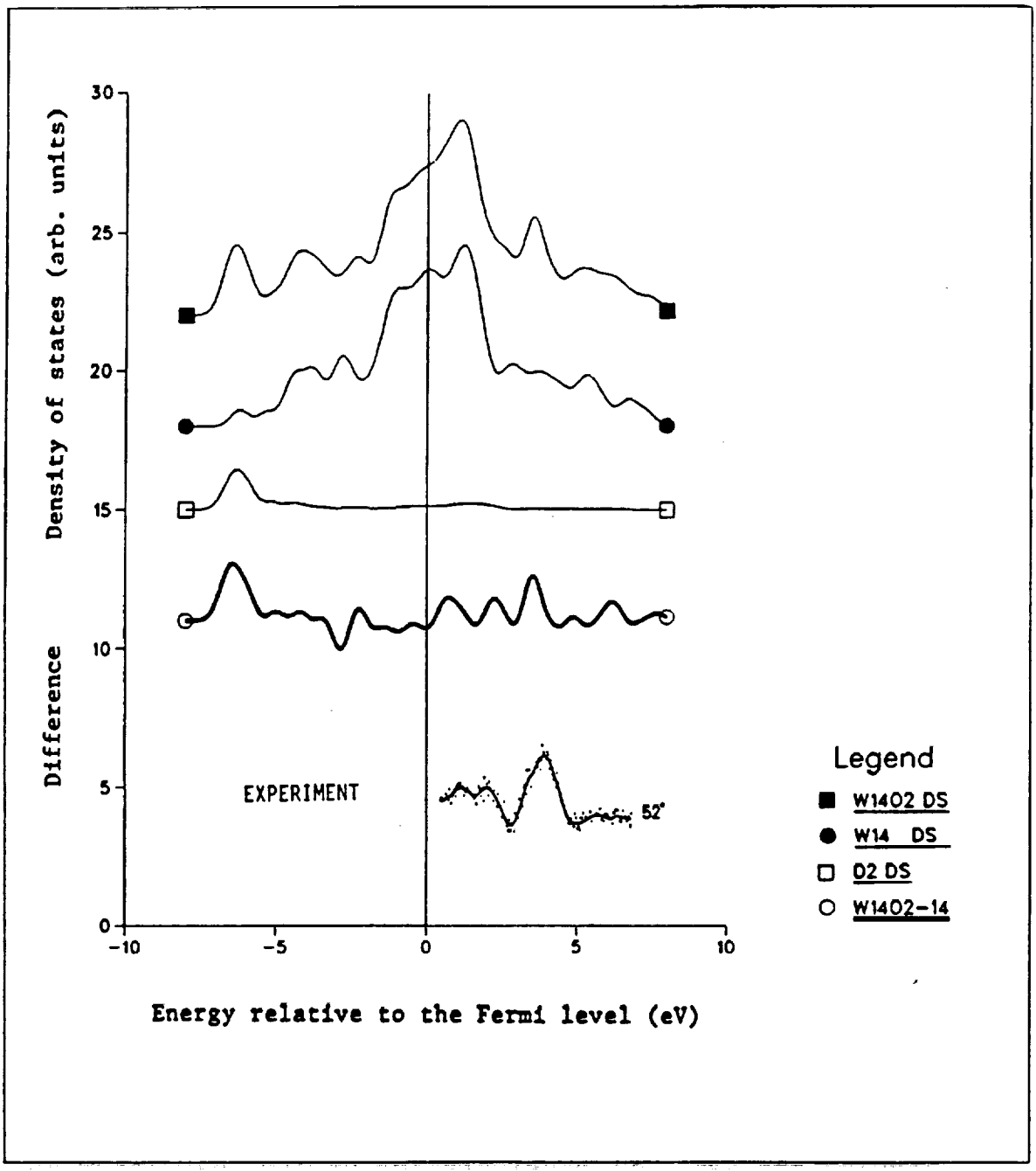

5. AB INITIO BaO RESULTS

Ab initio configuration interaction (CI) calculations, which are based on self-consistent-field (SCF) or multi-configuration (MC) wave functions, have been carried out for BaO. The electronic structure on Ba is described by using a previously developed 2-electron pseudopotential which includes relativistic and core polarization (CPP) effects (Müller, 1988). In Table XVIII the CI and MC-CI results are compared with earlier SCF and MC-SCF data.

The spectroscopic constants in this table include the equilibrium separation R_e, the rotational constant B_e, the harmonic vibrational frequency ω_e, the dissociation energies D_e and D_o, the dipole moment μ_e, and the net charge on Ba q_{Ba}. The calculation denoted as MC-CI+CPP' has been corrected for the Ba^{2+} (core) - O^- ($2p\sigma^{-1}$) exchange repulsion as obtained from the superposition of the O^- CI orbitals with an all-electron Ba^{2+} core, while for all other cases the O^- SCF orbitals have been used.

TABLE XVIII.

Spectroscopic constants for BaO at the SCF, MC and CI levels of calculation and from experiment (Huber and Herzberg, 1979).

Method	R_e(Å)	B_e(cm^{-1})	ω_e(cm^{-1})	D_e(eV)	D_o(eV)	μ_e(D)	q_{Ba}(e)
SCF	1.90	0.325	972	5.9	3.7	-12.2	1.2
SCF+CPP	1.89	0.328	976	6.5	4.3	-11.0	1.1
MC-SCF+CPP	1.92	0.319	813	7.0	4.8	-9.8	1.0
CI+CPP	1.91	0.324	944	8.5	6.3	-10.1	1.0
MC-CI+CPP	1.88	0.331	950	8.9	6.8	-9.2	0.9
MC-CI+CPP'	1.91	0.324	944	8.6	6.5	-9.2	0.9
Expt.	1.94	0.313	670	7.8	5.8	-8.0	0.9

The general conclusions are as follows:

- R_e and B_e are very well described at all levels.
- ω_e is still significantly too large at the CI level. This is most likely related to the approximate treatment of the Ba^{2+} core - O^- repulsion, in which the transfer of 1 electron is assumed for all R around R_e. A more rigorous treatment would require the explicit consideration of the next inner shell on Ba.

- The calculated dissociation energies are somewhat too small at the SCF and MC-SCF levels and appear to be too large at the CI level. A rigorous experimental value, however, is not known.

- The calculated dipole moment and charge transfer improve systematically with increasing level of computational effort.

In summary, it is found that the geometry and bonding in BaO is reasonably well described with the Ba 2-electron pseudopotential at the intermediate MC-SCF+CPP level, while a better description of the shape of the potential curve requires the explicit consideration of the next inner electronic shell on Ba and/or possibly also a larger basis set on oxygen.

6. YBaCuO SUPERCONDUCTOR ELECTRONIC STRUCTURE

The electronic structure of the high-temperature superconductor $YBa_2Cu_3O_7$ has been investigated with the relativistic cluster approach (Müller, Physica C, 1989). The results described here represent the first calculations for this system which include (a) all relativistic electronic effects and (b) final-state energy corrections for comparison with photoemission spectra.

The atomic clusters used for $YBa_2Cu_3O_7$ are shown in Figure 23. These include two small clusters modeling the Cu-O chains and planes, and larger clusters for two different unit cells with 3 and 4 Cu-O layers.

FIGURE 23. Cluster models for $YBa_2Cu_3O_7$.

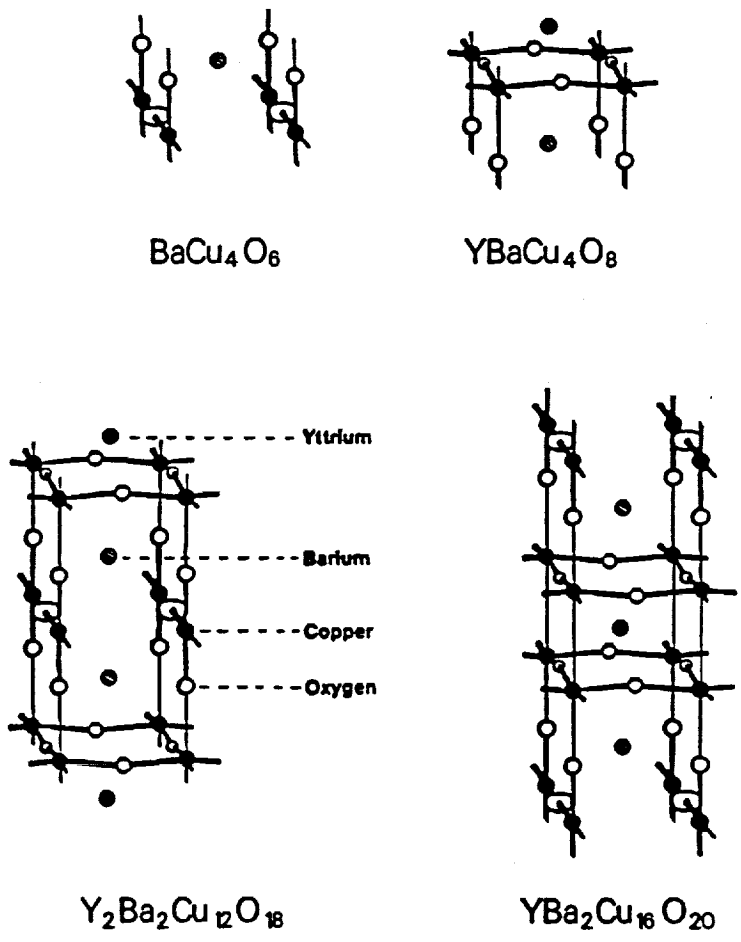

The valence densities of states (DOS) for the two small clusters and the $Y_2Ba_2Cu_{12}O_{18}$ unit-cell cluster are compared in Fig. 24. The DOS is generated from the calculated energy levels which are indicated as small vertical lines on the horizontal axis. The peaked and smooth density distributions were obtained by broadening the cluster energy levels with Gaussians using width parameters of 0.05 and 0.50 eV, respectively. The $BaCu_4O_6$ cluster, modeling the chains, already shows the characteristic double peak below the Fermi level that is observed in photoemission spectra. For $YBaCu_4O_8$, which models the planes, additional states appear in the center of the double-peak structure. For the unit-cell cluster, the width and shape of the double peak is in good agreement with experiment. The additional feature at -5 eV results from the planes. Above the Fermi level, the states at lower energy are due to Y and the states at higher energy are due to Ba.

The calculated total and partial densities of states for the Cu-O valence band of $Y_2Ba_2Cu_{12}O_{18}$ are shown in Figure 25, which shows the typical double maximum and additional features at higher and lower binding energies. The partial DOS from the cluster shows major copper contributions near the center of the double maximum and oxygen contributions more to its sides. These effects are analyzed in more detail in Fig. 26. In this figure, photoemission spectra for different photon energies are compared with calculated DOS for Cu-O in which the Cu contribution is varied from 0 to 100%. It can be seen that the double-peak structure of the high-energy, $h\nu$ = 70 eV, spectrum is well reproduced by the calculated Cu-O (both 100%) DOS, while the three-peak structure of the low-energy, $h\nu$ = 20 eV, spectrum resembles the Cu(0%)-O(100%) DOS. Low photon energies, therefore, emphasize the oxygen contribution to the Cu-O valence band.

In Fig. 27, the DOS are compared for different unit-cell clusters. $[Y_2Ba_2Cu_{12}O_{18}{}^{2-}]^{2+}$ contains two additional electrons and is surrounded by a "Watson" sphere with charge 2+, which represents an attempt to account for effects of the ionic environment in the crystalline material. If formal charges of +3 and +2 are assigned to Y and Ba, respectively, and -2 to O, then the formal charge of Cu in $YBa_2Cu_3O_7$ is +2.33. Because the clusters do not have the correct stoichiometry, the cluster of atoms in, e.g., $Y_2Ba_2Cu_{12}O_{18}$ requires 2 additional electrons for neutrality of the formal charges, which are balanced with 2 positive charges in the Watson sphere. Fig. 27 shows that this modification leads to a slight shift in the DOS of the order of -0.5 eV because of the occupation of a previously unoccupied orbital in $Y_2Ba_2Cu_{12}O_{18}$. The choice of a different unit cell, $YBa_2Cu_{16}O_{20}$, with the Cu-O planes and Y at the center of the cluster (instead of the Cu-O chains and Ba), has a somewhat larger effect on the DOS, but the calculated general structure remains the same.

FIGURE 24.

Densities of states for $BaCu_4O_6$, $YBaCu_4O_8$, and $Y_2Ba_2Cu_{12}O_{18}$.

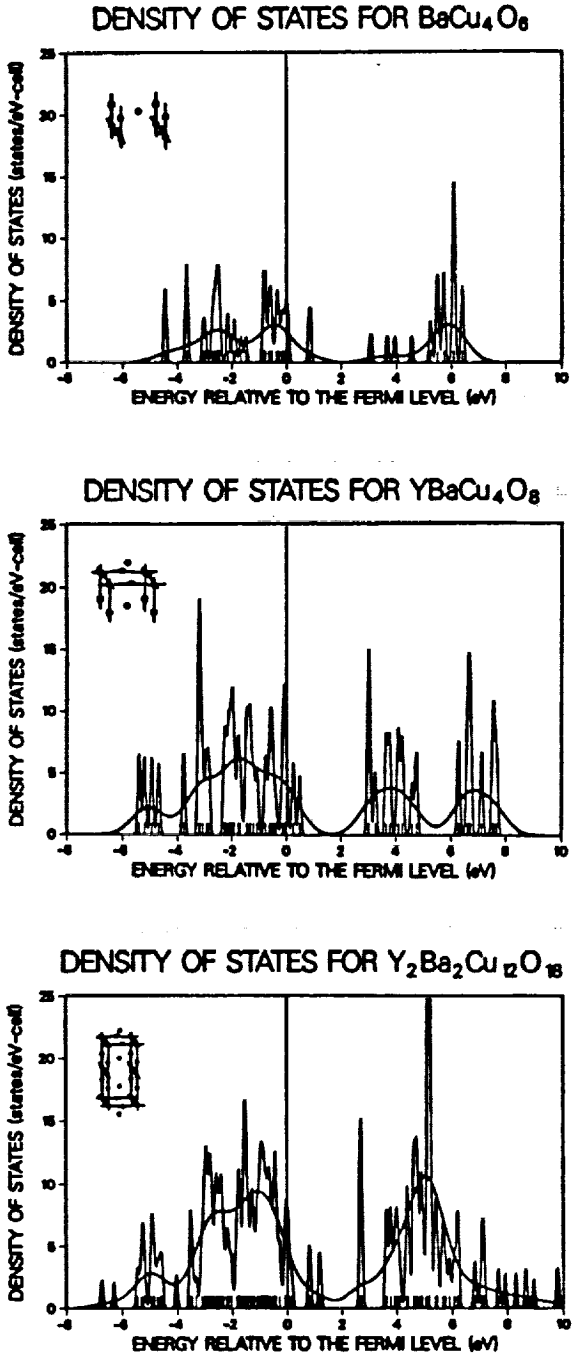

FIGURE 25.

Total (per $YBa_2Cu_3O_7$ cell) and partial (atomic) densities of states as derived from a $Y_2Ba_2Cu_{12}O_{18}$ cluster model.

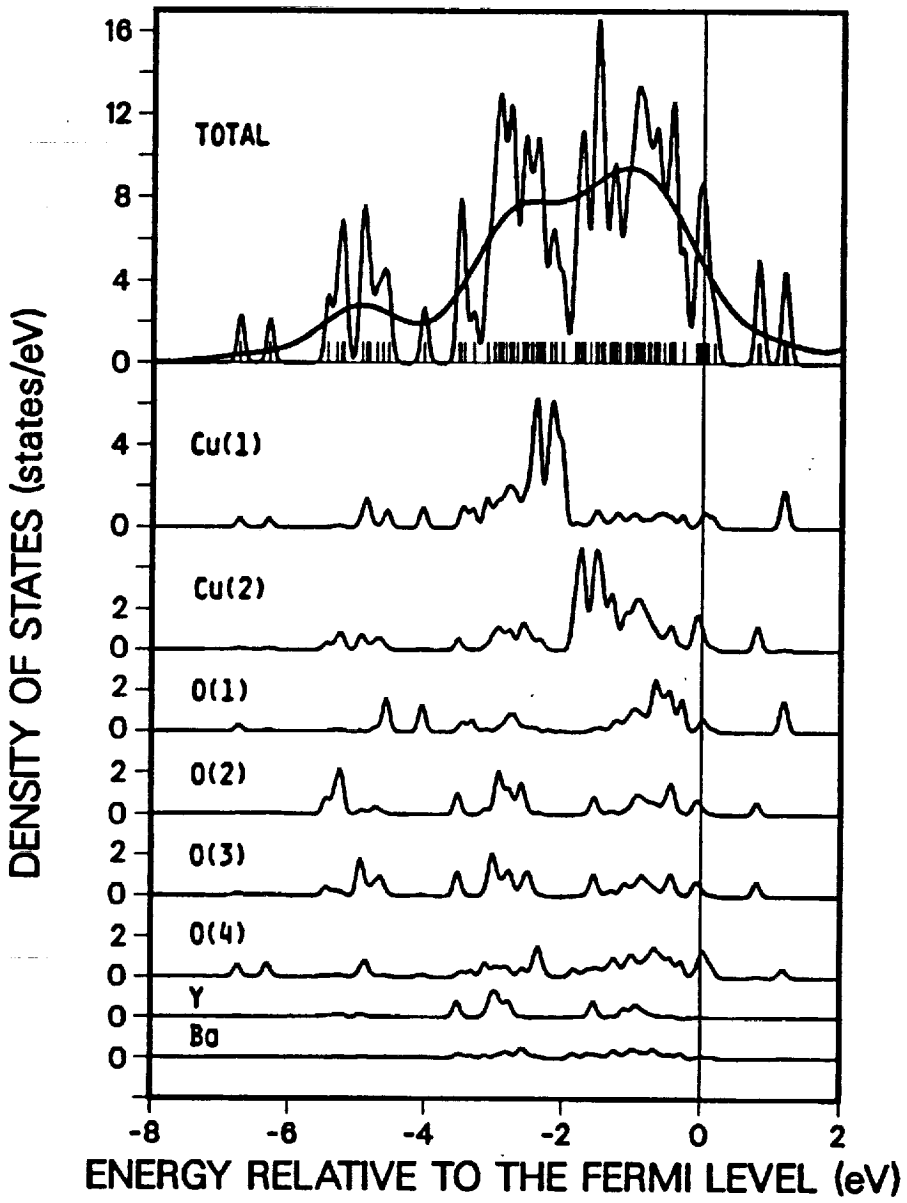

FIGURE 26.

Analyses of experimental and theoretical densities of states for Y-Ba-Cu-O near the Fermi level.

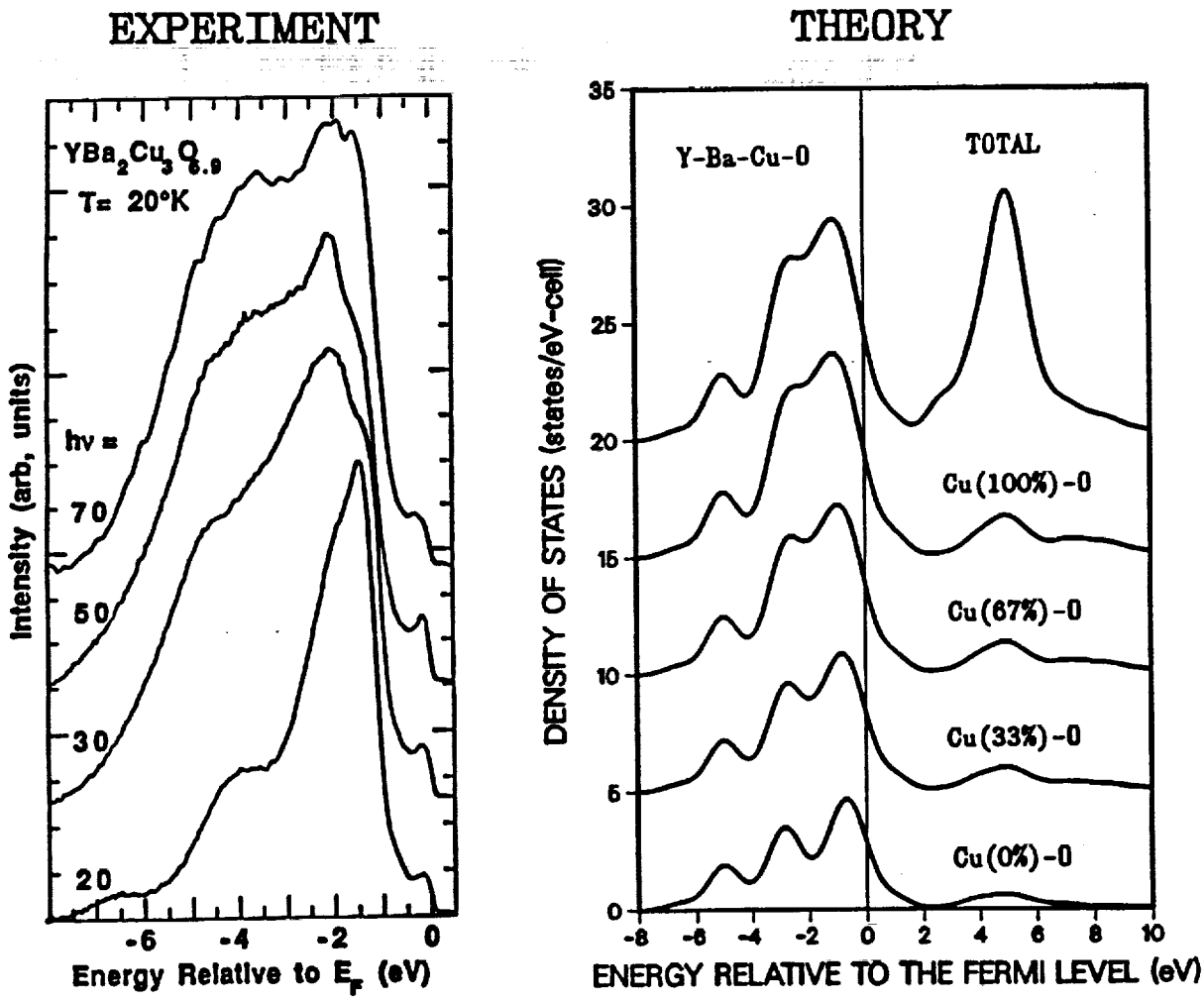

FIGURE 27. Densities of states for $Y_2Ba_2Cu_{12}O_{18}$ and $YBa_2Cu_{16}O_{20}$.

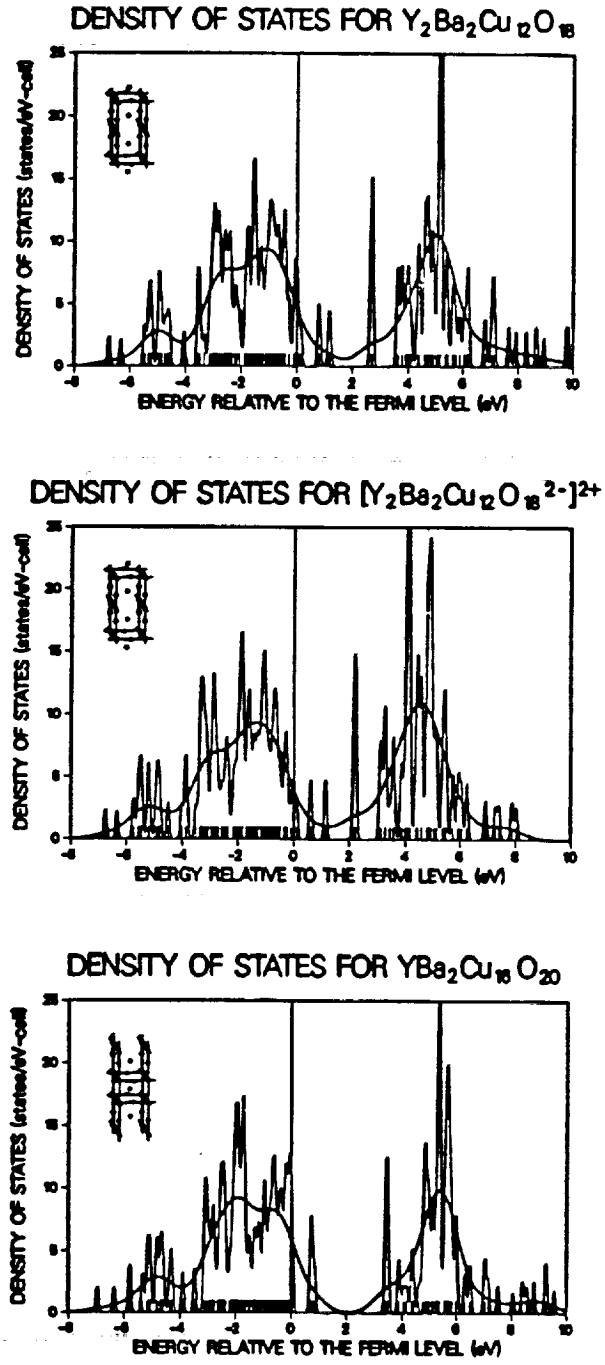

Overall, the cluster DOS is in good agreement with solid-state calculations and photoemission data. Relative to the results from both calculations, the observed valence band is shifted, however, by about 1.5 eV to higher binding energies (Johnson et al., 1987). This shift, as discussed below, has to be attributed to true electron correlation effects which are not included in calculations that are based on the density-functional approach.

The calculated charge distributions for the various clusters are given in Table XIX. For Ba, Cu, and O net charges of +/- 0.6 to 0.8 electrons are obtained. The net charge for Y shows the largest variation, with between +0.7 and +1.3 electrons. Although the real charges in the bulk material are certainly not as large as the formal charges given above, the true net charges in the bulk material are likely to be larger than as obtained in the cluster calculations because the long-range Madelung contribution to the potential is missing. This contribution is expected to stabilize additional electronic charge on oxygen and to increase the ionicity of the material. Because, however, the ionic environment is missing near the surface of a superconductor, the cluster results are believed to be representative of the surface electronic structure.

TABLE XIX.

Net atomic charges (in electrons) for different Y-Ba-Cu-O superconductor clusters from fully relativistic calculations.

Cluster	Y	Ba	Cu1	Cu2	O1-4
$BaCu_4O_6$	....	+0.8	+0.8	....	-0.7
$YBaCu_4O_8$	+1.3	+0.8	....	+0.8	-0.6/-0.7
$Y_2Ba_2Cu_{12}O_{18}$	+1.1	+0.6	+0.6	+0.8	-0.6/-0.8
$[Y_2Ba_2Cu_{12}O_{18}{}^{2-}]^{2+}$	+1.0	+0.5	+0.6	+0.7	-0.7/-0.8
$YBa_2Cu_{16}O_{20}$	+0.7	+0.6	+0.7	+0.8	-0.6/-0.8

Details of the calculated valence charge distributions for $Y_2Ba_2Cu_{12}O_{18}$ and $YBa_2Cu_{16}O_{20}$ are compared in Table XX. Although there are differences in the net atomic charges, in particular for Y which is either at the upper and lower ends or in the center of the cluster (see Fig. 23), the s, p, and d orbital populations for the various atoms are fairly similar in the two cases.

Barium has a 6sp population of 0.4 electrons and a 5d population of about 1 electron, i.e., a net positive charge of about 0.6 electrons, and oxygen has an excess of 0.6 to 0.8 electrons in the 2p shell. The Cu 4sp population varies between 0.6 and 1.1 electrons and the Cu 3d population between 9.3 and 9.8 electrons. The net charge on Cu is on the order of +0.7 electrons, and for Cu(1) approximately 0.15 electrons smaller than for Cu(2). The results for both clusters show that holes are present mainly in the O 2p shell. These holes are believed to be the charge carriers in the high-temperature superconductors. The charge distribution also indicates that there exist significant covalent contributions in the interatomic bonding near the surface.

The Cu 3d occupations of 9.3-9.6 electrons are in very good agreement with the estimate of 9.45 from the Larsson-Sawatzky model (Fujimori et al., 1987). The calculated Cu 3d spin-orbit splittings are 0.3 eV.

TABLE XX.

Valence charge distribution for unit-cell clusters of $YBa_2Cu_3O_7$ from relativistic Xα calculations.

Cluster	s	p	d	sum	net
$Y_2Ba_2Cu_{12}O_{18}$					
Y	0.26	0.24	1.41	1.91	+1.09
Ba	0.17	0.27	1.00	1.44	+0.56
Cu1	0.27	0.81	9.28	10.36	+0.64
Cu2	0.30	0.30	9.61	10.21	+0.79
O1	2.03	4.72	....	6.75	-0.75
O2	2.03	4.68	....	6.71	-0.71
O3	2.03	4.67	....	6.70	-0.70
O4	2.06	4.57	....	6.63	-0.63
$YBa_2Cu_{16}O_{20}$					
Y	0.27	0.41	1.60	2.28	+0.72
Ba	0.17	0.28	0.95	1.40	+0.60
Cu1	0.27	0.55	9.50	10.32	+0.68
Cu2	0.31	0.28	9.60	10.19	+0.81
O1	2.02	4.68	....	6.70	-0.70
O2	2.04	4.74	....	6.78	-0.78
O3	2.03	4.74	....	6.77	-0.77
O4	2.08	4.52	....	6.60	-0.60

Energy shifts due to the relaxation of the charge distribution upon ionization, which are the final-state contributions in the photoemission process, have been investigated for the first time. It is found that these effects are small for the valence states (for localized Cu 3d states up to 0.2 eV), and that the valence-band width is not affected. True correlation effects have, therefore, to be made responsible for the observed shifts.

The final-state contributions are, however, very large for the core states. They range from 160 eV for Cu 1s and 30 eV for O 1s to 1 eV for Cu 3s, 3p, and O 2s. The resulting core-electron binding energies for $Y_2Ba_2Cu_{12}O_{18}$ are given in Table XXI. The calculated values are in very good agreement with experimental data, with deviations of 1-5 eV only. Without consideration of the final-state contributions, the errors would be up to one order of magnitude larger.

TABLE XXI.

Calculated final-state contributions (ΔFS) and core-electron binding energies (eV) for $Y_2Ba_2Cu_{12}O_{18}$.

Atom	State	ΔFS	Calc.	Expt.
Cu(1,2)	1s	160	8999, 9004	---
	2s	17	1077, 1077	---
	3s	1	113, 112	---
	$2p_{1/2}$	23	953, 951	953
	$3p_{1/2}$	1	73, 72	76
	$2p_{3/2}$	23	932, 931	933
	$3p_{3/2}$	1	70, 69	74
O(1,4)	1s	30	533, 533	529
	2s	1	18, 17	(531,533)
O(2,3)	1s	30	534, 534	
	2s	1	19, 19	20
Ba	$3d_{3/2}$	23	794	---
	$3d_{5/2}$	23	778	779
Y	$3d_{3/2}$	10	160	158
	$3d_{5/2}$	10	158	156

A close examination of the results reveals that the calculated Cu levels are slightly lower and the O levels slightly higher than the corresponding experimental values. This is clear evidence that the calculated net charges on Cu and O are somewhat too small, and that the calculated electronic structure is more representative of the surface than of the bulk of the material. Higher binding energies for the O 1s level are in fact observed in surface-sensitive experiments, which are in excellent agreement with the calculated value of 533 eV. For the different inequivalent Cu and O atoms, no significant variations in the core-electron energies are found either in the experiment or in the calculation.

The unit-cell superconductor calculations have been carried out on the Cray supercomputers at the Numerical Aerodynamic Simulation (NAS) facility at Ames Research Center, whose support is gratefully acknowledged.

7. COMPUTATIONAL METHODS

Xα Methods. - The results for the low-work-function surfaces and high-temperature superconductors discussed in this report are based on the Xα scattered-wave approach. Fully relativistic (Case and Yang, 1980) and quasirelativistic (Cook and Case, 1989) computer programs have been employed for this research. In the quasirelativistic version, the relativistic mass-velocity and Darwin corrections to the energy are retained, but spin-orbit interaction is no longer taken into account. This reduces the computational effort considerably, and has enabled calculations for clusters with low symmetry and the study of adsorbate interactions as a function of coverage.

The original Xα scattered-wave programs have been significantly improved. In the quasirelativistic program, the input/output has been changed to conform with the fully relativistic version. An interpolation scheme for structure-factor matrices (G) has been implemented which doubled the computational speed of both programs on the Cray supercomputers. Because the off-diagonal elements of the G matrices show generally a smooth variation with energy, they can be precalculated for a specified energy grid, stored on disk, and interpolated during the iterative process. In the final iterations calculated G matrices are used without interpolation. Another new useful feature allows one to automatically compute all unoccupied electronic states for a given system by employing an in-line energy search procedure.

TABLE XXII.

Net atomic charges q (in electrons), dipole moments μ, and dipole energies E_{Ba} for BaO at R_e = 3.666 a_0 = 1.940 Å and BaO/W_9(100) with R(Ba-O) = 4.9 a_0 ~2.6 Å and R(Ba-surface) = 6.0 a_0 ~3.2 Å.

Property	BaO		BaO/W_9	
	quasi	fully rel.	quasi	fully rel.
q(Ba)	+0.82	+0.85	+1.50	+1.51
q(O)	-0.82	-0.85	-0.15	-0.24
$q(W_I)$	.....	.....	-0.08	+0.02
$q(W_{II})$	.....	.....	-0.00	-0.33
$q(W_{III})$	.....	.....	-0.25	-0.25
μ (Debyes)	9.5	7.0	38.4	37.5
E_{Ba} (eV)	4.0	6.1	6.1	6.4

A comparison between quasi- and fully relativistic results for BaO and $BaO/W_9(100)$ is made in Table XXII. The calculated charge distributions are in reasonable agreement, although there are some distinct differences in the net charges of O, W_I and W_{II} for BaO/W_9. The dipole properties differ quite significantly for BaO, but they are similar for BaO/W_9 at the two levels of calculation. Because the dipole energy E_{Ba} is defined as $q^3(Ba)/\mu$, small variations in q(Ba) have a relatively large effect on the value of E_{Ba}.

Quasi- and fully relativistic results for $BaO/M_4W_1W_4$ clusters with M = W, Os, and Pt are compared in Table XXIII. It can be seen that the dipole moments at the quasirelativistic level (in parentheses) are slightly larger, by 2-5%, and that the dipole energies are 5-9% smaller than the corresponding fully relativistic results. The calculated data are otherwise very similar.

The net charges for Ba and O on the different substrates vary only slightly (by 0.1 electrons or less), while the major charge redistributions occur inside the metal substrate and in the opposite direction of the Ba-substrate charge transfer. The consequences are a steady decrease in the dipole moments and an increase in the Ba binding energies in the series.

TABLE XXIII.

Comparison of fully and quasirelativistic (in parentheses) Xα results for $BaO/M_4W_1W_4$ clusters with M = W, Os, and Pt. R(Ba-O) = 4.9 a_0 ≈ 2.6 Å.

Property	$BaO/W_4W_1W_4$	$BaO/Os_4W_1W_4$	$BaO/Pt_4W_1W_4$
q(Ba)	+1.51 (+1.50)	+1.58 (+1.57)	+1.58 (+1.52)
q(O)	-0.24 (-0.15)	-0.17 (-0.15)	-0.14 (-0.25)
q(Substrate)	-1.27 (-1.35)	-1.41 (-1.42)	-1.44 (-1.27)
$q(M_I)$	+0.01 (-0.08)	-0.21 (-0.25)	-0.29 (-0.27)
$q(W_{II})$	-0.33 (-0.00)	-0.09 (+0.12)	+0.07 (+0.18)
$q(W_{III})$	-0.25 (-0.25)	-0.12 (-0.13)	-0.08 (-0.09)
μ (Debyes)	37.5 (38.4)	29.5 (31.1)	26.6 (25.8)
E_{Ba} (eV)	6.4 (6.1)	9.2 (8.6)	10.3 (9.4)

Benchmark calculations have been carried out on the different Cray supercomputers at NASA Lewis and Ames. In Table XXIV the timings are given for one iteration of the specified fully relativistic Xα calculations. The Cray-2 has only 60-70% of the speed of the Cray X-MP (in spite of a faster clock time, but due to a longer memory fetch time), while the Cray Y-MP is faster than the X-MP by 30-40% for the present code. Without vectorization the CPU time increases on the Cray Y-MP by a factor of 2.8, and without optimization by a factor of 4.8. For the present applications, the Cray Y-MP is clearly the favored machine.

TABLE XXIV.

CPU timings on different Cray supercomputers for Xα calculations, in seconds, and relative speedup/down for the Cray-2 and Y-MP relative to the Cray X-MP (in parentheses).

Calculation	Cray Y-MP	Cray X-MP	Cray-2
BaO/W_9	18.5" (1.0)	23.6" (1.3)	38.0" (2.1)
BaO/W_9 + G-Mat.	53.0" (1.0)	73.5" (1.4)	108.8" (2.1)
$Y_2Ba_2Cu_{12}O_{18}$	190.0" (1.0)	257.4" (1.4)	390.1" (2.1)

FLAPW Method. - The linearized augmented plane wave (LAPW) method is among the most accurate methods for performing band-structure calculations for solids or surfaces. Exchange and correlation are treated by using the local density approximation (LDA) to density-functional theory. Several forms of LDA potentials exist in the literature, the simplest being Slater's Xα potential. Relativistic effects can be included in a scalar-relativistic treatment for valence states and a fully relativistic one for core states.

The LAPW method is a procedure for solving the Kohn-Sham LDA equation for the ground-state density, total energy, and eigenvalues (bands) of a periodic many-electron system by employing a basis set which is highly adapted to the problem. The adaption is achieved by dividing the unit-cell into atomic spheres, interstitial, and vacuum regions. Inside the atomic spheres linear combinations of radial functions times spherical harmonics $Y_{lm}(r)$ are used, and plane waves exp(ikr) in the other regions. The solutions to the Kohn-Sham equation are expanded in this basis and the coefficients are determined by the Rayleigh-Ritz variational method.

In its general form the LAPW method expands the potential as follows:

$$V(r) = \begin{cases} \Sigma_{lm}\ V_{lm}(r)\ Y_{lm}(r) & \text{inside sphere,} \\ \Sigma_{k}\ V(k)\ \exp(ikr) & \text{else.} \end{cases}$$

Thus no shape approximations are made, and the method is then called a full-potential (FLAPW) method. The muffin-tin approximation corresponds to retaining only the l=0 and m=0 components in the first expression for V(r) and only k=0 in the second. This procedure corresponds to taking the spherical average inside the spheres and the volume average in the other regions.

A FLAPW program for solids (Blaha et al., 1990) has been obtained from Prof. Trickey at the University of Florida in Gainesville. It has been implemented on the Cray Y-MP at Lewis and some tests have been run for body-centered-cubic tungsten. The program consists of several independent packages. After a starting potential has been generated, the self-consistency cycle involves the following steps and programs:

1. Enter with density.
2. LAPW0: Generate potential from density.
3. LAPW1: Compute valence bands (eigenvalues and eigenvectors).
4. LAPW2: Compute valence density from eigenvectors.
5. CORE : Compute core states and densities.
6. Mixer: Mix input and output densities.
7. Loop to 2.

During his 1990 Summer Faculty Internship, Prof. K.S. Chu has developed a theoretical model for the treatment of surface relaxation effects within the FLAPW scheme by use of a deformation potential, which is based on elastic theory and lattice dynamics. This model and the implications for its implementation have been discussed with the Principal Investigator.

8. CONCLUSIONS

The quantum chemical cluster approach has been demonstrated to be a viable tool for the study of the electronic structure of low-work-function surfaces and high-temperature superconductors.

Very reliable and consistent results have been obtained for the minimum work functions of different model cathode surfaces. The calculated Ba binding energies are in very good agreement with experimental energies of desorption. The optimum coverages depend strongly on the magnitude of the charge transfer at the surface, and there are indications that the calculated surface dipoles are too large and the resulting optimum coverages too small in some cases. The derived work functions, however, do not seem to be affected.

For Ba and Cs on W(100) excellent results have been obtained for the minimum work functions and the adsorbate binding energies. In the case of Cs/W(100), the 0.25 monolayer coverage at the work function minimum is accurately reproduced. For Ba and BaO on W(100), optimum coverages of ~0.15 monolayers have been obtained, whereas higher coverages of up to 0.5 monolayers are expected. For BaO/W(110), on the other hand, the calculated optimum coverage of 0.1 monolayer is consistent with experimental results.

As a model for B-type cathode surfaces, it is found that the upright geometry for BaO on W(100) as suggested by Tuck and Norman et al. (1986 and 1987) provides a correct value for the B-type work function in relation to other low-work-function surfaces. The validity of this model has however been questioned by Shih et al. (1988), who find a shorter Ba-O distance for B-type surfaces and suggest a bridge-bonded BaO structure. While a shorter Ba-O distance gives better results in comparison with photoemission data, the assumption of a bridge-bonded structure leads to higher work functions in the investigated cases. The calculated work function of the BaO/W(110) surface is also higher than as observed for B-type cathodes, so that this surface is not expected to contribute significantly to the emission. The correct BaO geometry and the specific surface that are responsible for the high emission from operating B-type cathodes remain, therefore, uncertain.

The work function of BaO on hcp Os($10\bar{1}0$) is found to be lower by 0.2 eV and the work function of BaO on fcc Pt(111) higher by 0.4 eV than that for the model B-type BaO/W(100) surface. These results are in excellent qualitative agreement with the observed emission enhancement for Os-coated cathode surfaces and the degradation for Pt-coated surfaces. The variation in the work function is found to have its origin in the different substrate crystal structures and not the different electronegativities or work functions of the coating metals themselves.

If the calculated trends for the pure substrates can be verified also for M-type (alloy) surfaces, the credibility of the employed theoretical model would be significantly increased, and predictive capabilities could be achieved. Since the lowest work functions for dispenser cathodes are found for substrates with the hcp crystal structure, the interplay between the magnitude of the surface dipole and the depolarization is expected to explain also the low work functions for other surfaces with the same crystal structure, like Os-W and Ir-W.

The valence and core electronic structure of the 90K superconductor $YBa_2Cu_3O_7$ is found to be well described with atomic clusters of the size of the unit cell of the material. The experimentally observed intensity distribution and width of the Cu-O valence band are correctly described. The valence band observed in photoemission spectra is shifted, however, by about 1.5 eV to higher binding energies. This effect appears to be present in all density-functional calculations. Final-state energy corrections in the localized Cu 3d states are found to contribute 10-20% to the observed shift, while true many-electron effects have to made responsible for the majority of the shift. The calculated core-electron binding energies for Cu, O, and the 3d states of Y and Ba are, after inclusion of the final-state corrections, in excellent agreement with experiment. The charge distribution, as obtained with the cluster approach, is believed to be representative of the surface of the superconducting material.

9. REFERENCES

Blaha P., Schwarz K., Sorantin P., and Trickey S.B., Computer Phys. Commun. 59, 399 (1990).

Case D.A. and Yang C.Y., J. Chem. Phys. 72, 3443 (1980).

Cook M. and Case D.A., QCPE 21, 465 (1989).

Forman R., Appl. Surf. Sci. 17, 429 (1984).

Forman R., Appl. Surf. Sci. 29, 127 (1987).

Fujimori A., Takayama-Muromachi E., Uchida Y., and Okai B., Phys. Rev. B 35, 8814 (1987).

Haas G.A., Shih A., Marrian C.R.K., Appl. Surface Sci. 16, 139 (1983).

Hemstreet L.A., Chubb S.R., and Pickett W.E., Phys. Rev. B 40, 3592 (1989).

Huber K.P. and Herzberg G., in *Molecular Spectra and Molecular Structure*, Vol. IV (Van Nostrand, New York, 1979).

Johnson P.D., Qiu S.L., Jiang L., Ruckman M.W., Strongin M., Hulbert S.L., Garrett R.F., Sinković B., Smith N.V., Cava R.J., Jee C.S., Nichols D., Kaczanowicz E., Salomon R.E., and Crow J.E., Phys. Rev. B 35, 8811 (1987).

Krainsky I.L., J. Vac. Sci. Technol. A 6, 780 (1988).

Lamouri A. and Krainsky I.L., Surf. Sci. 278, 286 (1992).

Mueller D., Shih A., Roman E., Madey T., Kurtz R., and Stockbauer R., J. Vac. Sci. Technol. A 6, 1067 (1988).

Mueller D.R., Kurz R.L., Stockbauer R.L., Madey T.E., and Shih A., Surf. Sci. 237, 72 (1990).

Müller W., Final Technical Report: *Theoretical Study of Cathode Surfaces*, NASA CR-182166 (July 1988).

Müller W., IEEE Trans. Electron Devices 36, 180 (1989).

Müller W., Physica C 162-164, 1357 (1989).

Norman D., Tuck R.A., Skinner H.B., Wadsworth P.J., Gardiner T.M., Owen I.W., Richardson C.H., and Thornton G., Phys. Rev. Lett. 58, 519 (1987).

Schmidt L.D. and Gomer R., J. Chem. Phys. 45, 1605 (1966).

Shih A., Hor C., Elam W., Kirkland J., and Mueller D., Phys. Rev. B 44, 5818 (1991).

Shih A., Hor C., Mueller D., Marrian C.R.K., Elam W.T., Wolf P., Kirkland J.P., and Neiser R.A., J. Vac. Sci. Technol. A 6, 1058 (1988).

Skinner H.B., Tuck R.A., and Dobson P.J., J. Phys. D 15, 1519 (1982).

Swanson L.W. and Strayer R.W., J. Chem. Phys. 48, 2421 (1968).

Topping J., Proc. Roy. Soc. London A 114, 67 (1927).

Tuck R.A., Gardiner T.M., Skinner H.B., Norris R., Norman D., Thornton G., Owen I.W., and Richardson C.H., presented at the 1986 Tri-Service Cathode Workshop, Rome Air Development Center, Rome, NY (March 1986).

Wimmer E., Freeman A.J., Hiskes J.R., and Karo A.M., Phys.Rev. B 28, 3074 (1983).

Zalm P. and van Stratum A.J.A., Philips Tech. Rev. 27, 70 (1966).

10. TECHNICAL PRESENTATIONS AND PUBLICATIONS

- W. Müller, "Electronic Structure of BaO/W Cathode Surfaces", Tri-Service Cathode Workshop, Asbury Park, New Jersey, March 22-24, 1988.
- I.L. Krainsky and W. Müller, "Experimental and Theoretical Studies of Oxygen on W(100)", March Meeting of the American Physical Society, New Orleans, Louisiana, March 23, 1988.
- W. Müller, "Electronic Structure of High-Temperature Superconductors", HTS Research Review, NASA Lewis Research Center, Cleveland, Ohio, April 19, 1988.
- W. Müller, "Electronic Structure of $YBa_2Cu_3O_7$ from a Quantum Chemical Point of View", 5th North Coast Symposium of the American Vacuum Society, Cleveland, Ohio, June 2, 1988.
- W. Müller, "Electronic Structure and Emission Enhancement in Dispenser Cathodes", NASA Lewis Research Center, Cleveland, Ohio, December 5, 1988.

- W. Müller, "Electronic Structure of BaO/W Cathode Surfaces", IEEE Trans. Electron Devices 36, 180 (1989).

- W. Müller, "High-Temperature Superconductors" and "Mechanisms of Superconductivity", Florida A & M University, Tallahassee, Florida, March 1 and 2, 1989.

- W. Müller, "Cluster Modelling of Ceramic Superconductors", HTS Review, NASA-HQ, Washington, D.C., March 14, 1989.

- W. Müller, "Electronic Structure of Adsorbates at Surfaces", University of Akron, Ohio, April 5, 1989.

- W. Müller, "Relativistic Cluster Results for $YBa_2Cu_3O_7$", International Conference on Materials and Mechanisms of Superconductivity: High-Temperature Superconductors, Stanford, California, July 23-28, 1989.

- W. Müller, "Valence and Core Electronic Structure of the 90 K Superconductor Y-Ba-Cu-O", 10th Canadian Symposium on Theoretical Chemistry, Banff, Alberta, August 24-30, 1989.

- W. Müller, "Relativistic Cluster Results for $YBa_2Cu_3O_7$", Physica C 162-164, 1357 (1989).

- W. Müller, "Theoretical Cathode Research", 1990 Tri-Service/NASA Cathode Workshop, Cleveland, Ohio, April 3-5, 1990.

- W. Müller, "Electronic Structure of High-Temperature Superconductors", Annual HTS Review, NASA Lewis Research Center, Cleveland, Ohio, April 27, 1990.

- W. Müller, "A Comparison of Theoretical and Experimental Photoemission Data for $YBa_2Cu_3O_7$", 7th North Coast Symposium of the American Vacuum Society, Cleveland, Ohio, May 31, 1990.

- W. Müller, "Toward the Understanding of the Emission Enhancement in Modern Alloy Dispenser Cathodes", NASA Lewis Research Center, Cleveland, Ohio, November 5, 1990.

Results from the Y-Ba-Cu-O superconductor investigation have been published in the Annual Reports of the Numerical Aerodynamic Simulation (NAS) supercomputing program at Ames Research Center for the 1988-89, 1989-90, and 1990-91 operational years. Copies of the NAS reports (pages 73-75) and the journal articles (pages 76 ff.) are attached.

ELECTRONIC STRUCTURE OF SUPERCONDUCTORS

Wolfgang Mueller, Principal Investigator
Analatom, Inc./NASA Lewis Research Center

RESEARCH OBJECTIVE:

The primary objective of this work is to establish the validity of the quantum chemical cluster approach for the description of the electronic structure of the new high-temperature superconductors. This will justify theoretical analyses, enable predictions for materials properties, and contribute to a better understanding of the mechanism responsible for high-temperature superconductivity.

APPROACH:

Large cluster calculations are performed using the self-consistent relativistic scattered-wave method, which is based on the Dirac wave equation. The method employs the multiple scattering technique and Slater's statistical approximation for electron exchange and correlation.

ACCOMPLISHMENT DESCRIPTION:

The first fully relativistic unit-cell cluster results have been obtained for $YBa_2Cu_3O_7$. The accompanying figure shows the density of states (DOS) for a $Y_2Ba_2Cu_{12}O_{18}$ cluster. The DOS is generated from the calculated energy levels which are indicated as small vertical lines on the horizontal axis. The peaked and smooth density distributions were obtained by broadening the cluster energy levels with Gaussians using width parameters of 0.05 and 0.50 eV, respectively. The calculated DOS is in good agreement with solid-state results and experimental photoemission spectra. The calculated net atomic charges in $YBa_2Cu_3O_7$ are, approximately, for Y: +1.3; Ba: +0.6; Cu1: +0.6; Cu2: +0.8; O1, O2, O3: –0.7; and O4: –0.6. A typical calculation requires about 5 Cray-2 hours and 2 megawords of memory.

SIGNIFICANCE:

A thorough understanding of the electronic structure of the existing high-temperature superconductors will be crucial for the development and discovery of new materials with higher critical temperatures and current densities. The cluster approach is particularly well suited to provide direct insight into important molecular parameters through the analysis of the orbital structure at the Fermi energy.

FUTURE PLANS:

The code will be further used to investigate valence and core-level properties, relativistic electronic effects, and the coupling between Cu-O planes in other high-temperature superconductors. Based on the results of the scattered-wave study, calculations will be designed which employ more elaborate ab initio techniques.

PUBLICATIONS:

1 Relativistic Cluster Results for $YBa_2Cu_3O_7$, Wolfgang Mueller. To be presented at the International Conference on Materials and Mechanisms of Superconductivity: High-Temperature Superconductors, July 23-28, 1989, Stanford, California, and to be published.

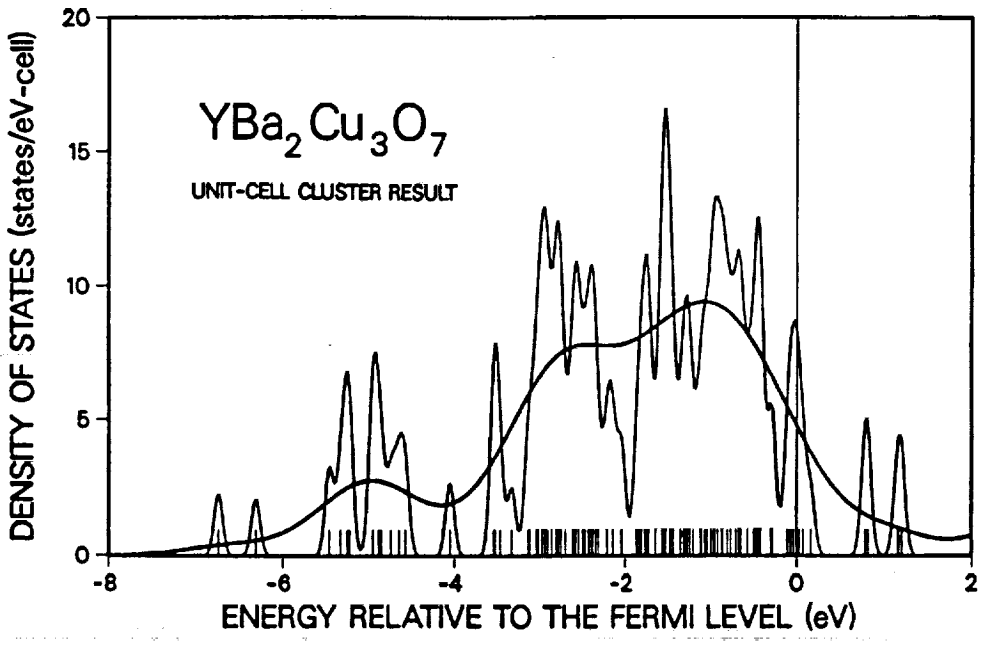

Electronic Structure of Superconductors

Wolfgang Mueller, Principal Investigator
Analatom, Inc./NASA Lewis Research Center

Research Objective
To investigate the electronic structure of high-temperature superconductors with the quantum chemical cluster approach, perform theoretical analyses for critical materials properties, and contribute to a better understanding of the mechanism responsible for high-temperature superconductivity.

Approach
Large-cluster calculations are carried out using the self-consistent, relativistic scattered-wave method, which is based on the Dirac wave equation. The method uses the multiple scattering technique and Slater's statistical approximation for electron exchange and correlation.

Accomplishment Description
Fully relativistic calculations have been performed for Y-Ba-Cu-O using two different clusters: $Y_2Ba_2Cu_{12}O_{18}$ with three Cu-O layers, and $YBa_2Cu_{16}O_{20}$ with four Cu-O layers. The accompanying figure shows the valence and conduction electronic structure per $YBa_2Cu_3O_7$ cell as derived from the two clusters, and a decomposition into atomic contributions. The prominent double peak just below the Fermi level, and other features that are observed in photoemission experiments, are clearly resolved. For $Y_2Ba_2Cu_{12}O_{18}$, final-state photoemission relaxation contributions have been calculated for about 25 valence and core states. Final-state effects (relative to the cluster Fermi level) are found to be small within the valence band, but significantly affect the core levels, where the remaining errors are 1 to 5 eV. A typical calculation requires about 5 Cray-2 hours and 2 megawords of memory.

Significance
The investigation of spin-orbit, relaxation, and correlation effects in cluster calculations is important for understanding the discrepancies between band structure results and photoemission data. Large clusters are shown to provide a good description of the electronic structure of these materials.

Future Plans
Extended cluster and plane-wave calculations will be performed for thin films of Y-Ba-Cu-O on various substrates.

Publications
1. Mueller, W. "Relativistic Cluster Results for $YBa_2Cu_3O_7$." *Physica C* 162-164 (1989): 1357.
2. Mueller, W. "Valence and Core Electronic Structure of the 90K Superconductor Y-Ba-Cu-O." Presented at the 10th Canadian Symposium on Theoretical Chemistry, Banff, Alberta, Aug. 1989.

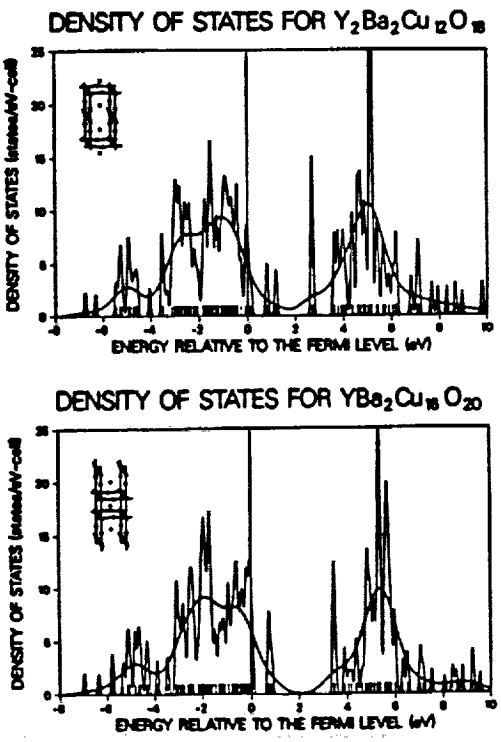

Density of states for (top) $Y_2Ba_2Cu_{12}O_{18}$ and (bottom) $YBa_2Cu_{16}O_{20}$.

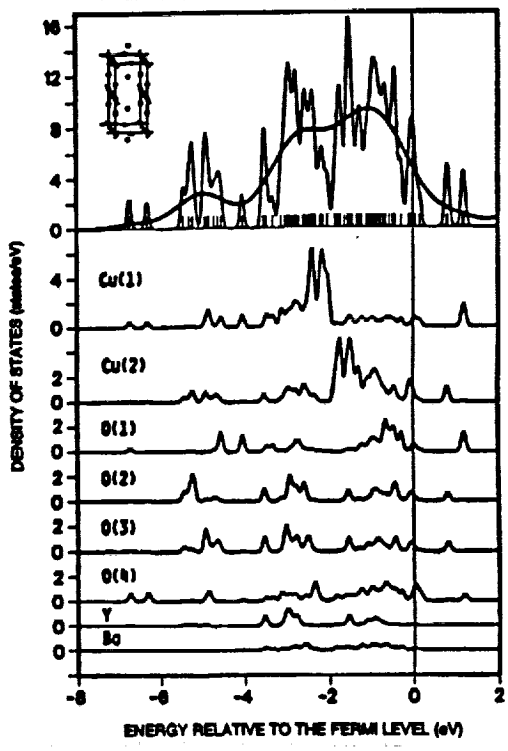

Atomic contributions to the density of states.

Electronic Structure of Superconductors

Wolfgang Mueller, Principal Investigator
Analatom, Inc./NASA Lewis Research Center

Research Objective
To investigate the electronic structure of high-temperature superconductors with the quantum chemical-cluster approach, to perform theoretical analyses for critical materials properties, and to contribute to a better understanding of the mechanism responsible for high-temperature superconductivity.

Approach
Large-cluster calculations are carried out using self-consistent ab initio and scattered-wave methods, which are based on the Schroedinger and Dirac wave equations.

Accomplishment Description
A comparison has been made among the results of fully, quasi-, and nonrelativistic scattered-wave calculations for Y-Ba-Cu-O; a representation of a $Y_2Ba_2Cu_{12}O_{16}$ cluster with three Cu-O layers was used. The cluster is shown schematically in the figures. The two figures depict the valence and conduction electronic structure per $YBa_2Cu_3O_7$ cell as derived from the fully and quasi-relativistic calculations, respectively. The densities of states have been generated from the calculated energy levels (which are indicated as small vertical lines on the horizontal axis) by Gaussian broadening with width parameters of 0.1 and 0.5 eV. Although the general electronic structure is similar in both calculations, especially with respect to the prominent double peak just below the Fermi level, there are significant differences in the shapes of the individual features and their positions relative to the cluster Fermi level. The density of states from the quasi-relativistic calculation is in good agreement with quasi-relativistic band structure results, which demonstrates the validity of the cluster approach. A typical calculation requires 5 to 10 Cray hours and 4 mega-words of central memory.

Significance
The investigation of relativistic, relaxation, and correlation effects in cluster calculations is important for a detailed understanding of the electronic structure and the coupling mechanism in high-temperature superconductors. Fully relativistic and correlated wave functions are required for high accuracy.

Future Plans
Embedded cluster and plane-wave calculations will be carried out to investigate differences in the surface, bulk, and interface electronic structure of Cu-O superconductors and films on various substrates. Electronic coupling parameters will be determined using the ab initio approach.

Publications
Mueller, W. "A Comparison of Theoretical and Experimental Photoemission Data for $YBa_2Cu_3O_7$." Presented at the 7th North Coast Symposium of the American Vacuum Society, Cleveland, OH, May 1990.

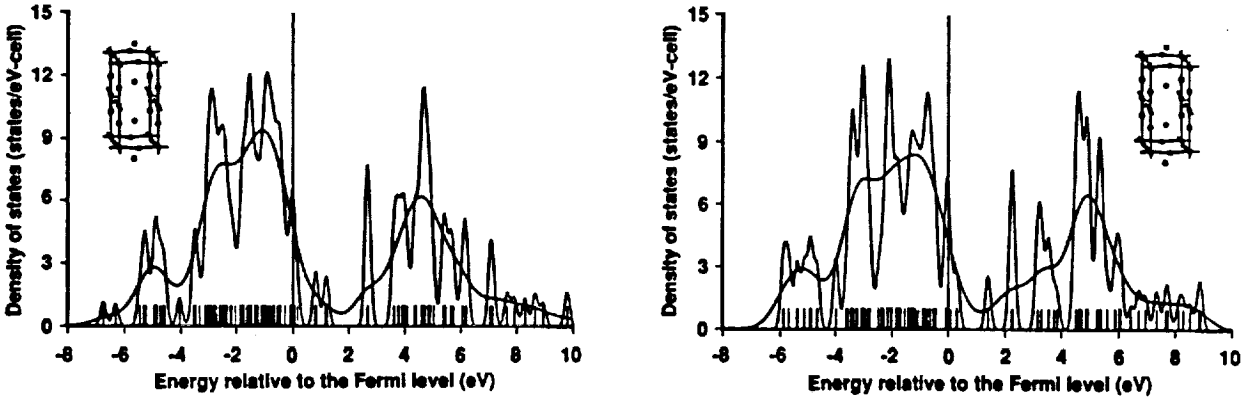

(a) Fully relativistic.

(b) Quasi-relativistic.

Electronic structure of Y-Ba-Cu-O.

Physica C 162-164 (1989) 1357-1358
North-Holland

RELATIVISTIC CLUSTER RESULTS FOR $YBa_2Cu_3O_7$*

Wolfgang MUELLER

Analatom, Inc., 29904 Sycamore Oval, Westlake, Ohio 44145, USA

The valence density of states, charge distribution, and core-level binding energies for a unit-cell cluster of Y-Ba-Cu-O are compared with solid state and experimental results. The cluster is shown to be a reasonable model, in particular for surface properties. Cu 3d spin-orbit effects and final state contributions in the photoemission process are investigated for the first time.

1. INTRODUCTION

It is known[1,2] that density-functional solid state calculations do not provide an accurate description of the Cu 3d - O 2p derived density of states (DOS) in the copper oxide superconductors. Although the general structure of the photoemission spectrum is well reproduced, the experimental spectra are shifted by 1-2 eV to higher binding energy, and the DOS at the Fermi level is much smaller than calculated. This discrepancy is attributed to many-electron effects in the highly localized Cu 3d states, which can be treated, in principle, with high accuracy in cluster calculations. As a test for the validity of the cluster approach, the electronic structure of large clusters is investigated, still within the density functional approach, but with consideration of Cu 3d spin-orbit effects and photoemission final state contributions. In these respects, the present calculations go beyond standard solid state techniques.

2. METHOD

Large cluster calculations are performed for $YBa_2Cu_3O_7$ using the self-consistent, fully relativistic Xα scattered-wave approach.[3] Final state contributions are calculated by employing Slater's transition state method. The results presented here are based on a $Y_2Ba_2Cu_{12}O_{18}$ unit-cell cluster, which consists of a central $Cu_4(1)O_2(1)$ plane, with $BaO_4(4)$, $Cu_4(2)O_4(2,3)$, and Y planes on both sides.

3. VALENCE DENSITY OF STATES

The total and partial densities of states for $YBa_2Cu_3O_7$ as derived from the 34-atom cluster are shown in Fig. 1. The peaked and smooth distributions for the total DOS per cell were obtained by broadening the indicated cluster energy levels with Gaussians using width

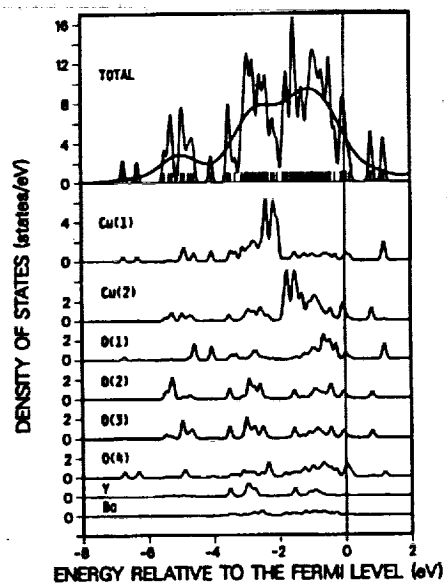

FIGURE 1. Total (per $YBa_2Cu_3O_7$ cell) and partial (atomic) densities of states as derived from a $Y_2Ba_2Cu_{12}O_{18}$ cluster model for Y-Ba-Cu-O.

* Work supported by NASA Lewis Research Center, Cleveland, and the NAS program at NASA Ames.

0921-4534/89/$03.50 © Elsevier Science Publishers B.V. (North-Holland)

parameters of 0.05 and 0.5 eV, respectively. The calculated DOS is in reasonable agreement with solid state results.[4] It shows the two major maxima observed in photoemission spectra, separated by about 2 eV, and additional features at higher and lower binding energies. The cluster DOS is shifted, however, by about 1.5 eV to lower binding energy, very similar to the DOS from solid state calculations. Apart from this shift, the partial DOS from the cluster show major copper contributions near the center of the double maximum and oxygen contributions more to its sides, in good agreement with experiment.[1] The Cu(1,2) 3d states near -2 eV are strongly localized and clearly show the spin-orbit splitting of about 0.3 eV. The Cu(1)-O(1,4) and Cu(2)-O(2,3) states are otherwise significantly hybridized. Without spin-orbit interaction, the Cu-derived DOS from solid state calculations exhibits much sharper peaks.

The calculated direct energy shift due to the relaxation of the charge distribution upon ionization, which is the final state contribution in the photoemission process, is very similar (1.4 eV) at the lower and upper ends of the valence band of the cluster. What counts in comparison with photoemission spectra is the shift of different states relative to the calculated shift at the Fermi level. The presence of an almost identical shift at both ends of the valence band therefore indicates that its width is not affected by final state contributions. The largest relative shifts of up to 0.2 eV are obtained for the strongly localized Cu 3d states near -2 eV. Although quite small, these final state effects account for about 10% of the observed shift of the experimental double peak relative to the calculation.

4. CHARGE DISTRIBUTION AND CORE-LEVEL ENERGIES

The analysis of the charge distribution shows a Cu 3d population of 9.3 for Cu(1) and 9.6 for Cu(2). These values are in very good agreement with the estimate of 9.45 from the Larsson-Sawatzky model.[5] Because of the presence of a strongly covalent electronic structure and the division of charge among overlapping spheres and from the interstitial space, the Cu atoms formally acquire also substantial amounts of valence s and p charge, so that their net charges become +0.6 and +0.8 electrons, respectively. With this subdivision of charge, the excess charge on oxygen, -0.7 for O(1,2,3) and -0.6 for O(4), as well as the ionicity of Y (+1.1) and Ba(+0.6) are small.

A comparison of calculated core-level binding energies with experiment is therefore of particular importance. The calculated Cu $2p_{1/2}$ energies, for both sites and including the final state contribution, are within 952±1 eV (expt. 953 eV),[6] and Cu $2p_{3/2}$ within 932±1 (933 eV).[6,7] The Y and Ba 3d energies are also within 1-2 eV of experimental values. The calculated O 1s energies for all four sites are within 533±1 eV. Peaks are observed at 533, 531,[6] and 529 eV;[7] however, only the latter peak is attributed to the bulk material. The fact that the cluster O 1s energies are all in the vicinity of the higher, surface-sensitive values indicates that the net charge on O in the isolated cluster is, due to the missing Madelung field, too small.

In conclusion, the electronic structure in Y-Ba-Cu-O is both ionic and covalent in character. The cluster valence DOS is in good overall agreement with solid state and experimental results. The charge distribution and core-level energies indicate, however, that an isolated cluster should be considered more as a model for the surface of the material than for the bulk.

REFERENCES
1. J.-M.Mariot et al., Z.Phys.B 75,1(1989).
2. J.A.Yarmoff et al., Phys.Rev.B 36,3967(1987).
3. D.A.Case and C.Y.Yang, J.Chem.Phys. 72,3443 (1980).
4. S.Massidda et al., Phys.Lett.A 122,198(1987).
5. A.Fujimori et al., Phys.Rev.B 35,8814(1987).
6. D.D.Sarma et al., Phys.Rev.B 36,2371(1987).
7. P.Steiner et al., Z.Phys.B 67,19(1987).

PRECEDING PAGE BLANK NOT FILMED

Electronic Structure of BaO/W Cathode Surfaces

WOLFGANG MÜLLER

Abstract—**The local electronic structure of the emissive layer of barium dispenser thermionic cathodes is investigated theoretically using the relativistic scattered-wave approach. The interaction of Ba and O with W, Os, and W-Os alloy surfaces is studied with atomic clusters modeling different adsorption environments representative of B- and M-type cathodes. Barium is found to be strongly oxidized, while oxygen and the metal substrate are in a reduced chemical state. The presence of oxygen enhances the surface dipole and Ba binding energy relative to Ba on W. Model results for W-Os alloy substrates show only relatively small changes in Ba and O for identical geometries, but very large charge redistributions inside the substrate, which are attributed to the electronegativity difference between Os and W. If Os is present in the surface layer, the charge transfer from Ba to the substrate and the Ba binding energy increase relative to W. The improved electron emission from modern alloy surfaces could therefore possibly be explained by higher coverages due to increased Ba binding energies. The different emission enhancement for different alloy substrates is likely to be related to a competition between electronegativity effects and the availability of unoccupied *d*-type orbitals in the substrate.**

I. Introduction

THERMIONIC cathodes have many important applications in the vacuum tube industry. In the field of power microwave devices [1], cathodes are major components in klystrons and traveling-wave tubes used as radio frequency signal amplifiers for communications. Other applications include high-resolution radar systems, plasma heating for fusion research, and free-electron lasers.

The basic and still most widely used type is the barium dispenser cathode, originally designed in 1955 by Levi [2] in which barium calcium aluminate is impregnated into a porous tungsten matrix. These so-called B-type cathodes have a work function of about 2 eV and operate at around 1400 K. The search for a cathode with a lower operating temperature and resulting longer life led in the 1960's to the development of M-type cathodes [3] in which the tungsten surface is coated with a film of rhenium, osmium, osmium-ruthenium, or iridium. A recently improved reservoir cathode developed by NASA and Varian [4], with a W-Os alloy emitting surface, has the potential to operate at current densities of 1–100 A/cm^2 and is expected to have a very long life. Contemplated applications are high-frequency/high-power tubes for space communications and microwave power transmission from satellites.

Extensive experimental efforts using modern surface analytical techniques like X-ray photoelectron (XPS) and Auger electron spectroscopies (AES) have been undertaken to characterize the electronic structure of the cathode emissive layer. The adsorbate structure is roughly described as a monolayer of barium above oxygen on the tungsten(-alloy) substrate (see, e.g., [5]). The detailed chemical and electronic structure of the cathode surface, however, has been found to be complex and is experimentally not well understood. Recent surface-extended X-ray absorption fine structure (SEXAFS) measurements [6], [7] of real cathode surfaces have resulted in conflicting assignments of atomic distances and even the geometrical arrangement of the Ba and O atoms in the emissive layer of impregnated tungsten cathodes.

Although the improved electron emission from modern low-work-function, cathode surfaces is experimentally well documented, basic structural and electronic surface properties and, in particular, and mechanism for the emission enhancement in alloy cathodes are not understood [8]. Because of the ever increasing demand for cathodes with higher current densities and longer life, a thorough theoretical understanding of the electronic properties of the surface at the atomic level is very much needed.

The work reported here represents the first quantum chemical investigation, based on the cluster model approach, of the emissive layer of barium dispenser thermionic cathodes. A preliminary account of the major results obtained from a BaO/W_9 cluster has been given elsewhere [9].

The paper is organized as follows: The relativistic cluster model approach and computational details are briefly discussed in Section II. The calculated electronic orbital structure of BaO/W(100) is compared with experimental photoemission data in Section III. In Section IV, the charge distribution at the surface is analyzed and the resulting dipole properties are investigated. In Section V the first computational results for models of W-Os alloy surfaces are presented. The conclusions from the present theoretical study are summarized in Section VI.

II. Relativistic Cluster Model Approach

Electronic structure calculations are performed for atomic clusters representative of the BaO/W(-Os) surface complex by employing the relativistic $X\alpha$ scattered-wave method.

The fully relativistic self-consistent field, $X\alpha$ scattered-wave method is based on the one-electron Dirac equation and has been developed by Yang and Case [10]–[12]. The general formulation follows the nonrelativistic approach of Slater and Johnson [13], [14] but includes all relativ-

Manuscript received July 15, 1988; revised September 29, 1988. This work was supported by the NASA Lewis Research Center under Contracts NAS3-24744 and NAS3-25085.

The author is with Analatom, Incorporated, Westlake, OH 44145.

IEEE Log Number 8825212.

0018-9383/89/0100-0180$01.00 © 1989 IEEE

istic electronic effects: the mass velocity and Darwin corrections to the energy, and spin–orbit interaction through the use of four-component electronic wave functions in the framework of double group theory. Electron exchange and correlation effects are taken into account by employing Slater's $X\alpha$ potential [15]. The program uses overlapping atomic spheres and thus goes beyond the basic muffin-tin approximation for the potential. The method contains no adjustable molecular parameters.

The substrate is modeled with atomic clusters representing the (100) face of the body-centered-cubic (bcc) crystal lattice of tungsten. Although real cathode surfaces are polycrystalline and (100) may not give the dominant contribution to the overall cathode emission, this surface has been chosen because of its high symmetry, which considerably facilitates the calculations. In a model for BaO adsorption on osmium, the $(10\bar{1}0)$ face of the hexagonal-close-packed (hcp) lattice has been chosen. W-W and Os-Os distances as present in the bulk are used, with lattice parameters of 3.165 Å for W and 2.74 and 4.32 Å for Os [16].

Atomic clusters with between 5 and 14 substrate atoms are investigated. The larger clusters with 9 and 14 substrate atoms are shown in Fig. 1. The smallest cluster, W_5, is derived from the body-centered-cubic W_9 cluster by considering only the 4 symmetry-equivalent atoms in the first layer and their nearest neighbor in the second layer. W_{10} contains in addition to W_9 the nearest neighbor in the fourth layer. In W_{14} two W_9 units are combined. Mixed W-Os substrate clusters are derived from W_9 by selectively replacing W atoms by Os.

For the bcc (100) clusters, oxygen adsorption is assumed in the fourfold hollow site with barium on top of oxygen. In the hcp BaO_2/Os_9 cluster, barium occupies the hollow site and is bridge-bonded to two oxygen atoms. A Ba-O bond length of 4.9 Bohrs ($\approx$2.6 Å) is used in all clusters, as determined by Norman *et al.* [6] from SEXAFS measurements for BaO on W and W-Os cathode surfaces. (Note, however, that Shih *et al.* [7] in a recent paper find 2.3 Å for the W substrate). The Ba-W distance used is 3.9 Å. This value is based on a fit of surface models to the Norman data and has been reported by Tuck *et al.* [17]. The Ba-Os distance used in BaO_2/Os_9 is 3.75 Å and taken the same as determined for BaO/W-Os [6]. This leads to the following heights above the surface (in Bohrs = 0.5292 Å): and 1.1 for O 6.0 for Ba in all bcc clusters, and 5.2 for Ba and 1.5 for O in BaO_2/Os_9.

Generally, the Ba electrons up to $4d$, the O $1s$ electrons, and the W and Os electrons up to $5p$ and including $4f$ are considered core electrons, for which spherical atomic potentials are assumed. The Ba $5s$ and $5p$ semi-core electrons and the remaining valence electrons are treated in the full cluster potential. The Ba_2O_2/W_{14}, BaO_2/Os_9, and $BaO/W_2Os_2W_1Os_2W_2$ clusters have C_{2v} point group symmetry, all other clusters C_{4v} symmetry. The radii of the atomic spheres are chosen as 88 percent of the sphere radii determined from the superposition of nonrelativistic atomic charge densities [18]. $X\alpha$ values of 0.74 for O and 0.70 for Ba, W, Os, and the outer sphere are used. For the largest cluster, Ba_2O_2/W_{14}, a total of 1164 electrons are treated self-consistently, which leads to 110 different core states and 58 valence states. With partial waves included up to $l = 1$ for O and $l = 2$ otherwise, the complex secular matrix for the semi-core and valence states of Ba_2O_2/W_{14} has a dimension of 161.

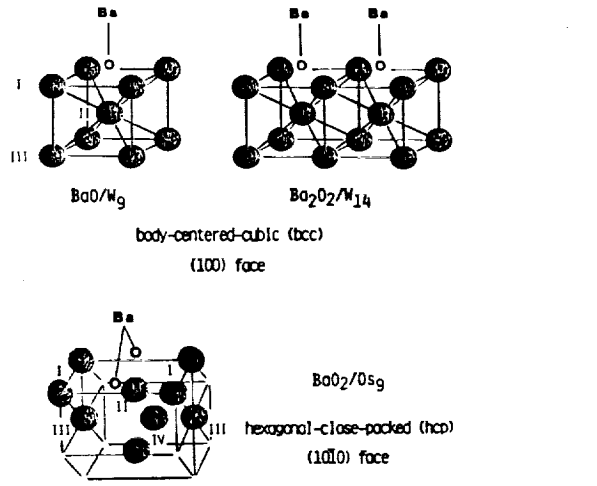

Fig. 1. Cluster models for BaO/W(Os). Mixed W-Os substrate clusters are derived from BaO/W_9 by selectively replacing W by Os.

III. BaO/W Electronic Structure

Fig. 2 displays the calculated outer electron density of BaO/W_9 in a plane perpendicular to the surface along the [110] direction, as indicated in the atomic cluster. Contributions from the W $5d$, $6s$, $6p$, O $2s$, $2p$, and Ba $5s$, $5p$, $5d$, $6s$, $6p$ electronic levels are included. The electronic configuration of tungsten in the clusters is approximately $5d^5 6s^1$, including some $6p$ character. The d orbital structure on W with a characteristic density of four lobes is clearly visible in the figure.

The electron density around the barium atom is largely spherically symmetric due to a high level of oxidation; what is seen is essentially the completely filled $5s$ and $5p$ semi-core shell. The oxygen atom is embedded in the first tungsten layer and exhibits a large interaction in particular with the second-layer tungsten atom. The population analysis shows that the oxygen orbitals are strongly mixed with tungsten orbitals: The O $2s$ orbital has 10 percent and the O $2p$ orbitals have each about 30 percent of W character, mainly in W $5d$ orbitals.

The orbital energy structure of BaO/W_9 gives rise to the density of states (DOS) shown in Fig. 3, in which the discrete cluster levels have been broadened by a Gaussian distribution with a half width of 0.3 eV. The arrows indicate observed energies from the photoemission study of Mueller *et al.* [19] for a BaO overlayer on W(100). The calculated density of states below the Fermi level down to -6 eV originates from electronic states related to occupied W $5d$ and $6s$ orbitals. The BaO/W_9 spectrum shows the well-known W surface states at the Fermi level, the prominent surface resonance state at -1.3 eV (experimentally at -1.9 eV), and a three-peak structure be-

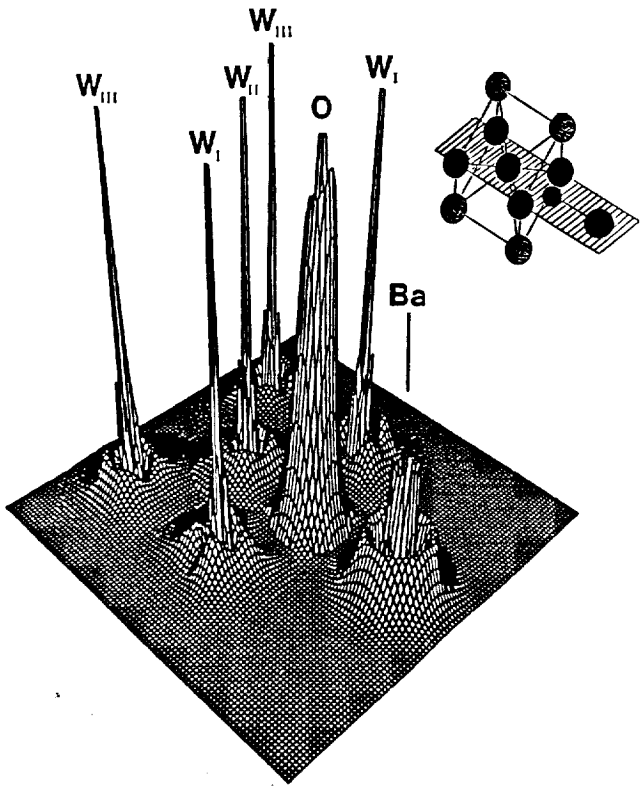

Fig. 2. Cluster model and calculated outer electron density of BaO/W_9 in a plane perpendicular to the surface.

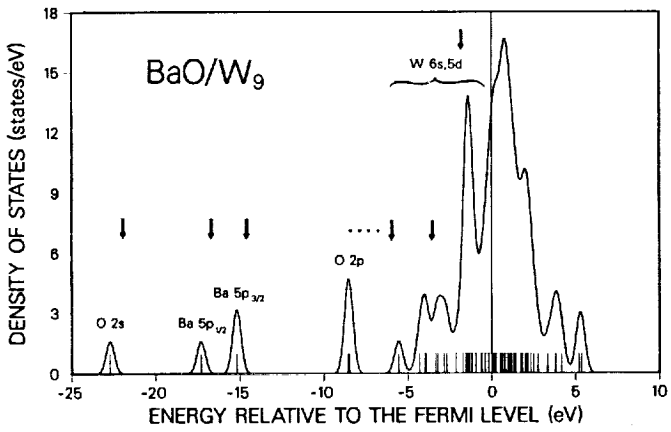

Fig. 3. Calculated density of states for BaO/W_9. The vertical lines on the horizontal axis indicate the discrete electronic levels of the cluster and the arrows experimental photoemission energies for BaO/W(100) [19].

tween −3 and −6 eV. The surface resonance state and the two peaks between −3 and −4 eV are shifted relative to clean W_9 by 0.2–0.3 eV to higher binding energies, while the peak below −5 eV is shifted by 0.4 eV to lower binding energy. The intensity of the peak near −4 eV is increased relative to clean W_9. The three-peak structure is weakly seen in the experimental spectrum for clean W(100) but is not well resolved for BaO/W(100) [19]. The intensity increase around −4 eV, however, is clearly observed. In the experimental spectrum, the structure at higher energies overlaps significantly with a broad O 2*p* band with a maximum at −5.9 eV, which is shifted to −8.5 eV in the theoretical spectrum. The calculated peak positions are otherwise in good agreement with experiment (within 0.5–1.0 eV).

The calculated electronic energies for three different clusters are compared in Table I with the experimental photoemission energies from Mueller *et al.* [19] and calculated energies based on the full-potential linearized augmented plane wave (FLAPW) thin film method from Hemstreet *et al.* [20]. The model used in the FLAPW calculation was a $c(2 \times 2)$ BaO overlayer on W(100) with R(Ba-O) = 2.375 Å and R(Ba-W) = 3.617 Å.

A close similarity is observed for the calculated electronic energies, which differ for the various orbitals in the quite different clusters by no more than 0.5 eV. This result is particularly significant, since the energies in Table I are binding energies relative to the highest occupied (cluster Fermi) level, which changes from 4.8 eV for BaO/W_5 to 5.4 eV for BaO/W_9 and to 7.3 eV for Ba_2O_2/W_{14}, i.e., by as much as 2.5 eV. Cluster size effects thus appear to be not very crucial for electronic binding energies.

The comparison of the cluster results with experiment for binding energies less than 50 eV shows good agreement (within 1 eV) for W $5p_{3/2}$, Ba $5p_{1/2}$ and $5p_{3/2}$, and O 2*s*. The Ba 5*s* level overlaps with W 4*f* and no experimental value was given. The W 4*f* electrons are more weakly bound in the calculation by about 3.5 eV, which could have resulted from the constraints imposed by the treatment as core orbitals. The calculated spin-orbit splittings, however, of the W 4*f* as well as the Ba 5*p* levels are in excellent agreement with experiment, within 0.1 eV of the total spin-orbit separations of 2 eV.

The most significant discrepancy is in the O 2*p* binding energy, which is calculated about 2.5 eV higher than observed. This suggests that the height of oxygen above the W(100) surface of 0.6 Å as derived from the geometry proposed by Tuck *et al.* [17] may not be correct. For larger oxygen-surface separations a larger charge transfer to O and up to 2–3 eV smaller O 2*p* binding energies are obtained [21]. The FLAPW calculation for a 0.1 Å smaller oxygen-surface separation gives a split O 2*p* peak with maxima at 7.8 and 8.8 eV, which is otherwise in the same energy range as the present results. The deviations of the FLAPW binding energies from experiment for the non spin-orbit split Ba 5*p* levels and the O 2*s* level are 3–4 times larger than for the cluster results.

It should be noted at this point that the quoted orbital binding energies are, per definition, not equivalent to observed photoemission energies, but have to be corrected for self-energies and final state effects. These corrections are generally small for energies close to the Fermi level and are known to increase the calculated values for higher binding energies. The fact that the calculated Ba 5*p* and O 2*s*, 2*p* energies are higher than the experimental values for all clusters therefore indicates that the Ba^+ character is slightly too high and the O^- character too low. This is to be expected because the surface coverage in the largest cluster (Ba_2O_2/W_{14}, which gives the best agreement with experiment) is only 1/3 and in the photoemission exper-

TABLE I
ELECTRONIC ENERGIES RELATIVE TO THE HIGHEST OCCUPIED (FERMI) LEVEL FOR SELECTED ORBITALS OF BaO/W(100) IN ELECTRONVOLTS (The W energies given are those for the surface layer.)

Orbital		BaO/W_5	BaO/W_9	Ba_2O_2/W_{14}	Expt.[19]	FLAPW [20]
W	$5p_{1/2}$	45.5	45.8	45.7	....	....
	$5p_{3/2}$	35.8	36.0	36.0	36.8	....
	$4f_{5/2}$	29.8	30.0	29.8	33.5	....
	$4f_{7/2}$	27.5	27.7	27.6	31.3	....
Ba	5s	31.0	30.9	30.5	....	....
	$5p_{1/2}$	17.5	17.3	17.1	16.6	13.8
	$5p_{3/2}$	15.4	15.2	14.9	14.6	13.8
O	2s	22.9	22.7	22.5	21.9	25.8
	2p	8.7	8.5	8.3	5.9	8.8,7.8

iment presumably 1/2. At higher coverages, the net positive charge on Ba will decrease because of dipole-dipole depolarization effects, and the net negative charge on O may increase because the oxygen-surface distance could be larger than assumed. There is also the possibility that the vertical arrangement for BaO on W(100) is not correct.

IV. Charge Distribution and Dipole Properties

In this section the charge distribution in BaO/W clusters will be analyzed. The results will be studied as a function of cluster size and compared with Ba/W in order to analyze the roles of the metal adsorbate and oxygen.

The first basic quantity that can be calculated from the charge distribution is the surface dipole moment. Although the surface coverage in the clusters is in most cases equal to 1/4, the calculated dipole moments are not to be understood as the effective dipoles that determine the value of the work function for this coverage. Rather, the calculated dipole moments reflect initial dipoles, governing the initial change of the work function with coverage in the low coverage regime. This is so because the interaction between the dipoles from different adsorbates is not present in most of the clusters considered. The depolarization resulting from the repulsive interaction of two BaO adsorbate dipoles in Ba_2O_2/W_{14} is found to be very strong. The present results, therefore, emphasize fundamental properties of an individual adsorbed molecule rather than properties of a more complete overlayer. The cluster results thus complement thin film calculations in which dipole properties and data for low coverages are not easily accessible. Symmetry considerations in thin film (slab geometry) calculations require the adsorbate to be placed on both sides of the film. The dipole moment for the system is, therefore, by definition equal to zero.

A second basic quantity that can be derived from the charge distribution and calculated dipole moment is the dipole energy that is an estimate for the binding energy of an ionic adsorbate. In the classical picture, the net charge on the adsorbate interacts with its image inside the substrate to form an ionic adsorbate–substrate bond. The dipole binding energies obtained from the calculated actual charge distributions will be compared with those obtained from the classical image charge concept and with experimental energies for desorption.

The calculated properties for the different clusters are presented in Table II. These include the charge distribution, the Ba 5*d* orbital occupation, the dipole moment, and estimates for the Ba binding energy based on the electrostatic dipole and image charge concepts. Results for a stretched BaO molecule and for Ba on W are given for comparison, with the same distances used as in the BaO/W surface clusters. The roman subscripts on W denote the different substrate layers.

The charge distribution in the BaO/W clusters shows that electrons have been transferred from Ba to O and W. The charge transfer increases significantly from the two-layer W_5 to the three-layer W_9 cluster, but stabilizes very well with the four-layer W_{10} cluster for the single-BaO-adsorbate systems. The differences in the individual net atomic charges are around 0.1 electrons, with the largest variation in the substrate atoms. In the larger clusters, the first W layer is almost neutral, while the electronic charge from Ba has been transferred to the second substrate layer and to a large extent also to the third layer. Because the W_5 cluster does not include third-layer atoms, the charge distribution in the first two layers is completely different. The net charge on Ba in stretched BaO, Ba/W_9, and BaO/W_5 is +1 electron.

For the larger single-BaO-adsorbate clusters, the oxidation level of Ba is about +1.5. The Ba 5*d* occupation is of the order of 0.3 electrons and the Ba 6*sp* occupation about one half of the *d* occupation. This indicates a strong Ba 5*d* contribution to the bonding. The net charge on oxygen is −0.2 electrons and surprisingly small. In the Ba_2O_2/W_{14} cluster with two BaO adsorbates in neighboring sites, the net positive charge on Ba decreases to +1.2 electrons and the net negative charge on O increases to −0.35 electrons. For larger oxygen-surface distances, for which the O 2*p* binding energies would be in better agreement with experiment, the net charge on O may increase up to −0.5 electrons [21].

The important general results from the analyses of the cluster charge distributions are summarized as follows: First, electronic charge is removed from Ba and found in form of a screened image charge inside the substrate cluster. Second, the net negative charge on O is small. And third, the tungsten substrate is not oxidized, it is in a reduced metallic state with the surface layer of W atoms almost neutral and metal-like. The electronic structure of the emissive layer, therefore, is described as largely ionic between Ba and the O/W substrate, while oxygen forms covalent donor bonds to tungsten. The Ba-O overlayer is completely different from either molecular or bulk barium oxide. According to the present results, the chemical structure is best characterized as a Ba salt of the O/W substrate.

The large charge transfer from Ba into the substrate re-

TABLE II
NET CHARGES q (ELECTRONS), DIPOLE MOMENTS μ, AND DIPOLE AND IMAGE CHARGE BINDING ENERGIES E FOR BARIUM IN Ba, BaO/W CLUSTERS (R(Ba-O) = 4.9 Bohrs ≈ 2.6 Å, R(Ba-surface) = 6.0 Bohrs ≈ 3.2 Å.)

Property	BaO	Ba/W_9	BaO/W_8	BaO/W_9	BaO/W_{10}	Ba_2O_2/W_{14}
q(Ba,tot)	+1.03	+1.04	+0.98	+1.51	+1.47	+1.22*2
q(Ba,5d)	0.76	0.53	0.76	0.34	0.35	0.62*2
q(O)	-1.03	....	-0.12	-0.24	-0.22	-0.35*2
q(BaO)	0.00	....	+0.86	+1.27	+1.25	+0.87*2
$q(W_I)$	....	-0.21	-1.05	+0.06	-0.07	+0.01[a]
$q(W_{II})$	....	-0.30	+0.19	-0.33	-0.23	-0.89
$q(W_{III})$	....	-0.53	....	-1.00	-0.87	-0.86[a]
$q(W_{IV})$	....	....	....	....	-0.08	....
μ (Debye)	13.8	25.1	14.9	37.5	36.2	24.6*2
E_{dipole} (eV)	5.5	3.1	4.4	6.4	5.8	5.1*2
$E_{im.ch.}$ (eV)	...	2.5	(2.2)	5.2	4.9	3.4*2

[a] -0.18 for W_I (center), +0.19 for W_I (periphery), -0.38 for W_{III} (center), -0.48 for W_{III} (periphery).

sults in very large dipole moments of about 38 Debyes for the larger single-BaO-adsorbate clusters. The dipole moment for BaO/W_9 is 1.5 times larger than for Ba/W_9, assuming the same Ba-surface distance. The presence of oxygen thus strongly enhances the charge transfer from Ba into the W substrate, which leads to the observed lowering of the work function [22], [23]. The large initial dipole moment for BaO/W(100) of about 38 Debyes per BaO adsorbate will be significantly reduced in a completed overlayer because of repulsive dipole-dipole interactions. The result for Ba_2O_2/W_{14} with a net charge of +1.2 electrons on Ba and an effective dipole of 25 Debyes per BaO adsorbate shows the expected strong depolarization of interacting dipoles.

The maximum coverage on W(100) and real cathode surfaces is probably 1/2 or less, and the BaO–BaO separation is therefore likely to be larger than in the W_{14} cluster. On the other hand, there will be more nearest neighbors that may offset the possibly too large depolarization resulting from one neighbor at a closer distance. The net charge on Ba and the dipole moment for the single-BaO-adsorbate clusters with a formal coverage 1/4 are therefore expected to be reduced for larger coverages on real, polycrystalline cathode surfaces, and the results for Ba_2O_2/W_{14} are certainly considered to be more realistic. Analyses of Auger spectra suggest that Ba is in a mixed metal–metal oxide valence state [24].

An additional test for the accuracy of the calculated charge distribution in the surface clusters is provided by Ba binding energies obtained from simple electrostatic and image charge concepts, which are also given in Table II. The dipole and image charge binding energies are defined as, respectively,

$$E_{dipole} = q_{Ba}^2/R_{dipole} = q_{Ba}^3/\mu$$

and

$$E_{im.ch.} = q_{Ba}^2/2R_{Ba\text{-}surface}.$$

Atomic units are used with q in electrons, R in Bohrs and μ in a.u. (1 Å ≙ 0.5292 Bohrs, 1 Debye ≙ 2.542 a.u., and 1 eV ≙ 27.21 Hartrees); $R_{Ba\text{-}surface} = 6.0$ Bohrs.

The validity of the dipole expression for the binding energy in ionic systems has been tested for molecular BaO at the equilibrium separation, $R_e = 1.94$ Å [25]. Assuming point charges, the experimental dipole moment of 7.93 Debyes corresponds to a transfer of 0.85 electrons from Ba to O. The resulting dipole binding energy is 5.4 eV, which is in reasonable agreement with the experimental value for molecular dissociation of 5.8 eV. Relativistic $X\alpha$ calculations give binding energies of 6.1 eV for R_e and 5.5 eV for the stretched molecule with $R = 4.9$ Bohrs.

The calculated Ba binding energy for the larger single-BaO-adsorbate clusters is of the order of 6 eV and reduced by dipole–dipole interaction to 5.1 eV in Ba_2O_2/W_{14}. The latter value is in excellent agreement with the experimental value of 4.8 ± 0.2 eV for Ba desorption [22]. If simple image charges for q_{Ba} are assumed inside the substrate and $R_{im.ch.} = 2\,R_{Ba\text{-}surface} = 12$ Bohrs are used (rather than the actual center of the negative charge via the calculated dipole moment), the Ba binding energies are reduced by about 1 eV. The reduction is related to the fact that the actual dipole length $R_{dipole} = \mu/q_{Ba}$ is smaller than $R_{im.ch.}$ because of the presence of a small negative charge on oxygen and screening effects inside the W substrate. The calculated dipole binding energy for Ba/W_9 at $R = 6$ Bohrs is 3.1 eV, which may be compared with the experimental value of 3.8 eV for Ba desorption from a clean tungsten surface [22].

In summary, it is found that the electronic structure of the BaO/W emissive layer appears to be reasonably well described by the present calculation. The net positive charge of 1.2 electrons on Ba for the largest cluster gives rise to a Ba binding energy of about 5 eV in agreement with experiment. The net negative charge on O is less than 0.5 electrons. There are, however, indications from the comparison of calculated and experimental densities of states for BaO/W(100) that the O-W distance may be larger than assumed. The comparison of the Ba/W and BaO/W interaction shows that the O/W electronic structure provides for a substantially increased charge transfer from Ba into the metal and a larger binding energy. The resulting very large surface dipole is responsible for the lowering of the work function and related improvement in the emission properties of the cathode. The strong ionic bond in the Ba-O/W complex explains the high thermal stability of the surface.

V. BaO/W-Os Model Results

As a first step toward the theoretical investigation of alloy cathode surfaces, different bcc unit-cell substrate

clusters have been considered in which W atoms were selectively replaced by Os. All other computational parameters and the adsorption geometry are kept the same in order to emphasize the effects due to the atomic substitution and eliminate geometrical and cluster size and shape effects.

Three different BaO/W-Os clusters are derived from W_9 by replacing either the W_I, W_{II}, or W_{III} atoms by Os, which leads to substrate clusters denoted as $Os_4W_1W_4$, $W_4Os_1W_4$, or $W_4W_1Os_4$. In the $W_2Os_2W_1Os_2W_2$ cluster, two first- and two third-layer W atoms in the [110] and [1$\bar{1}$0] directions, respectively, are replaced by Os.

The calculated charge distributions, dipole moments, and Ba binding energies for these clusters are given in Table III together with the results for BaO/W_9 and the Ba bridge-bonded BaO_2/Os_9 cluster. The comparison of the data for the mixed BaO/W-Os clusters with BaO/W_9 shows two significant results: First, the net charges on Ba and O are very similar, with a maximum variation of 0.1 electrons only. Second, very large charge redistributions, however, occur in the substrate which affect in a systematic way the cluster dipole moments and Ba dipole binding energies. This situation is illustrated in Fig. 4.

The charge redistribution in the substrate has to be attributed to the electronegativity difference between W (1.40) and Os (1.52) [26]. The higher electronegativity value for Os indicates that Os has a larger tendency to attract electrons of chemical bonds than W, which results in a net charge transfer from W to Os. This has the following consequences for the surface dipoles as qualitiatively indicated with $-/+$ charges and dipole arrows at the bottom of Fig. 4: If all W_I atoms are replaced by Os, charge is transferred from W_{II} and W_{III} to Os_I opposing the Ba-substrate charge transfer, and the BaO/W_9 (reference) dipole is lowered by 8 Debyes. If all W_{III} atoms are replaced by Os, charge is transferred from W_I and W_{II} to Os_{III} in the direction of the Ba-substrate charge transfer, and the BaO/W_9 dipole is increased by 4 Debyes. If W_{II} or half of the W atoms in the first and third layers are replaced by Os, the resulting cluster dipoles are within about 1 Debye of BaO/W_9.

If Os is present in the first layer, as in $BaO/W_2Os_2W_1Os_2W_2$ or $BaO/Os_4W_1W_4$, the net charge on barium is increased relative to BaO/W_9, which results in a larger Ba dipole binding energy. If Os is not present in the first layer, the Ba binding energy is smaller than in BaO/W_9. In the hcp BaO_2/Os_9 cluster, where Ba is closer to the surface, the net positive charge on Ba is reduced from about 1.5 to 1.3 electrons and the dipole moment is reduced to almost one half of the BaO/W_9 value, which results in a net increase in the Ba dipole binding energy.

The present theoretical results for simple model alloy systems suggest that the following general trends should hold: 1) For similar BaO geometries, the presence of Os in the first layer leads to a smaller surface dipole and larger Ba binding energy compared to pure W. 2) If Ba is bridge bonded to O and consequently closer to the surface than in the on-top position the surface dipole decreases. 3) For different alloy substrates, the largest changes in the charge distribution occur in the substrate, which can either compete with or enhance the Ba-substrate charge transfer, depending on the location of the different metal atoms in the first few layers.

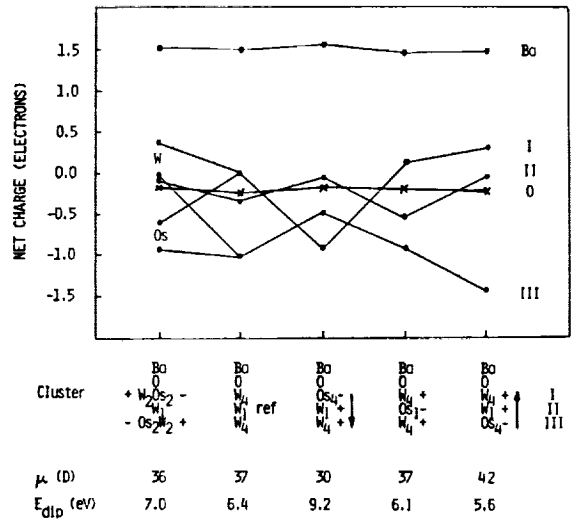

Fig. 4. Charge distribution in $BaO/(W\text{-}Os)_9$ clusters. The $+/-$ signs indicate the charge redistribution in the substrate layers and the arrows the dipole contribution relative to the BaO/W_9 reference cluster.

TABLE III
NET CHARGES q (ELECTRONS), DIPOLE MOMENTS μ, AND Ba DIPOLE BINDING ENERGIES E_{dipole} FOR BaO/W-Os CLUSTERS
(R(Ba-O) = 4.9 Bohrs ≈ 2.6 Å.)

Property	$W_2Os_2W_1Os_2W_2$	W_9	BaO/ $Os_4W_1W_4$	$W_4Os_1W_4$	$W_4W_1Os_4$	BaO_2/ Os_9(hcp)
q(Ba)	+1.54	+1.51	+1.58	+1.48	+1.50	+1.31
q(O)	-0.22	-0.24	-0.17	-0.21	-0.24	-0.36×2
q(BaO)	+1.32	+1.27	+1.41	+1.27	+1.26	.....
$q(W_I)$	+0.38	+0.06	.....	+0.15	+0.29	.....
$q(Os_I)$	-0.63	.....	-0.84	.....	.....	+0.05
$q(W_{II})$	-0.11	-0.33	-0.09	.....	-0.09	.....
$q(Os_{II})$	.....	.....	.....	-0.54	.....	-0.15
$q(W_{III})$	-0.04	-1.00	-0.48	-0.88	.....	.....
$q(Os_{III})$	-0.92	.....	.....	.....	-1.46	-0.25
$q(Os_{III'})$	.....	.....	.....	.....	.....	-0.24
μ (Debye)	36.2	37.5	29.5	36.6	41.8	19.7
E_{dipole} (eV)	7.0	6.4	9.2	6.1	5.6	7.9

A higher Ba binding energy is experimentally observed for osmium-ruthenium coated W surfaces as present in commercial M-type thermionic cathodes. The binding energy increases from 4.8 eV for B-type to 5.4 eV for M-type cathodes [27]. The difference correlates very well with the calculated increase from 6.4 eV for BaO/W_9 to 7.0 eV for $BaO/W_2Os_2W_1Os_2W_2$ at presumably lower coverages. The calculated Ba binding energy on a pure Os substrate in BaO_2/Os_9 is 7.9 eV.

The question of the lowering of the work function in alloy cathodes cannot easily be addressed from the pres-

ent results for individual surface dipoles because the work function is an extended surface property. The minimum work function results from the competition of an increase in the total surface dipole due to additional adsorbate dipoles and the depolarization that occurs with increasing coverage. Simple models for work function versus coverage curves suggest that the maximum work function change is determined by the magnitude of the initial surface dipole, while the optimum coverage is determined by the strength of the depolarization [28]. A larger surface dipole would therefore be indicative of a lower work function, and the on-top arrangement should theoretically lead to a lower work function at smaller coverages. Because, however, the work function versus coverage curve for the BaO/W system does not exhibit a minimum but continues to decrease with increasing coverage [23], the bridge-bonded BaO overlayer with smaller individual dipoles could lead to a lower work function at higher coverages.

The difference between B- and M-type cathodes has been related by Norman *et al.* [6], in part, to the different on-top (BaO/W) versus bridge-bonded (BaO/W-Os) geometries, which were questioned, however, by Shih *et al.* [7] and are inconsistent with the model for the bonding proposed by Green [29]. Drawing on theories of heterogeneous catalysis, Green had postulated that the Ba-O surface bond is tilted on the tungsten substrate and linear on alloy substrates. From the present model results for linear geometries, the lower work function for M-type cathodes could possibly be explained by a higher final coverage due to reduced dipole–dipole interaction and/or higher Ba binding energy.

VI. Summary and Conclusions

Detailed analyses have been presented for the electronic structure of the BaO/W surface complex as obtained from self-consistent relativistic scattered-wave cluster calculations. The effects of mixed W-Os alloy substrates are investigated with computational methods for the first time. Calculated properties include electronic energies, densities of states, electron densities, charge distributions, surface dipoles, and barium binding energies on different model substrates.

Barium is found to be heavily oxidized in the BaO/W surface complex, with an oxidation level greater than 1, while both oxygen and the tungsten substrate are in a partially reduced chemical state. The net negative charge on oxygen is less than 0.5 electrons and thus surprisingly small. The remaining negative charge balancing the large positive charge on barium is found in the form of a screened image charge inside the substrate cluster. The bonding is largely ionic between Ba and the O/W substrate, while oxygen forms covalent bonds with tungsten. The chemical structure of the surface is therefore characterized as a Ba salt of the O/W substrate. These theoretical findings are consistent with available experimental data which describe the barium oxidation state as intermediate between metal and oxide, oxygen in an environment different from bulk BaO, and the W substrate as not being oxidized [29].

The presence of oxygen leads to a significant enhancement of the surface dipole relative to Ba/W. The theoretical population analyses indicate that the O $2p$ orbitals are strongly mixed with W $5d$ orbitals and thus provide for an effective charge transfer from Ba into the W substrate. The large charge transfer leads to a very large initial surface dipole of up to 40 Debyes for the assumed geometry of Ba on top of O in the fourfold hollow site of W(100). The repulsion between interacting adsorbate-induced dipoles, however, causes substantial depolarization. The analysis of the charge distribution shows that the relevant surface dipole is the Ba-substrate and not the Ba-O dipole. The calculated Ba binding energy for an individual BaO adsorbate is about 6 eV. For strongly interacting BaO adsorbates this value is reduced to 5 eV, which is in excellent agreement with the experimental energy for Ba desorption from BaO/W surfaces.

The comparison of theoretical and experimental O $2p$ binding energies in the BaO/W(100) system suggests that the oxygen-surface distance of 0.6 Å as derived from a fit of surface models to experimental SEXAFS data [17] may be too small. For a larger oxygen-surface distance in BaO/W, the net charge transfer from W to O increases and the surface dipole decreases [21]. The surface dipole also decreases when barium is bridge-bonded to two oxygen atoms (and is consequently closer to the surface) as shown with the model for adsorption on a hexagonal-close-packed osmium cluster.

The analysis of the charge distributions in BaO/W-Os model alloy clusters with identical adsorbate and substrate geometries shows similar net charges on Ba and O but very large charge redistributions inside the substrate clusters. The charge redistribution is attributed to the higher electronegativity of Os relative to W and varies systematically with the positions of the Os and W atoms in the clusters. The surface dipole may either increase, decrease, or remain similar to BaO on pure W. If Os is present in the surface layer, the charge transfer from Ba to the substrate and the Ba binding energy increase relative to W. The calculated Ba binding energy for a more or less random W-Os substrate cluster is found to be 0.6 eV higher than for the equivalent pure W cluster, a result that is in striking agreement with the experimentally observed increase in the energy for Ba desorption from B- to M-type surfaces.

The results from the present theoretical investigation suggest that for assumed similar BaO geometries the observed lowering of the work function and related emission enhancement for alloy versus tungsten cathode surfaces could be explained by higher Ba coverages due to higher Ba binding energies. The higher Ba binding energies result from an increased charge transfer from Ba to the surface and the charge redistribution within the first substrate layers due to electronegativity differences between the alloy component metals.

On the basis of the electronegativity argument for Os

and W, one might speculate that a Pt-W surface should also show an improved emission relative to W, since the electronegativity for Pt (1.44) is also slightly higher than for W (1.40) [26]. This is, of course, well known to be not the case. A significant difference between Pt and the emission enhancing transition elements Re, Os, Ru, and Ir is the fact that Pt has an almost completely filled $5d$ shell and forms intermetallic compounds with Ba [30]. The electronegativity argument, therefore, is not equally applicable to Pt, and these other properties are obviously much more important.

A consideration of different bonding geometries in the Ba-O overlayer shows that the surface dipole for an individual adsorbate decreases when changing from on-top to bridge-bonded BaO (with Ba closer to the surface). The larger dipole for the on-top orientation would favor a lower work function at smaller coverages, if such an overlayer actually forms and Ba and O are not initially adsorbed in different sites. Because of the strong repulsive interaction between adsorbate-induced dipoles, however, the bridge-bonded BaO overlayer with smaller individual dipoles would tend to be more stable at higher coverages and could thereby lead to a lower effective work function.

ACKNOWLEDGMENT

The author would like to thank E. G. Wintucky and Dr. R. Forman for stimulating and very fruitful discussions, and Dr. D. A. Case for having provided the basic relativistic X_α computer code.

REFERENCES

[1] A. S. Gilmour, Jr., in *Microwave Tubes*. Norwood, MA: Artech House, 1986.
[2] R. Levi, *J. Appl. Phys.*, vol. 26, p. 639, 1955.
[3] P. Zalm and A. J. A. van Stratum, *Philips Tech. Rev.*, vol. 27, p. 69, 1966.
[4] E. G. Wintucky, M. C. Green, and M. Feinleib, *Research & Develop.*, vol. 29, no. 10, p. 93, 1987.
[5] *Proc. 1982 Tri-Service Cathode Workshop*, in *Appl. Surface Sci.*, vol. 16, nos. 1 and 2, 1983.
[6] D. Norman, R. A. Tuck, H. B. Skinner, P. J. Wadsworth, T. M. Gardiner, I. W. Owen, C. H. Richardson, and G. Thornton, *Phys. Rev. Lett.*, vol. 58, p. 519, 1987.
[7] A. Shih, C. Hor, D. Mueller, C. R. K. Marrian, W. T. Elam, P. Wolf, J. P. Kirkland, and R. A. Neiser, *J. Vac. Sci. Technol. A*, vol. 6, p. 1058, 1988.
[8] R. A. Tuck, *Vacuum*, vol. 33, p. 715, 1983.
[9] W. Müller, *J. Vac. Sci. Technol. A*, vol. 6, p. 1072, 1988.
[10] C. Y. Yang and S. Rabii, *Phys. Rev. A*, vol. 12, p. 362, 1975.
[11] C. Y. Yang, *J. Chem. Phys.*, vol. 68, p. 2626, 1978.
[12] D. A. Case and C. Y. Yang, *J. Chem. Phys.*, vol. 72, p. 3443, 1980.
[13] J. C. Slater, *J. Chem. Phys.*, vol. 43, p. S228, 1965.
[14] K. H. Johnson, *J. Chem. Phys.*, vol. 45, p. 3085, 1966.
[15] J. C. Slater, *Adv. Quantum Chem.*, vol. 6, p. 1, 1972.
[16] C. Kittel, in *Introduction to Solid State Physics*. New York: Wiley, 1976.
[17] R. A. Tuck, T. M. Gardiner, H. B. Skinner, R. Norris, D. Norman, G. Thornton, I. W. Owen, and C. H. Richardson, presented at the 1986 Tri-Service Cathode Workshop, Rome Air Development Center, Rome, NY, Mar. 1986.
[18] J. G. Norman, Jr., *Mol. Phys.*, vol. 31, p. 1191, 1976.
[19] D. Mueller, A. Shih, E. Roman, T. Madey, R. Kurtz, and R. Stockbauer, *J. Vac. Sci. Technol. A*, vol. 6, p. 1067, 1988.
[20] L. A. Hemstreet, S. R. Chubb, and W. E. Pickett, *J. Vac. Sci. Technol. A*, vol. 6, p. 1063, 1988.
[21] W. Müller and E. G. Wintucky, to be published.
[22] R. Forman, *Appl. Surface Sci.*, vol. 17, p. 429, 1984.
[23] G. A. Haas, A. Shih, and C. R. K. Marrian, *Appl. Surface Sci.*, vol. 16, p. 139, 1983.
[24] W. V. Lampert, K. D. Rachocki, B. C. Lamartine, and T. W. Haas, *Appl. Surface Sci.*, vol. 8, p. 66, 1981.
[25] K. P. Huber and G. Herzberg, in *Molecular Spectra and Molecular Structure*. New York: Van Nostrand, 1979, vol. IV.
[26] F. A. Cotton and G. Wilkinson, in *Advanced Inorganic Chemistry*. New York: Wiley, 1966.
[27] R. Forman, *Appl. Surface Sci.*, vol. 29, p. 127, 1987.
[28] J. Hölzl, F. K. Schulte, and H. Wagner, in *Solid Surface Physics*. Berlin: Springer, 1979.
[29] M. C. Green, "Dispenser cathode physics," Final Tech. Rep. RADC-TR-81-211, Rome Air Development Center, Rome, NY, July 1981.
[30] W. B. Pearson, in *A Handbook of Lattice Spacings and Structures of Metals and Alloys*. Oxford: Pergamon, 1967.

*

Wolfgang Müller received the M.S. degree in chemistry and the Ph.D. degree in physical chemistry from the University of Basel, Switzerland, in 1973 and 1978, respectively.

During his postdoctoral years he worked in the field of computational quantum chemistry at the University of Kaiserslautern, West Germany, from 1979 to 1984, and was a Visiting Scientist at the IBM Research Laboratory in San Jose, from 1984 to 1985. In 1986, he joined Analatom, Inc., as a Senior Research Scientist. His current research interests include thermionic cathode surfaces and high-temperature superconductors.

Dr. Müller is a member of the American Physical Society and the Physical Chemistry Division of the American Chemical Society.

REPORT DOCUMENTATION PAGE

Form Approved
OMB No. 0704-0188

Public reporting burden for this collection of information is estimated to average 1 hour per response, including the time for reviewing instructions, searching existing data sources, gathering and maintaining the data needed, and completing and reviewing the collection of information. Send comments regarding this burden estimate or any other aspect of this collection of information, including suggestions for reducing this burden, to Washington Headquarters Services, Directorate for Information Operations and Reports, 1215 Jefferson Davis Highway, Suite 1204, Arlington, VA 22202-4302, and to the Office of Management and Budget, Paperwork Reduction Project (0704-0188), Washington, DC 20503.

1. AGENCY USE ONLY (*Leave blank*)	2. REPORT DATE	3. REPORT TYPE AND DATES COVERED
	October 1994	Final Contractor Report

4. TITLE AND SUBTITLE

Theoretical Study of Cathode Surfaces and High-Temperature Superconductors

5. FUNDING NUMBERS

WU-235-01-0A
C-NAS3-25085

6. AUTHOR(S)

Wolfgang Mueller

7. PERFORMING ORGANIZATION NAME(S) AND ADDRESS(ES)

Analatom, Inc.
29904 Sycamore Oval
Westlake, Ohio 44145

8. PERFORMING ORGANIZATION REPORT NUMBER

E-9264

9. SPONSORING/MONITORING AGENCY NAME(S) AND ADDRESS(ES)

National Aeronautics and Space Administration
Lewis Research Center
Cleveland, Ohio 44135-3191

10. SPONSORING/MONITORING AGENCY REPORT NUMBER

NASA CR-195407

11. SUPPLEMENTARY NOTES

Project Manager, Edwin G. Wintucky, Space Electronics Division, NASA Lewis Research Center, organization code 5620, (216) 433-3510.

12a. DISTRIBUTION/AVAILABILITY STATEMENT

Unclassified - Unlimited
Subject Categories 23 and 76

This publication is available from the NASA Center for Aerospace Information, (301) 621-0390.

12b. DISTRIBUTION CODE

13. ABSTRACT (*Maximum 200 words*)

The surface-dipole properties of model cathode surfaces have been investigated with relativistic scattered-wave cluster calculations. Work-function/coverage curves have been derived from these data by employing the depolarization model of interacting surface dipoles. Accurate values have been obtained for the minimum work functions of several low-work-function surfaces. In the series BaO on bcc W, hcp Os, and fcc Pt, BaO/Os shows a lower and BaO/Pt a higher work function than BaO/W, which is attributed to the different substrate crystal structures involved. Results are also presented on the electronic structure of the high-temperature superconductor $YBa_2Cu_3O_7$, which has been investigated with fully relativistic calculations for the first time.

14. SUBJECT TERMS

Thermionic cathodes; Work function calculations; Electronic structure calculations; High temperature superconductors

15. NUMBER OF PAGES
92

16. PRICE CODE
A05

17. SECURITY CLASSIFICATION OF REPORT	18. SECURITY CLASSIFICATION OF THIS PAGE	19. SECURITY CLASSIFICATION OF ABSTRACT	20. LIMITATION OF ABSTRACT
Unclassified	Unclassified	Unclassified	

PRECEDING PAGE BLANK NOT FILMED